# TIDE- AND WIND-FORCED CURRENTS IN BUZZARDS BAY, MASSACHUSETTS

by

Richard Peter Signell

B.S., University of Michigan
(1983)

SUBMITTED TO THE DEPARTMENT OF EARTH, ATMOSPHERIC AND PLANETARY SCIENCES IN PARTIAL FULFILLMENT OF THE REQUIREMENTS FOR THE DEGREE OF

MASTER OF SCIENCE IN PHYSICAL OCEANOGRAPHY

at the

MASSACHUSETTS INSTITUTE OF TECHNOLOGY

January 1987



Signature of Author _____
Department of Earth, Atmospheric and Planetary Sciences

Certified by _____
R. C. Beardsley
Thesis Supervisor

Accepted by _____
W. F. Brace
Chairman, Department Graduate Committee

# TIDE- AND WIND-FORCED CURRENTS IN BUZZARDS BAY, MASSACHUSETTS

by
Richard Peter Signell

Submitted to the Department of Earth,
Atmospheric, and Planetary Sciences
on January 16, 1987 in partial fulfillment of the
requirements for the Degree of Master of Science in
Physical Oceanography

## ABSTRACT

Buzzards Bay is a embayment located in southeastern Massachusetts which is roughly 50 km long, 15 km wide, and has an average depth of 11 m. Freshwater input is minimal (15 $m^3$ $s^{-1}$) and currents over most of the bay are dominated by tides. The tidal current is basically rectilinear in the along-bay direction, and the amplitude decreases from a maximum of 50–60 cm $s^{-1}$ near the mouth to 10–15 cm $s^{-1}$ at the head, exhibiting a standing wave response.

Subtidal currents in Buzzards Bay were examined from six current meters on three moorings near the mouth from August 1984 to January 1985. Conditions were vertically well mixed over most this period, and measurements made at 5 and 10 m in roughly 15 m of water show barotropic mean flow dominated by tidal rectification. These Eulerian mean observations are shown to be consistent with the predictions of a nonlinear numerical tidal model of the region, which indicates that the lower bay Eulerian mean field is dominated by small scale (2–5 km) tide-induced residual eddies with magnitudes of 1–5 cm $s^{-1}$.

Subtidal current variability is polarized along the axis of the bay, and appears driven by local wind stress. Local wind stress acting along the bay drives a coherent up-wind response at 10 m depth, but is not coherent at 5 m. In addition, along-bay current energy levels are higher at the central, deepest mooring. A constant depth, steady 1-D model predicts a zero-crossing in current at 1/3 the water depth, providing an explanation for the lack of coherence at the upper instruments. When cross-channel structure is added, the model successfully predicts higher energy levels at the deeper mooring but erroneously predicts a coherent response at the surface instrument.

Transport of material should be due dominantly to the interaction of the local wind response and the tide-induced dispersion indicated by the small scale Eulerian residual field.

## ACKNOWLEDGEMENTS

Many people have contributed to make this thesis a rewarding and largely enjoyable project. I thank Bob Beardsley for his many insights and suggestions, and especially for his unflagging enthusiasm and support. Bill Grant, Brad Butman and Rocky Geyer were also generous with their time and advice. My fellow Joint Program students have helped make the semesters pass quickly. Thanks especially to Libby for sticking it out for better and worse.

The New England Division of the U.S. Army Corps of Engineers and Brad Butman of the U.S. Geologic Survey in Woods Hole kindly allowed the use of their data.

This study was supported by the Department of Commerce, NOAA Office of Sea Grant under Grant R/P-13 and R/P-21, the National Science Foundation Grant OCE 84-17769, the Battelle Memorial Institute Subcontract C-8184(8818)-381, the Woods Hole Oceanographic Institution Coastal Research Center, and the Woods Hole Oceanographic Institution Education Program.

# Contents

# List of Figures

# List of Tables

# Chapter 1

# Introduction

The transport and dispersion of waterborne tracers (e.g. pollutants, larvae, salt) are often of primary interest in shallow bays and estuaries. These processes often depend most importantly on the low-frequency and mean currents even when the instantaneous flow is dominated by tidal currents. The focus of this thesis, therefore, is to describe and explain the mean and low-frequency current response in a typical tidally dominated coastal embayment with a contamination problem: Buzzards Bay, Massachusetts.

Buzzards Bay is a coastal embayment located in southeastern Massachusetts (Fig. 1.1 and Fig. 1.2). As in many estuaries and bays, there is a rich variety of use by the coastal population: New Bedford, on its northwestern shore, is the largest revenue-producing port on the United States east coast (Weaver, 1984), while the beaches, warm water and superb fishing and sailing conditions make Buzzards Bay popular with summer visitors. In addition, its salt marshes are unique ecosystems supporting a wide variety of wildlife. While these characteristics create public interest in Buzzards Bay, the recent discovery of polychlorinated biphenyl (PCB) contamination in New Bedford Harbor (Gilbert, 1974) has caused intense scientific activity to be focused on the bay. The PCB problem in New Bedford has been described in detail by Weaver (1984) and Farrington (1982). When the pollution problem arose, it was discovered that little was known about physical processes in the bay, and a series of hydrographic and moored array experiments were conducted by Woods Hole Oceanographic Institution (WHOI) and United States Geologic Survey (USGS) scientists to obtain basic water structure and current measurements. With the addition of data from the United States Army Corps of Engineers and National

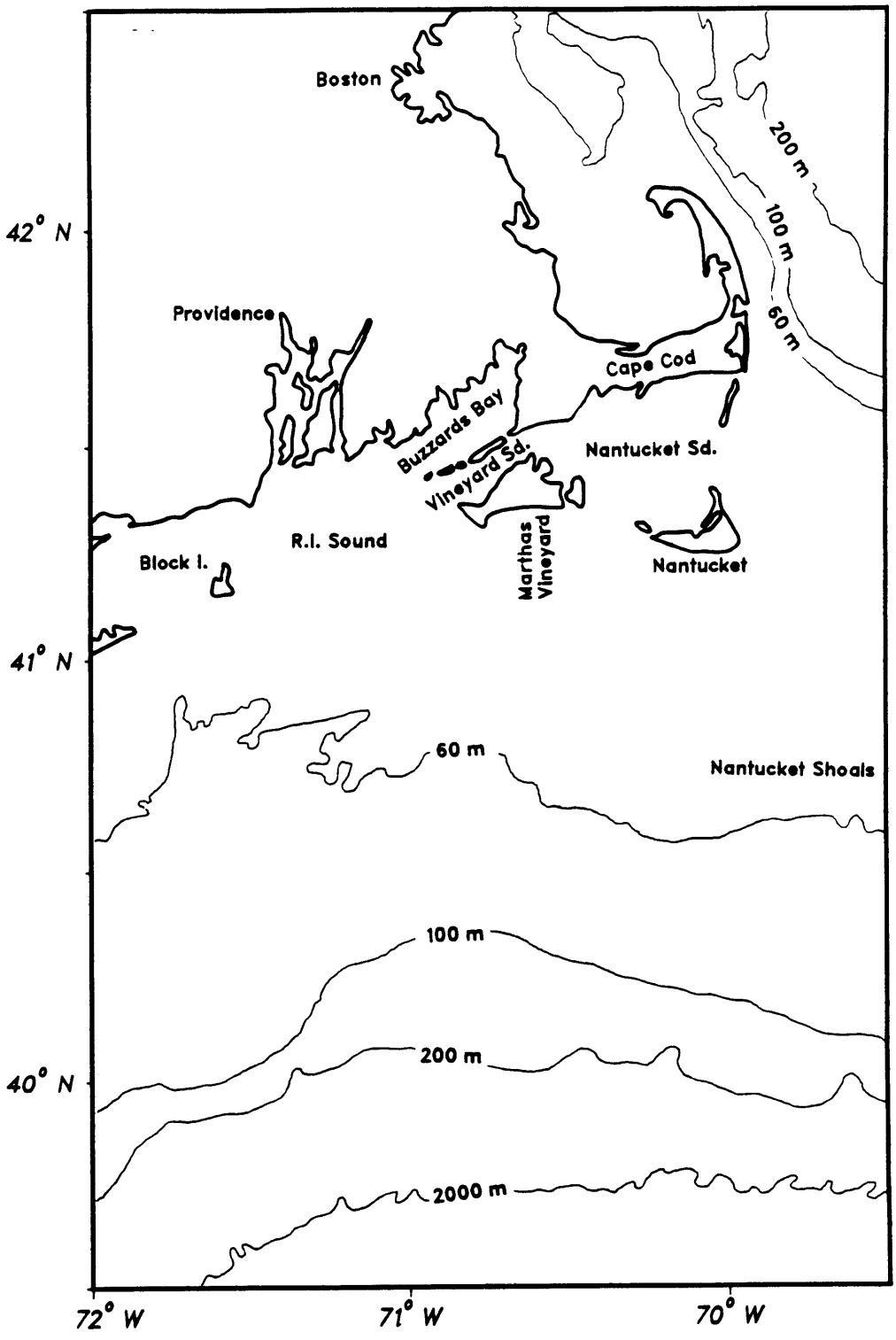


Figure 1.1: Buzzards Bay, Massachusetts and surrounding region.

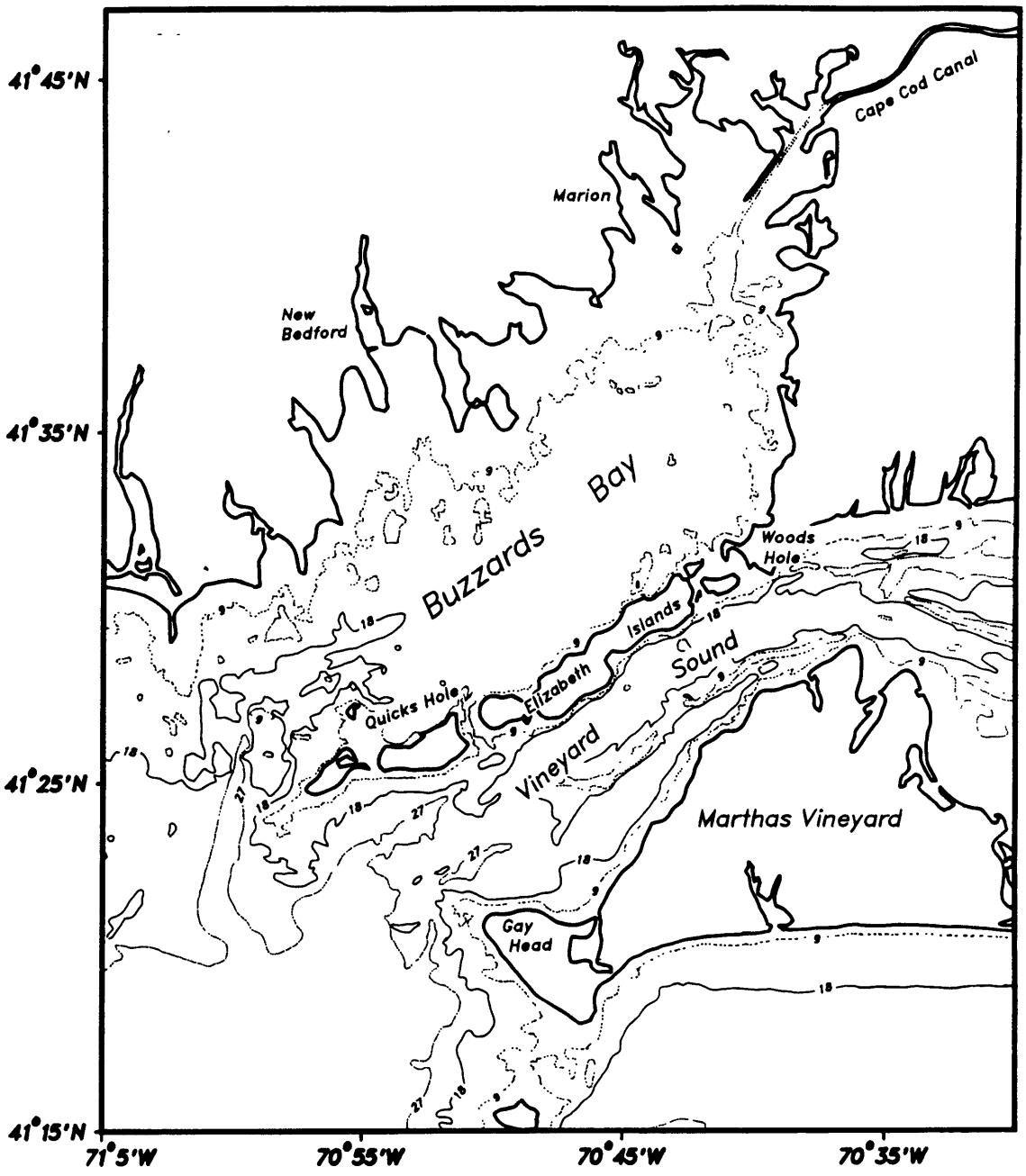


Figure 1.2: Detail of Buzzards Bay and Vineyard Sound. The bay is separated from the sound by several holes in the Elizabeth Islands. Contour interval is 9 m.

Ocean Survey, there is a growing set of hydrographic, current, wind and sea level data for the region. The time series data used in this study is summarized in Fig. 1.3 and Table 1.1.

For this study, Buzzards Bay is defined as the body of water extending southwestward from the west end of Cape Cod Canal, opening onto Rhode Island Sound at its mouth, and bounded to the southeast by the Elizabeth Islands. The bay so defined is approximately 40 km long, and varies in width from 10 km near the mouth to a maximum of 20 km at New Bedford. The formation of the bay occured during the last ice age (15,000 years ago), and the glaciers retreat is evidenced in the numerous elongate inlets along the northwestern shore, with variations in width comparable to the width of the bay itself. The southeastern side of the bay, consists of glacial debris which constitutes the recessional Buzzards Bay Moraine. Consequently, it has a relatively smooth shoreline, interrupted by a series of passages between the Elizabeth Islands, of which Quicks Hole is the largest in cross-sectional area. The bay communicates with Rhode Island Sound through its mouth, with Vineyard Sound through the holes and with Cape Cod Bay through the Cape Cod Canal.

Buzzards Bay is quite shallow, with an mean depth from digitized isobaths of 11 m at Mean Low Water (MLW). Depths near the head average 5-10 m at MLW and increase seaward to over slightly over 20 m at the mouth (Fig. 1.2). Gradations in bathymetry are generally weak over most of the central area of the bay, but depth profiles of transects across the bay are typically asymmetric, with shallow water to the northwest (Fig. 1.4). Near the mouth, the bottom topography becomes complex and convoluted, with depths of 20–30 m. Offshore to the southwest is Rhode Island Sound (RIS) with more gradually varying depths from 20–40 m. Vineyard Sound, to the southeast, is also generally deeper than Buzzards Bay, with an average depth of 18 m between Woods Hole and Gay Head.

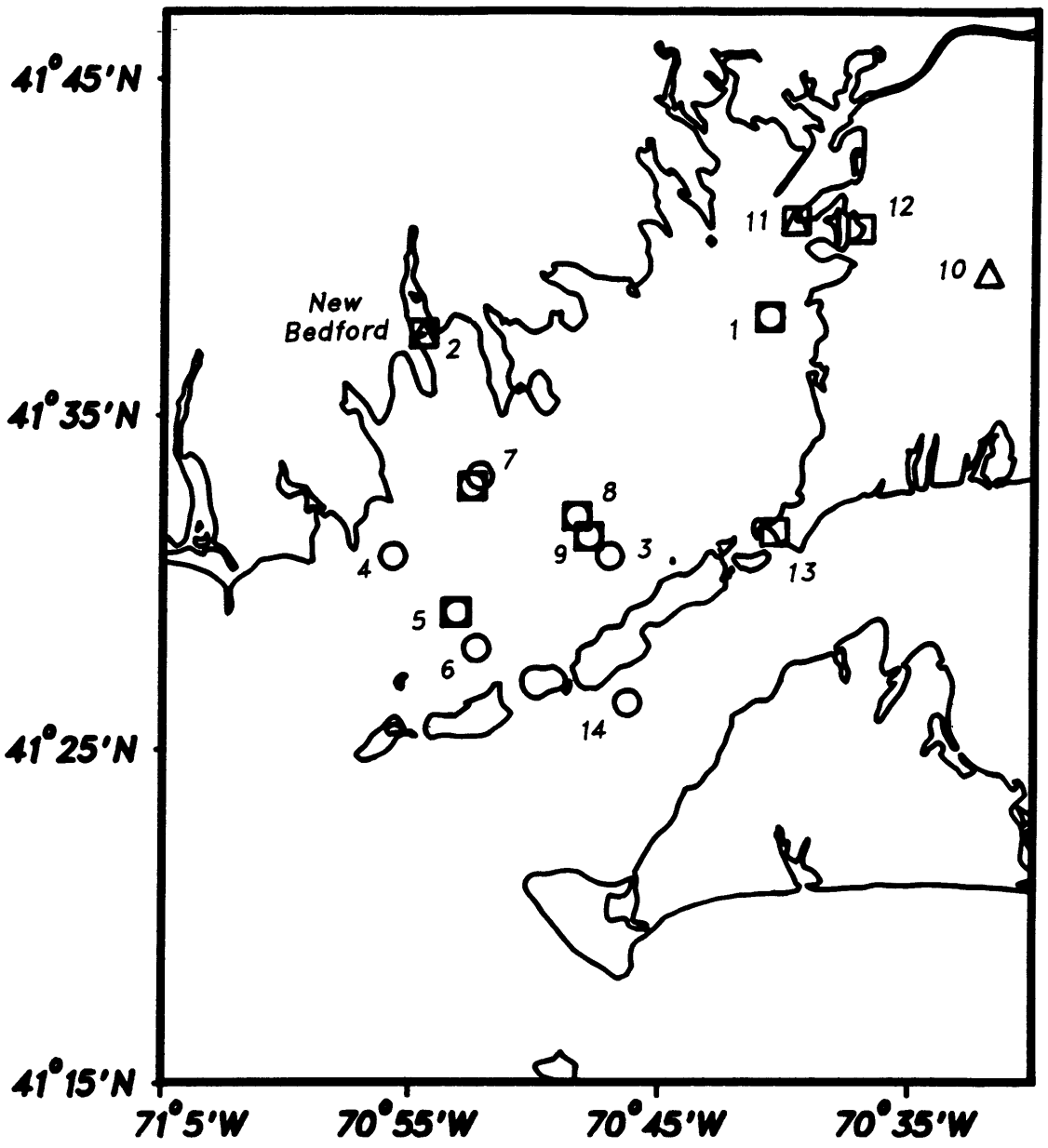


Figure 1.3: Station map for time series data used in study. Circles denote current measurements, squares denote pressure or tide gauge measurements and triangles denote wind measurements. Refer to Table 1.1 for further explanation of data.

| Station | Water depth (m)[1] | Lat.(N.)/Lon.(W.) | Instrument type[2] | Instrument depth | Start (YrMoDy) | Stop (YrMoDy) |
|---|---|---|---|---|---|---|
| 1 | 13.0 | 41°37.9′ 70°40.6′ | T | 12.0 | 841108 | 850114 |
| | 13.1 | | T | 12.1 | 850128 | 850329 |
| | 13.3 | | T | 12.3 | 850409 | 850619 |
| | 12.0 | | T | 11.0 | 850626 | 850814 |
| 2 | – | 41°35.4′ 70°54.0′ | A | – | 840820 | 850913 |
| | – | | TG | – | 840809 | 850119 |
| 3 | 14.2 | 41°30.8′ 70°47.0′ | T | 13.2 | 840821 | 841022 |
| 4A | 15.4 | 41°30.8′ 70°55.7′ | VMCM | 5.0 | 840824 | 850116 |
| 4B | | | VMCM | 10.0 | 840824 | 841208 |
| 5A | 18.1 | 41°29.1′ 70°53.1′ | VMCM | 5.0 | 840827 | 841219 |
| 5B | | | VMCM | 10.0 | 840827 | 841219 |
| | | | TDR | 18.1 | 841109 | 841212 |
| 6A | 16.0 | 41°28.0′ 70°52.3′ | VMCM | 5.0 | 840828 | 850116 |
| 6B | | | VMCM | 10.0 | 840828 | 841208 |
| 7 | 12.8 | 41°32.9′ 70°52.5′ | T | 11.8 | 840906 | 841022 |
| | 12.6 | 41°33.2′ 70°52.2′ | VACM | 8.6 | 841025 | 850114 |
| | 12.6 | | VACM | 8.6 | 850114 | 850328 |
| | 13.3 | | VACM | 9.3 | 850328 | 850619 |
| | 12.6 | | VACM | 8.6 | 850619 | 850814 |
| 8 | 16.6 | 41°32.0′ 70°48.3′ | T | 15.6 | 841025 | 850114 |
| | 16.6 | | T | 15.6 | 850128 | 850328 |
| | 16.6 | | T | 15.6 | 850329 | 850628 |
| 9 | 15.4 | 41°31.4′ 70°27.8′ | T | 14.4 | 850619 | 850807 |
| 10 | – | 41°39.2′ 70°31.9′ | A | – | 840701 | 850131 |
| 11 | – | 41°40.8′ 70°39.6′ | TG | – | 840824 | 850118 |
| 12 | – | 41°30.6′ 70°37.0′ | TDR | – | 841127 | 850303 |
| 13 | – | 41°31.5′ 70°40.4′ | TG | – | 840101 | 850101 |
| 14 | – | 41°26.4′ 70°46.2′ | VACM | – | 860225 | 860428 |

[1] Water depth not corrected for tide.

[2] A= Anemometer; T=tripod with current (Savonius rotor) and pressure, described in Butman and Folger (1979); TDR=Temperature-Depth Recorder TG=Tide gauge; VACM=Vector Averaging Current Meter; VMCM=Vector Measuring Current Meter.

Table 1.1: Description of Buzzards Bay time series data used in this study (see Fig. 1.3 for locations).

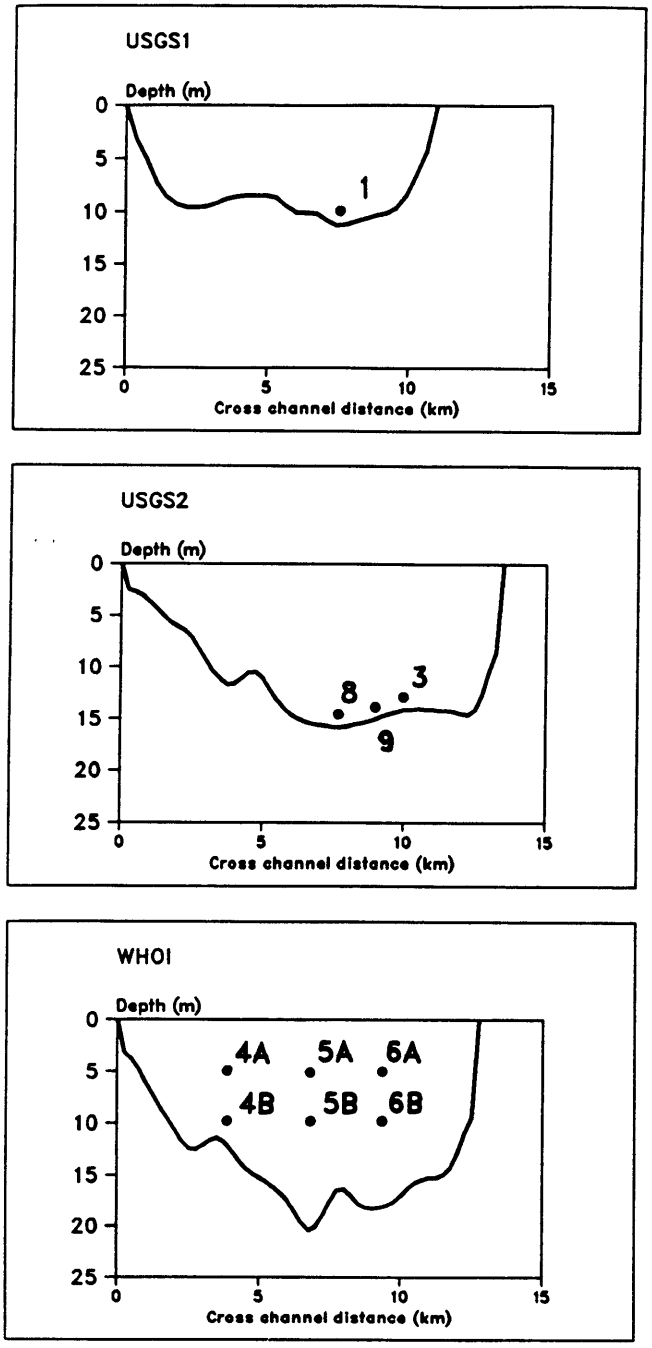


Figure 1.4: Cross-section profiles at three transects: (a) USGS1 (stn. 1) at the head of the bay; (b) USGS2 (stns. 8, 9 & 3) at mid-bay; and (c) WHOI (stns. 4, 5 & 6) in the lower bay.

# Chapter 2

# Hydrography

## 2.1 Introduction

The purpose of this chapter is to examine the major hydrographic characteristics of Buzzards Bay. This is essential, for the density field may drive thermohaline circulation and substantially alter the structure of forced and free motions. In addition, the temperature and salinity fields are important biological factors affecting species productivity and diversity. While a detailed description in time and space is difficult due to the complexity of the physical processes and lack of a comprehensive data set, the gross features of the temperature, salinity and density fields in Buzzards Bay are well defined by existing measurements and can be related to freshwater input, the surface heat flux cycle, turbulent mixing and lateral exchange with shelf water. Seperate overviews of factors affecting the salinity and temperature fields are followed by a review of hydrographic surveys.

## 2.2 Factors affecting the salinity field

The salinity distribution dominates the density variation in Buzzards Bay from fall to spring. This distribution is determined by inputs of freshwater from streams and groundwater, precipitation minus evaporation, and the results of mixing with the surrounding waters of Rhode Island Sound, Vineyard Sound, and Cape Cod Bay. These influences are first examined using historical data.

Buzzards Bay drains approximately 780 $km^2$ of land, based on drainage basin data for the northwest side of the bay (Wandle and Morgan, 1984) and contours of groundwater elevation from Cape Cod (Guswa and LeBlanc, 1981). Most of the inflow enters along the northwestern side with a concentration at the head of the bay, where the Wankinko, Agawam and Weweantic Rivers discharge (Fig. 2.1). Stream gauge data is limited, the only long term station operated by the United States Geologic Survey (USGS) at the Westport River, a nearby tributary which empties into Rhode Island Sound. The monthly mean discharge over 38 years, normalized by drainage area, is presented in (Fig. 2.2a). Evident is the distinct seasonal variation of discharge due to the rise and fall of the water table, which in this region is due primarily to increased evaporation and transpiration in the summer since the seasonal variation in rainfall is relatively small (Goldsmith, 1986). There is considerable interannual variability in rainfall, however, resulting in large fluctuations about the climatological monthly means. Nevertheless, if recharge and usage rates of groundwater are similar enough over the region of interest, the ratio of runoff to drainage area from the Westport River can be used to estimate freshwater input for Buzzards Bay. In support of this approach, normalized monthly discharge from two partial years of data at the Weweantic River (located in the bay proper) compare well with data collected simultaneously from the Westport River (Fig. 2.2b). The similarity of the two stations suggests that an estimate of stream flow for the entire bay is possible. From the Westport River data, the mean stream flow to drainage area with one standard deviation is .0198$\pm$.0051 ($m^3$ $s^{-1}$) $km^{-2}$ or 62.5$\pm$16.0 cm $yr^{-1}$ (Linney, written communication). This compares favorably with the .0191 ($m^3$ $s^{-1}$) $km^{-2}$ from Reach 11 of Bue (1970), which encompassed the freshwater input from Orleans, MA to the Taunton River in Rhode Island. Using the drainage area of the entire bay, a total mean inflow of 15.4$\pm$3.9 $m^3$ $s^{-1}$ is obtained[1]. The drainage areas and estimated mean stream flows for the larger rivers are presented in table 2.1, and the standard deviations from these means are $\pm$26%.

The other factor effecting fresh water input in the bay is precipitation minus evaporation (P-E). Evaporation was determined from the archived

[1]Bumpus (1973) estimated 27 $m^3$ $s^{-1}$ for Buzzards Bay from Bue's (1970) data, but apparantly considered the shoreline of the bay relative to the total shoreline of Reach 11 rather than considering the drainage area of the bay.

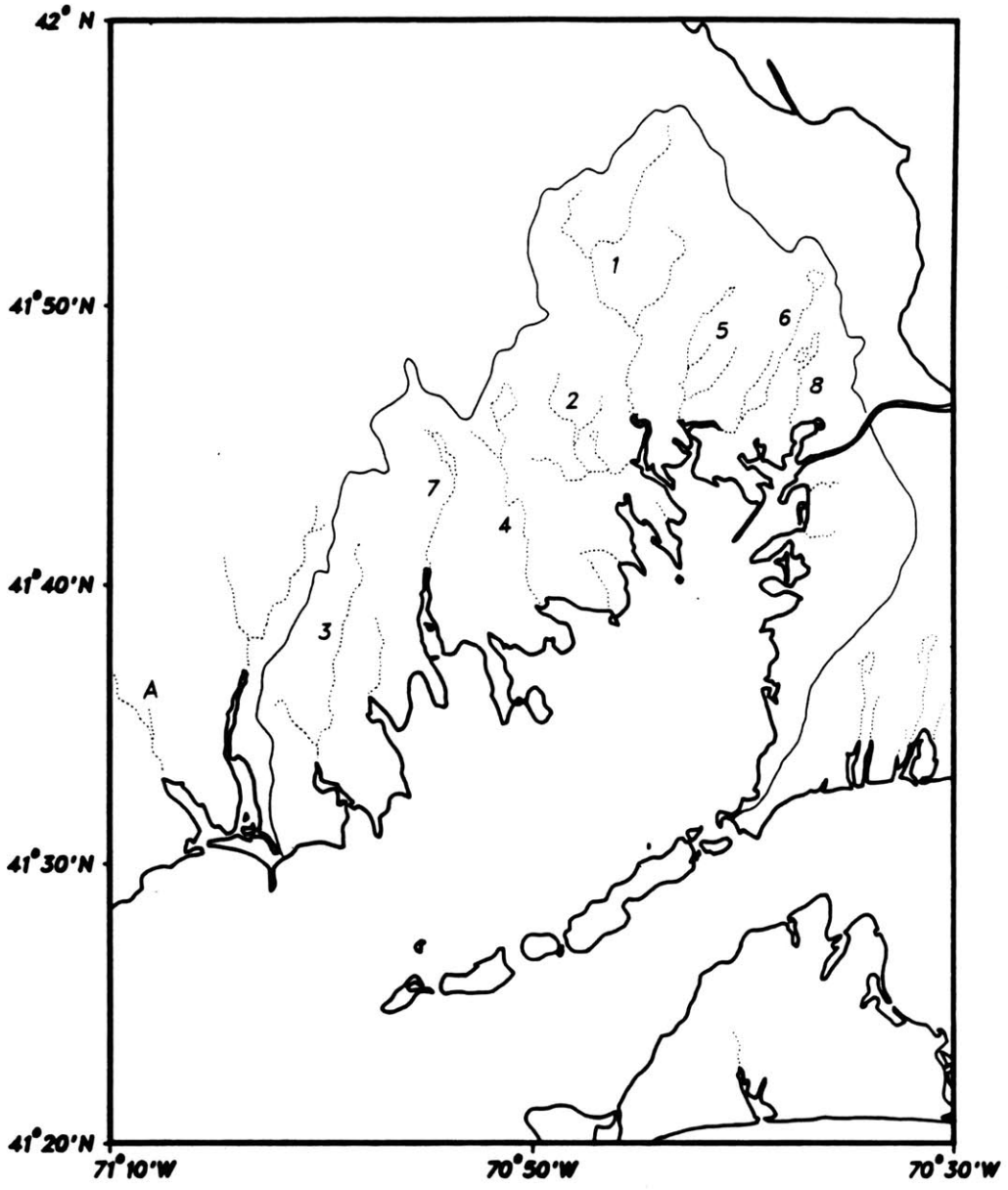


Figure 2.1: Drainage basin and location of major streams emptying into Buzzards Bay. Numbered rivers are listed in table 2.1. The Westport River (A) has the only long term stream gauge in the region.

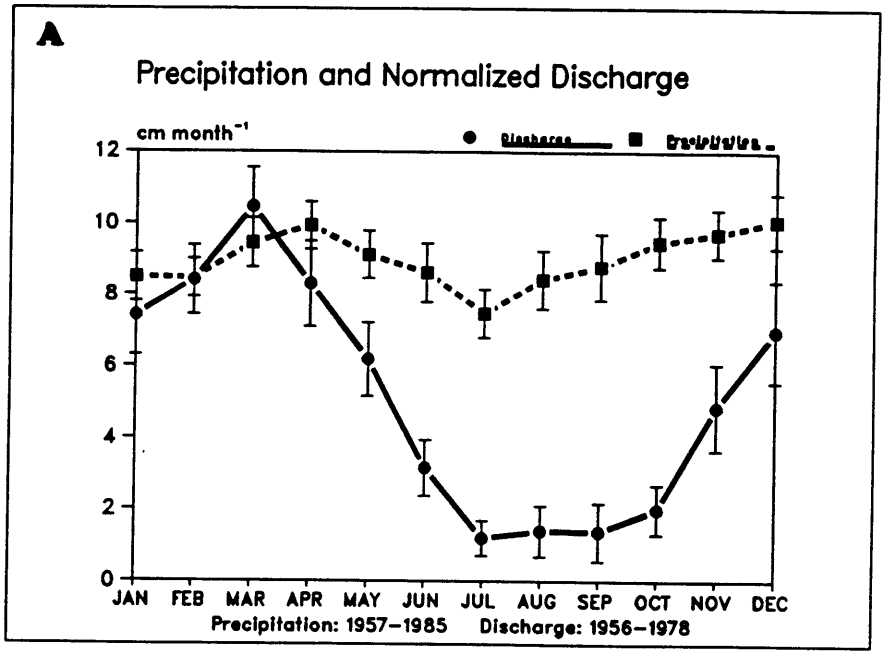


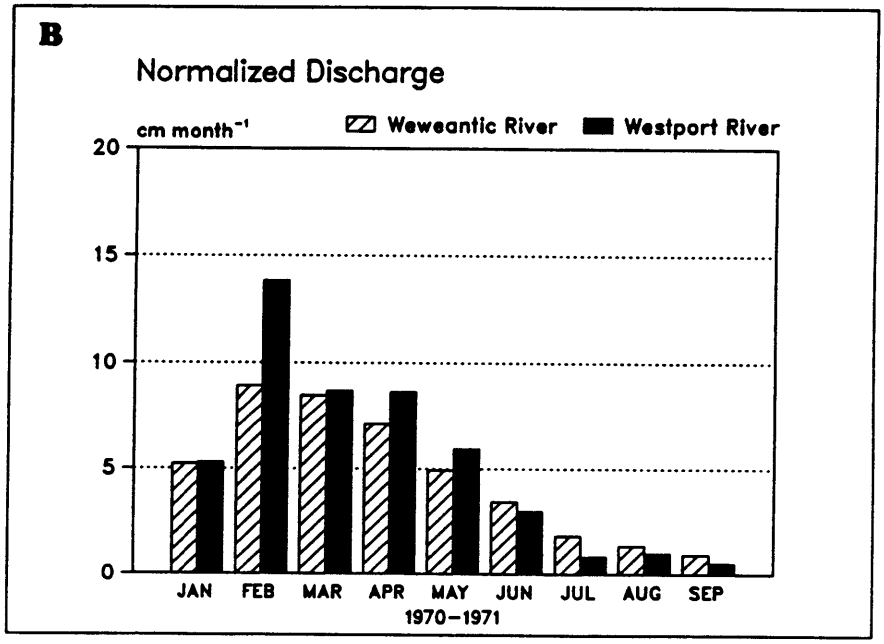


Figure 2.2: (a)Precipitation and mean monthly discharge of the Westport River, normalized by its drainage area. (b)Comparison of normalized discharge from two years of data from the Westport and Weweantic Rivers.

| Rank | River | Drainage Area $km^2$ | Inferred Inflow $m^3$ s | Percent Total % |
|---|---|---|---|---|
| 1. | Weweantic | 145.3 | 2.9 | 18.6 |
| 2. | Sippican | 72.8 | 1.4 | 9.3 |
| 3. | Paskamenet | 67.6 | 1.3 | 8.7 |
| 4. | Mattapoisett | 62.2 | 1.2 | 8.0 |
| 5. | Wankinko | 53.1 | 1.1 | 6.8 |
| 6. | Agawam | 44.1 | .9 | 5.7 |
| 7. | Acushnet | 42.5 | .8 | 5.4 |
| 8. | Red Brook | 23.5 | .5 | 3.3 |
| | Smaller rivers & ground water | 266.9 | 5.3 | 34.2 |
| | TOTAL | 780.0 | 15.4 | 100.0 |

Table 2.1: Inferred annual average freshwater volume flux into Buzzards Bay.

| Bay | Drainage area $km^2$ | Surface area $km^2$ | Depth m | Volume $m^3$ | Inflow $m^3\ s^{-1}$ |
|---|---|---|---|---|---|
| San Francisco Bay | 153,000 | 1240 | 6 | $6.7\times10^9$ | 600 |
| Chesapeake Bay | 166,000 | 11400 | 6 | $7.4\times10^{10}$ | 2100 |
| Delaware Bay | 33,000 | 1870 | 10 | $1.8\times10^{10}$ | 590 |
| Buzzards Bay | 800 | 550 | 11 | $6.1\times10^9$ | 15 |

Table 2.2: Drainage characteristics of several North American bays. Delaware and Chesapeake data from Bumpus (1973), San Francisco data from Conomos *et al.*, (1985).

heat flux calculations of A. Bunker, who applied bulk formulas to ship observations collected over the period 1946–1972. Monthly averages were then computed for 1 degree rectangles along the Atlantic Coast. Quadrant 71–72°W, 41–42°N was selected to represent Buzzards Bay, an area encompassing Rhode Island Sound and Narragansett Bay (Fig. 2.3). The quadrant 72–73°W, 41–42°N included Cape Cod Bay, which has a much colder average sea surface temperature. Variation in P-E (Fig. 2.4a) is chiefly due to seasonal change in evaporation and ranges from a high of 6–8 cm $month^{-1}$ in the spring and early summer, when the winds are light, the air temperature is comparable to the sea surface temperature and the air is moist due to the seabreeze and prevailing southwesterly wind, to a low of $-5$ cm $month^{-1}$ in the fall and early winter due to drier, colder, and stronger winds blowing over relatively warmer water. In Fig. 2.4a it can be seen that the dominant contribution to the total freshwater input is from stream inflow, but is modified by the P-E value. The total inflow, compared to several prominent U.S. estuaries with observed density driven circulations, is relatively modest (Table 2.2). For example, the time scale determined by the volume of the basin divided by the inflow is 4 months for San Fransisco Bay, 12 months for Delaware Bay, 13 months for Chesapeake Bay, and 156 months for Buzzards Bay. Given the same mixing conditions, it would be expected that the effects of freshwater input would be an order of magnitude less important than in these bays.

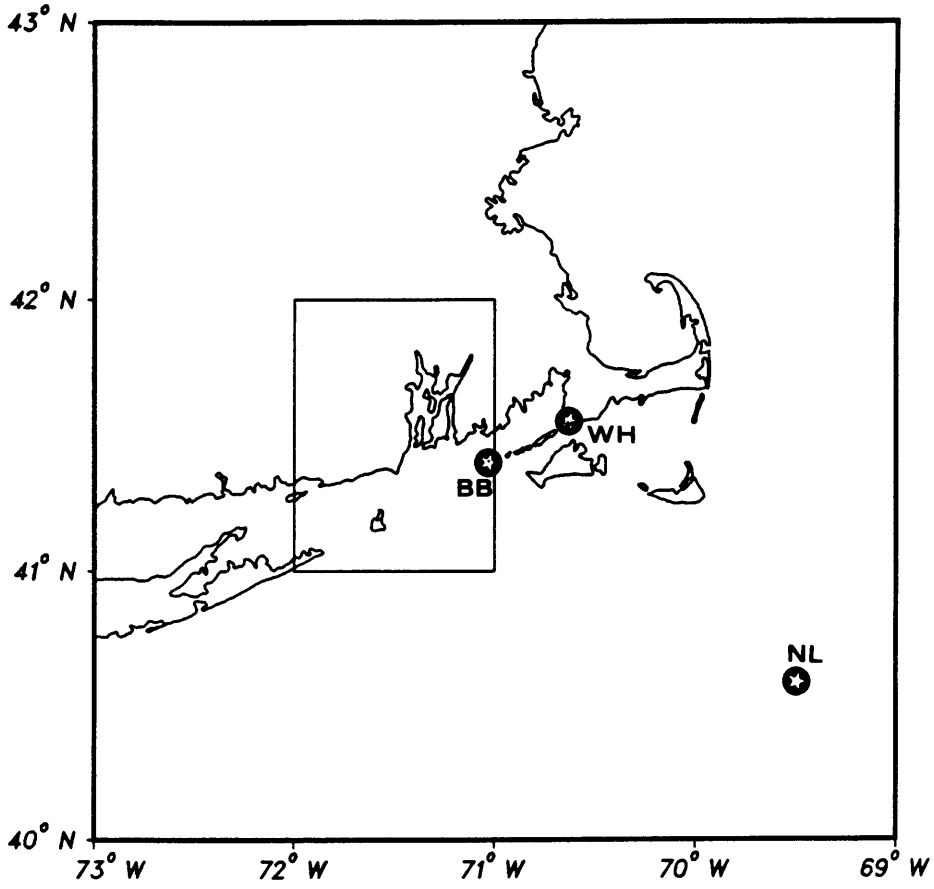


Figure 2.3: Quadrant for heat flux estimates derived from ship observations from A. Bunker. The location of long term surface temperature and salinity stations from Chase (1972) are also shown: Woods Hole (WH), Buzzards Bay Lightship (BB), and Nantucket Shoals Lightship (NL).

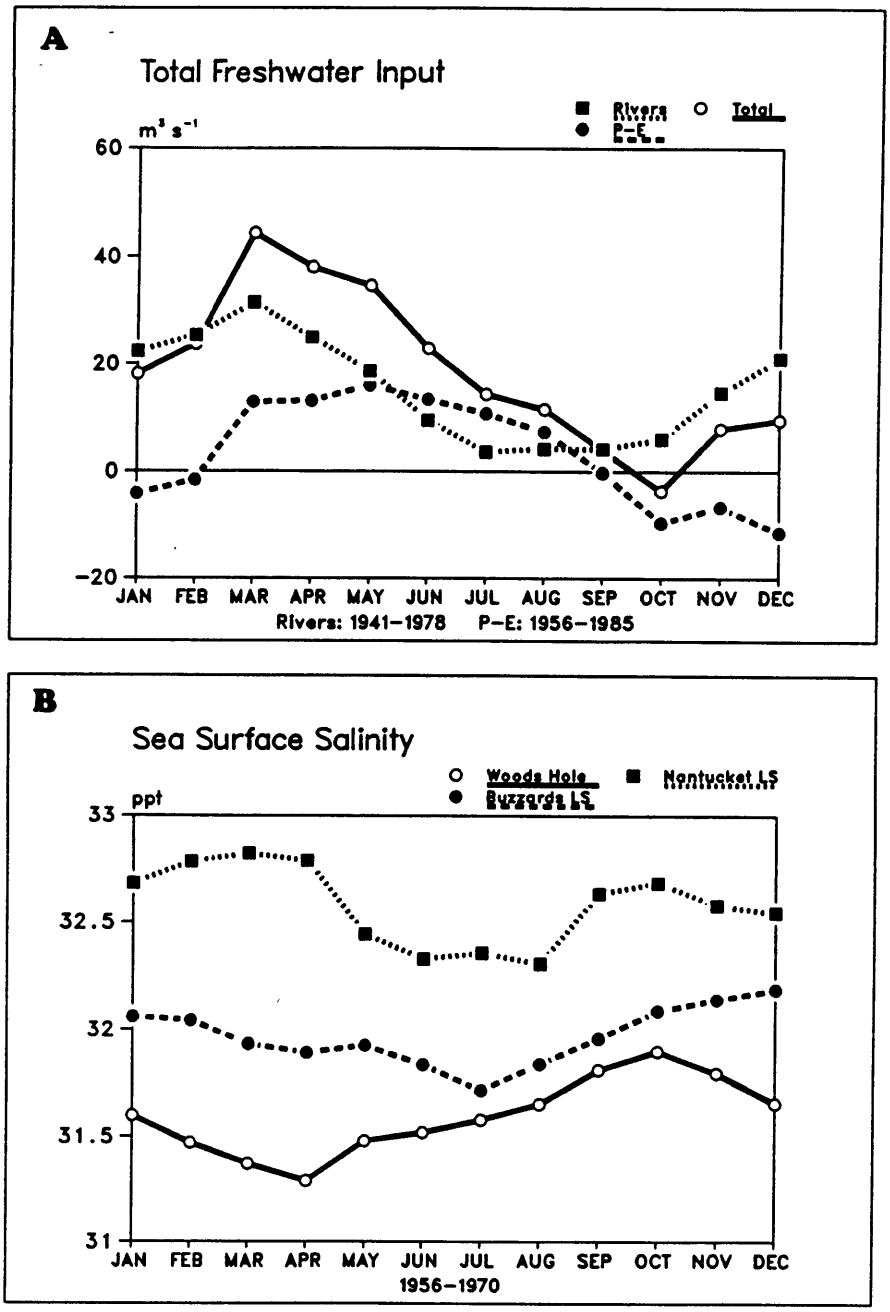


Figure 2.4: (a)Total inferred freshwater input into Buzzards Bay from rivers and precipitation minus evaporation. (b)Sea surface salinity from Woods Hole, Buzzards Bay Lightship, and Nantucket Lightship (see Fig. 2.3 for location map).

To examine the influence of the freshwater input in the region, mean monthly surface salinities from 14 years of daily measurements at Woods Hole, the Buzzards Bay Lighttower, and the Nantucket Shoals Lightship from Chase (1972) were examined. The Buzzards Bay Lightship (now a light tower) is located just off the mouth of the bay while the Nantucket Shoals Lightship lies on the shelf to the southeast(Fig. 2.3). Although Woods Hole is located between Buzzards Bay and Vineyard Sound, it may be more representative of Bay conditions, since Mangelsdorf (1963) observed a mean mass flux from Buzzards Bay into Vineyard Sound through Woods Hole.

Fig. 2.4b shows the monthly values averaged over 14 years. Salinity has a small annual range (less than 1 ppt), and gradually increases offshore. In Woods Hole, the salinity minimum (31.3 ppt) occurs in April and lags the freshwater input maximum by one month. The salinity maximum (31.9 ppt) occurs in October, simultaneously with the minimum in freshwater input. At Nantucket Lightship, the salinity minimum does not occur until mid-June to late August, perhaps reflecting the advection of freshwater from the Gulf of Maine (Beardsley and Boicourt, 1981). The Buzzards Bay Lightship has salinity values between that of Woods Hole and Nantucket and shows that the salinity difference between Woods Hole and the mouth of the bay is greatest when the freshwater input is the greatest. The maximum difference, however, is only about 0.5 ppt.

## 2.3 Factors affecting the temperature field

During the summer, the temperature field primarily determines density variations in Buzzards Bay, the high surface heat flux stratifying the bay and the differential heat capacity of shallower and deeper waters giving rise to horizontal gradients. The surface heat flux data from A. Bunker is presented in Fig. 2.5. Heat flux becomes positive in March, and reaches a maximum in June, the summer solstice accompanying light winds (Fig. 2.5a). Heat flux out of the bay begins in October as the winds and drier air increase latent heat flux and the days shorten, decreasing radiative heat flux. Radiative heat flux is responsible for most of the heating in the summer, while latent and senesible heat loss dominate cooling in the winter. The mean heat flux over the year is negligible, only 8.1 W $m^{-2}$ into the bay. The

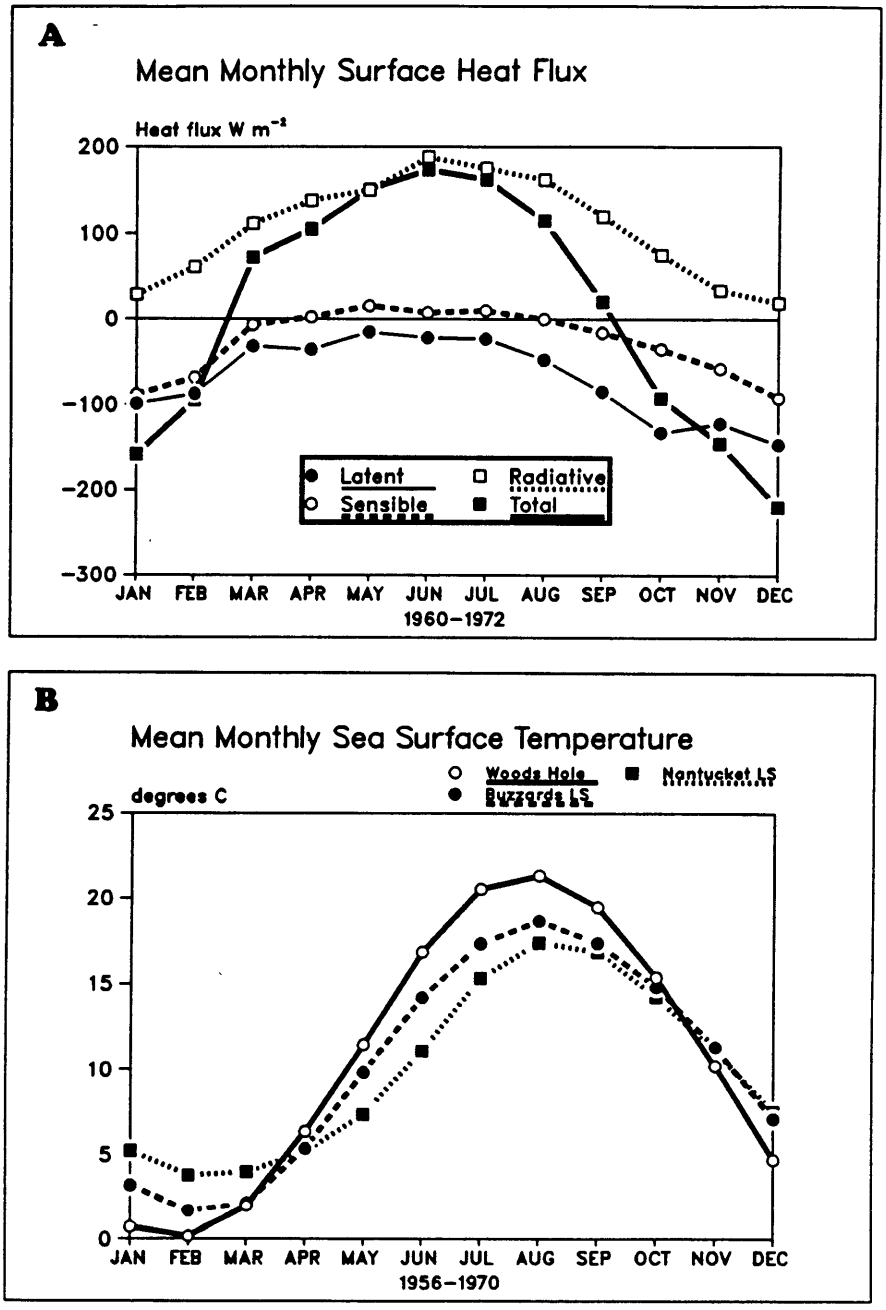


Figure 2.5: (a) Mean monthly surface latent, sensible, radiative and total heat flux from A. Bunker for the quadrant shown in Fig. 2.3. (b) Mean monthly sea surface temperature from Woods Hole, Buzzards Bay Lightship, and Nantucket Shoals Lightship (from Chase (1972).

effect on the monthly mean surface temperature measurements reported by Chase (1972) is illustrated in Fig. 2.5b. When the heat flux becomes positive in March, all stations respond with no resolvable lag, although Woods Hole temperatures increase more rapidly than either Buzzards Bay Lightship or Nantucket. This reflects the decreased heat capacity of shallower waters in both Buzzards Bay and Vineyard Sound, assuming there are mixing processes that can carry the heat from the surface to the rest of the water column. This mechanism also results in an increased annual temperature range for shallower waters. Considering vertical temperature structure, stratification under warming conditions will be dependent on the strength of turbulent mixing from the surface due to wind stress and from the bottom due to tidally produced turbulence. Since radiative heating has a strong diurnal signal it should be expected that the thermal stratification in summer may vary significantly with timescales around one day. Under cooling conditions, the column will readily mix once the salinity stratification is overcome, and stratification should disappear.

## 2.4 Hydrographic surveys

Although the climatalogical fluxes of heat and salt in Buzzards Bay are reasonably well understood, the density distribution depends on the processes of vertical and horizontal mixing, which are less well understood. Hydrographic surveys provide insight into these mechanisms, although it must be realized that these 1–3 day surveys are essentially snapshots of highly time dependent processes. Advection and mixing by tidal currents, diurnal heating, mixing by wind events all significantly effect the observed structures.

The first large scale survey which included Buzzards Bay was reported by F.B Sumner in 1913 (Sumner, et al, 1913), a naturalist surveying the biological conditions of the waters of Woods Hole. Two cruises were conducted in August and November of 1907 and two in March and June of 1908, with an areal extent covering most of Buzzards Bay and Vineyard Sound (Fig. 2.6a). The temperature of top and bottom water samples was recorded and the salinity was inferred from a specific gravity device judged accurate to .1 part per thousand. The resulting data is sparce and noisy from the standpoint of determining vertical structure (many show density

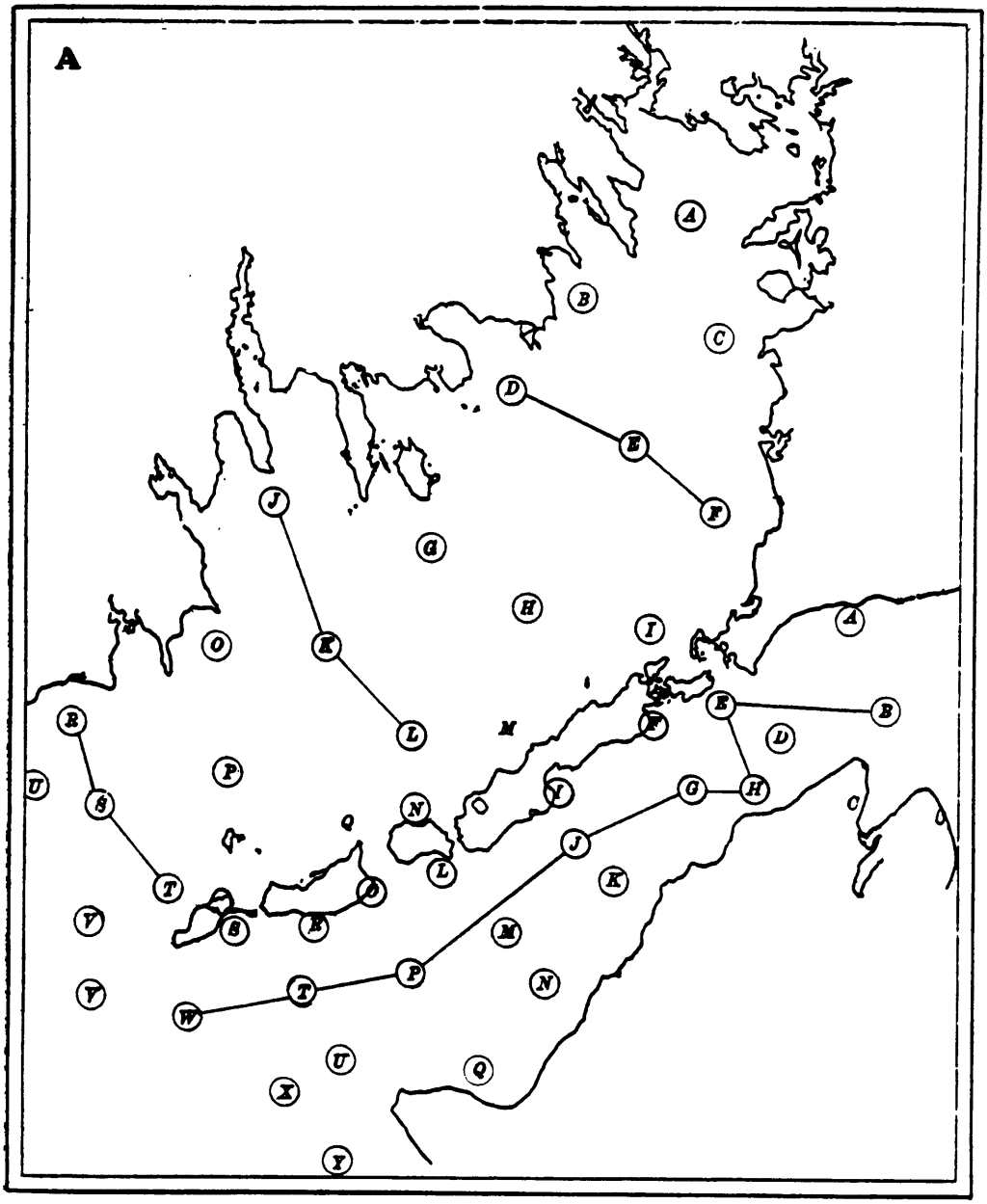


Figure 2.6: (a)Station map for the hydrographic cruises of Sumner (1913). Connected stations indicate selected transects. (b)T-S diagram for stations from cruises in August and November, 1907 and, March and June, 1908. There is a clear seperation between Buzzards Bay (BB) and Vineyard Sound (VS) stations.

B

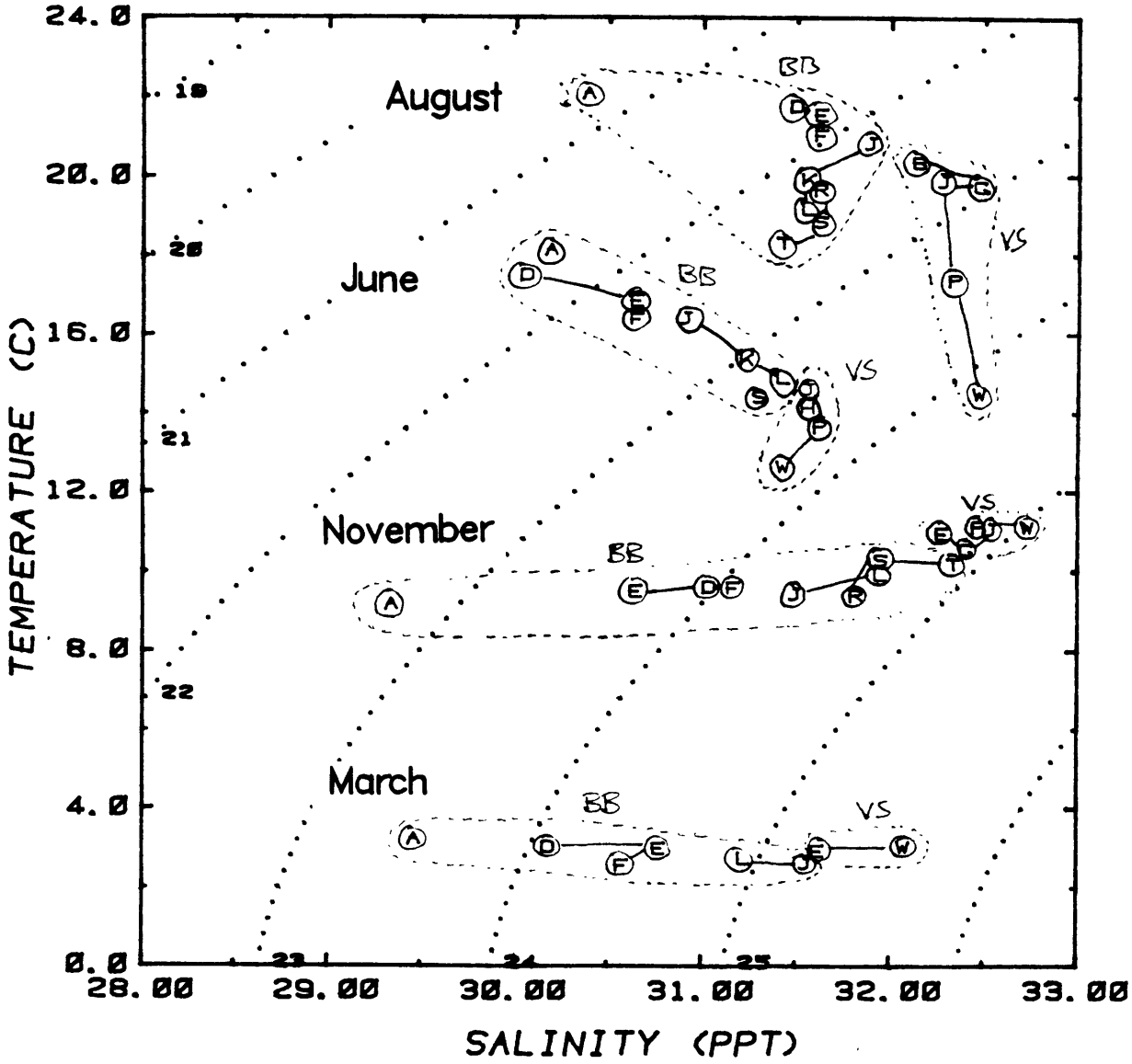
August
June
November
March
BB
VS
TEMPERATURE (C)
SALINITY (PPT)
24.0
20.0
16.0
12.0
8.0
4.0
0.0
28.00
29.00
30.00
31.00
32.00
33.00

inversions), but clearly resolves many features of the horizontal temperature and salinity fields.

Fig. 2.6b shows the temperature-salinity (T-S) plot of selected stations from the four cruises, with the top and bottom samples averaged to reduce noise. As expected, Buzzards Bay and Vineyard Sound have salinity minima furthest from the open ocean and values gradually increase seaward. Vineyard Sound is more saline than Buzzards Bay thoughout the year, due to increased exchange with Rhode Island Sound from strong tidal mixing and minimal freshwater input, but is colder in the summer and warmer in the winter due to its greater heat capacity (average depth 18 m). The salinity field dominates the horizontal density structure in November and March when conditions are nearly isothermal, but in June and August the temperature field makes a comparable contribution.

The second significant hydrographic study was conducted by Anruku (1964) who, from June 1959 to May 1961, conducted seventeen surveys along an axial line extending from the middle of Buzzards Bay through the Cape Cod Canal into Cape Cod Bay (Fig. 2.7a). These studies serve to define the seasonal conditions in Cape Cod Bay, as well as providing the first description of vertical stratification in the upper half of Buzzards Bay. A bathythermograph was used to obtain continuous profiles of temperature, and surface and bottom salinities were recorded.

Three representative vertical sections show that Buzzards Bay (average depth 10 m), being slightly shallower than Cape Cod Bay (average depth 15 m), becomes slightly colder in winter and warmer in the summer (Fig. 2.7b). Cape Cod Bay is cooled considerably by cold Scotian Shelf water and as a result is much cooler in summer than Buzzards Bay. Salinities in Buzzards Bay are lower than Cape Cod Bay in all cruises and have a minima at the head of Buzzards Bay where the chief river input occurs.

Anraku's surveys indicate that both bays become temperature and salinity stratified in summer and well mixed in winter. Analysis of seventeen surveys indicate well mixed conditions by the end of October, salt stratification in the head of Buzzards Bay by late February and temperature stratification by mid-April. Salinities are lowest in Buzzards Bay in April, and remain lower through the spring, indicating again the influence of spring runoff. Conditions in the canal are well mixed at all times due to the strong tidal flows (200 cm $s^{-1}$) present.

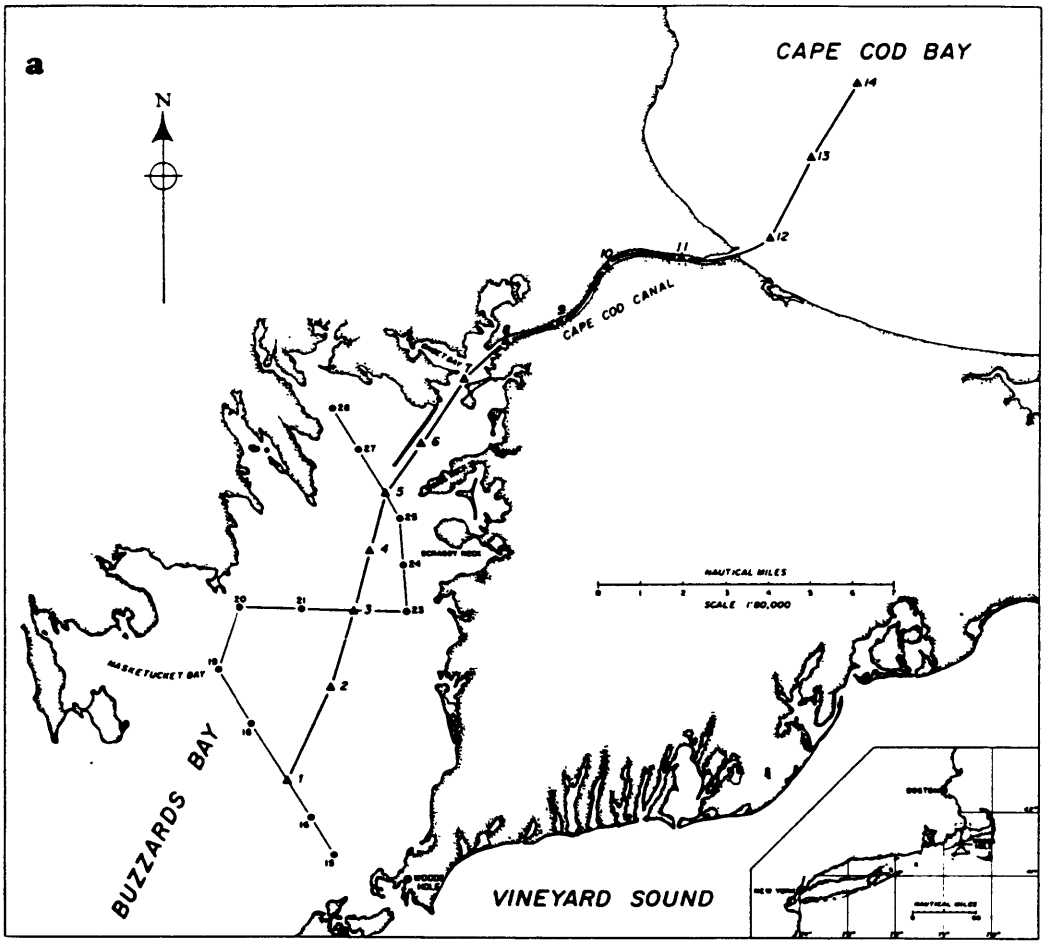


Figure 2.7: (a)Station map of Anraku (1964). Vertical Sections from three representative cruises: (b) August 12, 1959; (c) December 1, 1959; and (d) April 11, 1960.

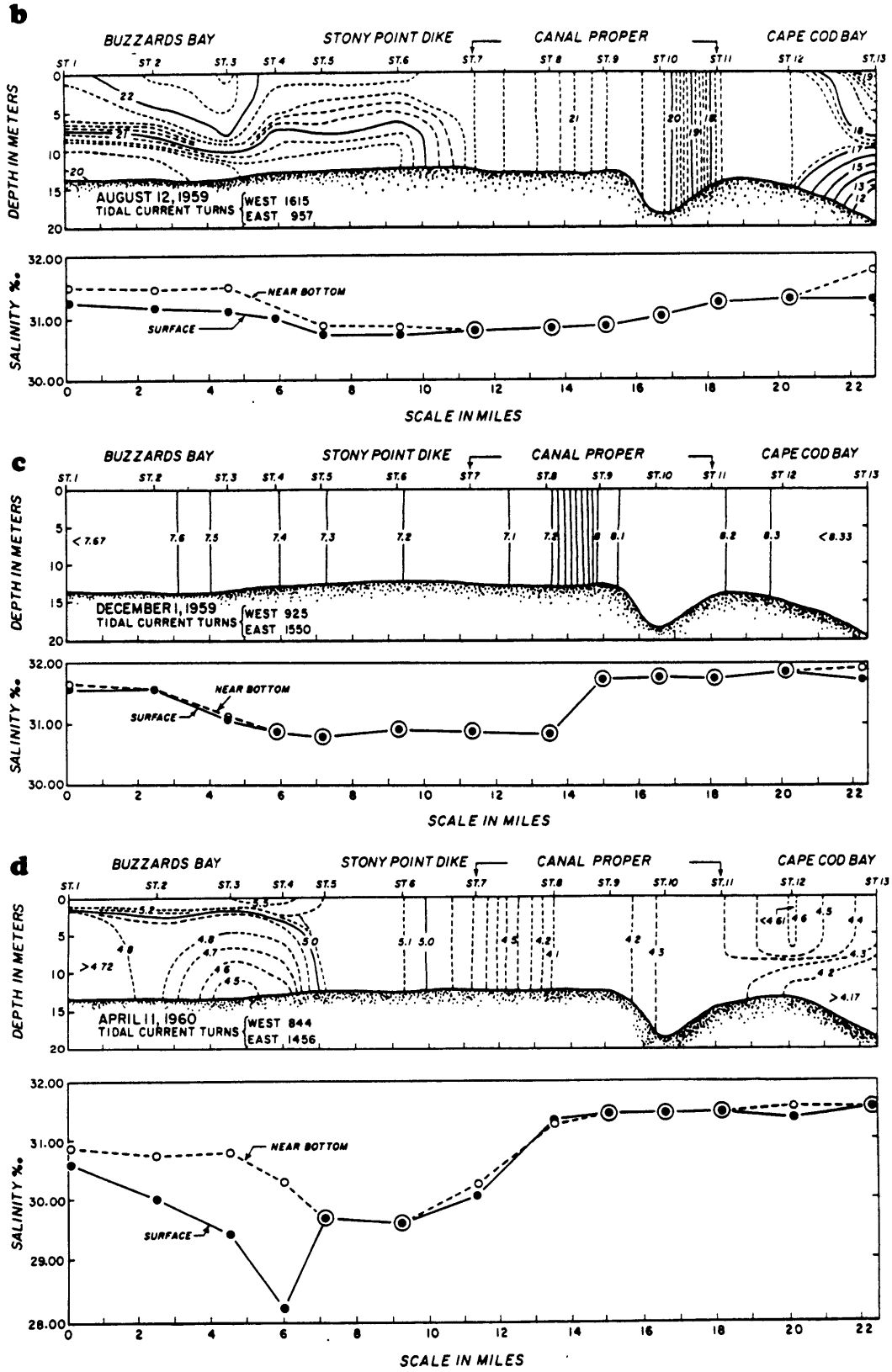
b
BUZZARDS BAY
STONY POINT DIKE
CANAL PROPER
CAPE COD BAY
ST.1 ST.2 ST.3 ST.4 ST.5 ST.6 ST.7 ST.8 ST.9 ST.10 ST.11 ST.12 ST.13
DEPTH IN METERS
AUGUST 12, 1959
TIDAL CURRENT TURNS {WEST 1615
EAST 957
SALINITY ‰
NEAR BOTTOM
SURFACE
SCALE IN MILES
c
DECEMBER 1, 1959
TIDAL CURRENT TURNS {WEST 925
EAST 1550
d
APRIL 11, 1960
TIDAL CURRENT TURNS {WEST 844
EAST 1456

To investigate the hydrographic structure in Buzzards Bay in more detail, four modern hydrographic cruises were carried out in 1982–83 obtaining the first continuous profiles of temperature and salinity (Rosenfeld, Signell and Gawarkiewicz, 1984). Shown in Fig. 2.8 are vertical sections of density along the axis of the bay. On June 29, the upper bay is well mixed while the lower bay shows vertical stratification of order 0.5 $\sigma_t$ unit top to bottom density difference. This stratification is due almost entirely to temperature, and reoccupation of the upper bay stations three tidal cycles later showed similar stratification, indicating that significant variation in vertical stratification occurs at periods on the order of a tidal cycle (12 hours). The October and January sections are vertically well mixed over most of the bay. In April, record monthly rainfall was recorded and the May 5 section shows strong vertical stratification in the upper bay due to salinity, with top to bottom density differences of 1.6 $\sigma_t$ units. The lower bay is also stratified due to the combined effects of salinity and temperature with top to bottom differences of 0.5 $\sigma_t$ units.

The horizontal density structure is stronger on July 29 and May 5, with large scale gradients of 2 $\sigma_t$ units in 50 km, while on October 28 and January 13, the large scale gradient is less than 1 $\sigma_t$ unit. Within 5 km of the river discharge at the head of the bay, the gradients are stronger is all four cruises, with a maximum of 1 $\sigma_t$ unit in 5 km on May 5.

The magnitude of the large scale low-frequency circulation driven by these density gradients may be estimated by a simple 1-D channel model closed on one end. With a constant buoyancy source at the head of the channel and constant mixing parameters, a steady salt field and circulation pattern will develop. The salt balance depends strongly on diffusion as well as advection, but the current field is chiefly dependent on the surface slope, horizontal density gradient and the vertical stress divergence. Since the frictional time scale in the bay is only 2–3 hours, adjustments take place quickly (less than the time scale of density variation). Assuming there are processes that maintain a steady salt field, the current can be calculated from the static pressure gradient. The momemtum equation is

$$0 = -g\frac{\partial \eta}{\partial x} - \frac{\partial}{\partial x}\left(\frac{g}{\rho_0}\int_z^h \rho'(\mathrm{x,z})dz\right) + \frac{1}{\rho_0}\frac{\partial \tau^x}{\partial z},$$

where $z$ is distance from the bottom, $x$ is distance along-channel, $h$ is the depth of the water column, $g$ is gravitational acceleration, $\eta$ is the free

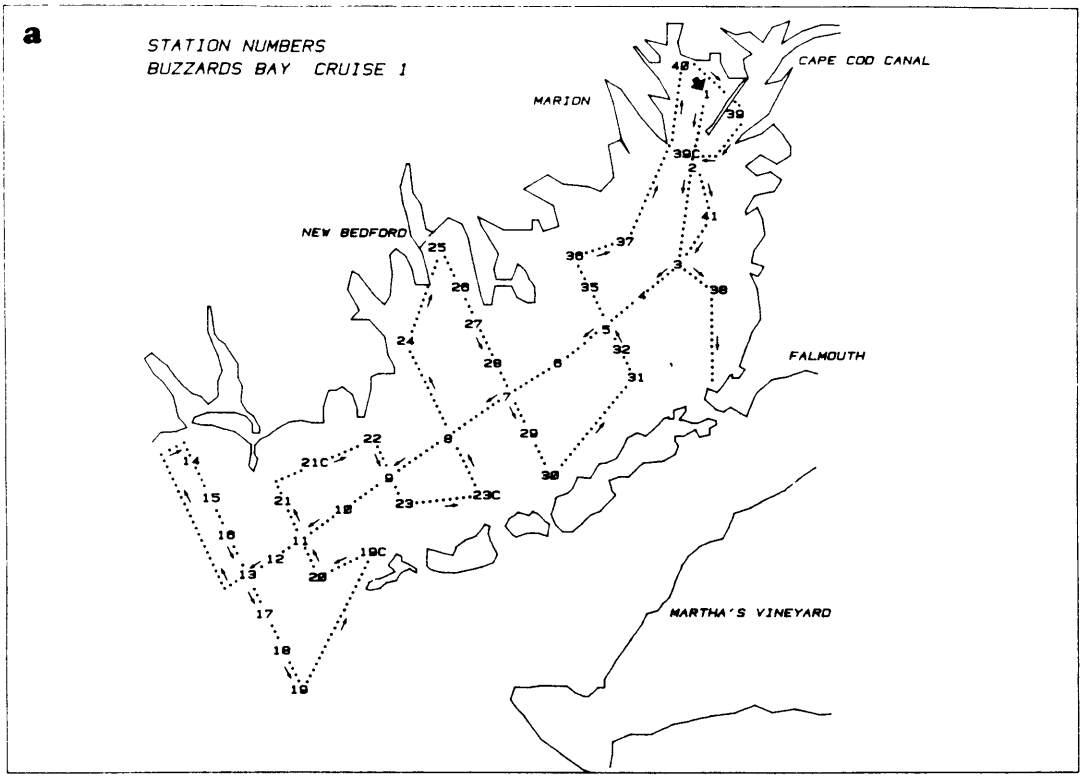


Figure 2.8: (a) Station map from Rosenfeld *et al.* (1984) and along-axis vertical density sections: (b) July 19, 1982; (c) October 29, 1982; (d) January 13, 1983; and (e) May 5, 1983.

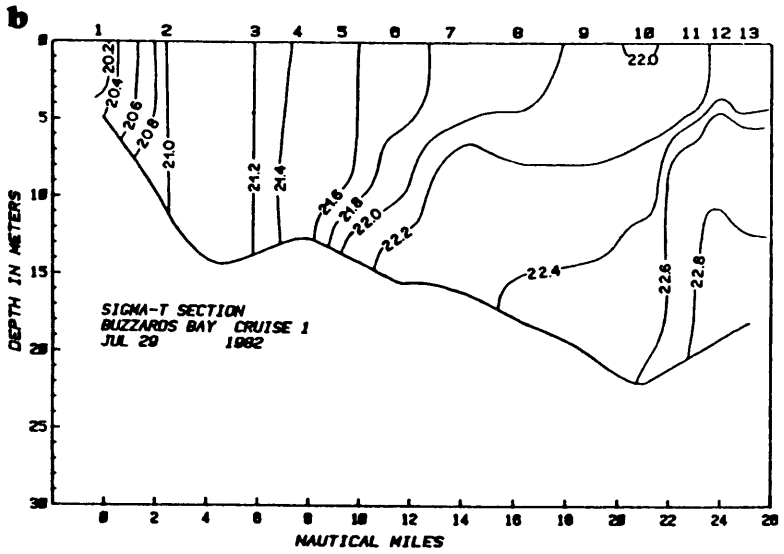
b
DEPTH IN METERS
NAUTICAL MILES
SIGMA-T SECTION
BUZZARDS BAY CRUISE 1
JUL 29 1982
20.2
20.4
20.6
20.8
21.0
21.2
21.4
21.6
21.8
22.0
22.2
22.4
22.6
22.8

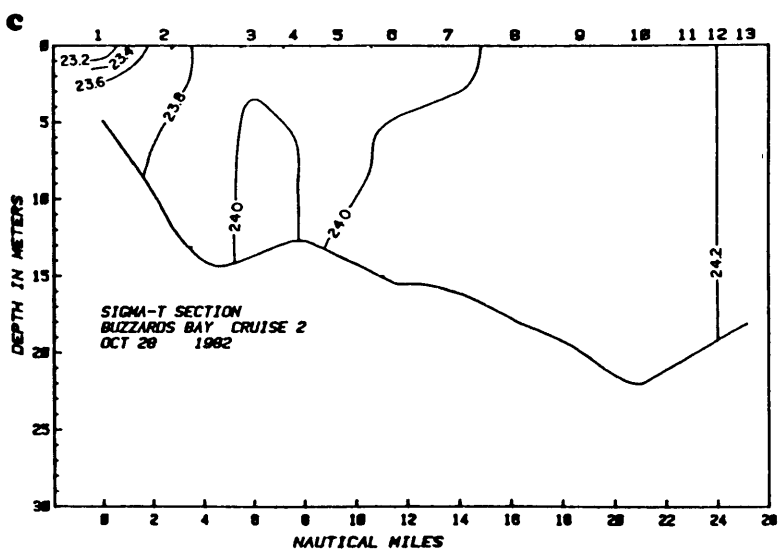
c
DEPTH IN METERS
NAUTICAL MILES
SIGMA-T SECTION
BUZZARDS BAY CRUISE 2
OCT 28 1982
23.2
23.4
23.6
23.8
24.0
24.2

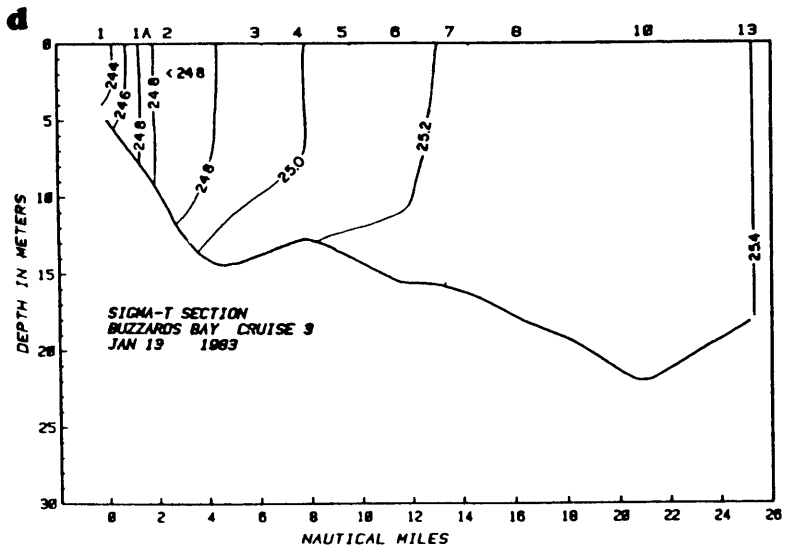
d
DEPTH IN METERS
NAUTICAL MILES
SIGMA-T SECTION
BUZZARDS BAY CRUISE 3
JAN 19 1983
24.4
24.6
24.8
<24.8
25.0
25.2
25.4

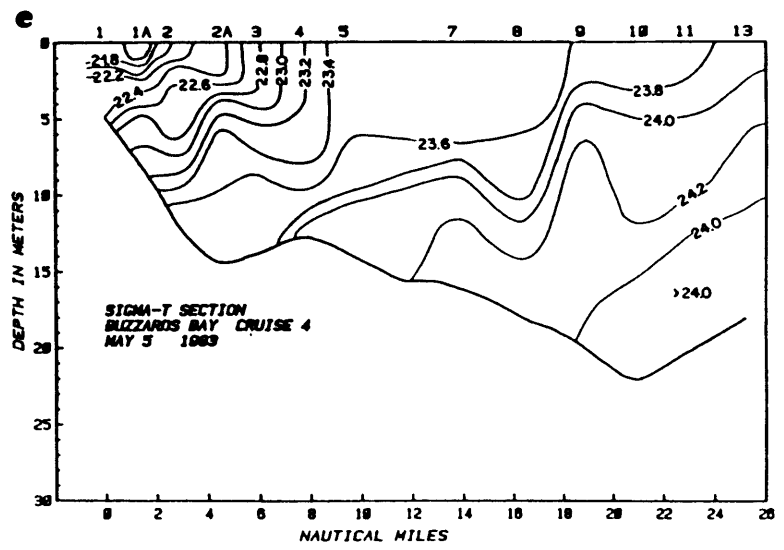
e
DEPTH IN METERS
NAUTICAL MILES
SIGMA-T SECTION
BUZZARDS BAY CRUISE 4
MAY 5 1983
21.8
22.2
22.4
22.6
22.8
23.0
23.2
23.4
23.6
23.8
24.0
24.2
>24.0

surface displacement, $\tau^x$ is the stress in the $x$ direction, and the density field has been decomposed into a constant part and a fluctuating part, $\rho(\mathrm{x,z}) = \rho_0 + \rho'(\mathrm{x,z})$.

The channel is bounded at the head, so that the vertically averaged transport must be zero. For the simplest parameterization of the bottom boundary layer, a no-slip bottom boundary is chosen. At the water surface, a zero stress condition is appropriate, so

$$\frac{\partial u}{\partial z} = 0 \text{ at } z = h,$$

$$u = 0 \text{ at } z = 0.,$$

Interior stresses are represented by a eddy viscosity formulation,

$$\tau^x = A_v \frac{\partial u}{\partial z},$$

and it is assumed that vertical stratification does not effect the eddy visocity so that a constant $A_v$ will give the right magnitude, if not the detail of the density driven flow.

For a horizontal density gradient constant with depth, the problem is simplified, and integration of the momentum equation with application of the boundary conditions yields

$$g\frac{\partial \eta}{\partial x}\left(hz - \frac{z^2}{2}\right) + \frac{\partial \rho}{\partial x}\frac{g}{\rho_0}\left(\frac{h^2 z}{2} - \frac{hz^2}{2} + \frac{z^3}{6}\right) + A_v u(z) = 0.$$

Applying the zero transport condition yields the relation between the barotropic and baroclinic pressure gradients,

$$g\frac{\partial \eta}{\partial x} = -\frac{3g}{8\rho_0}\frac{\partial \rho}{\partial x},$$

so that the velocity profile is given by

$$u = -\frac{g}{A_v \rho_0}\frac{\partial \rho}{\partial x}\left(-\frac{5}{16}hz^2 + \frac{1}{8}h^2 z + \frac{1}{6}z^3\right),$$

which has maxima at $z = h/4$ and $z = h$. For a reasonable value of $A_v = 40$ $\mathrm{cm^2\ s^{-1}}$ (chosen from the average value of a parabolic eddy viscosity profile

that would approximate surface and bottom log layers), a gradient of 2 $\sigma_t$ in 50 km (in 15 m of water) gives .70 cm $s^{-1}$ at the surface, 1 $\sigma_t$ in 50 km gives .35 cm $s^{-1}$, and 1 $\sigma_t$ in 5 km (in 10 m of water) gives 1.0 cm $s^{-1}$. Therefore, the model suggests that the large scale circulation driven by density gradients is of order 1 cm $s^{-1}$. The large scale thermohaline driven currents in spring and summer should be twice as strong as in fall and winter, and should be locally higher near the freshwater input at the head of the bay due to the enhanced density gradient there.

## 2.5 Summary

The salinity, temperature and density structure of Buzzards Bay have been described in order to assess the magnitude of density driven currents and degree of vertical stratification. The drainage area of the bay (780 $km^2$) is only slightly larger than the area of the bay itself (550 $km^2$), and the mean freshwater input (15 $m^3$ $s^{-1}$) is relatively small. When scaled by the bay volume, it is an order of magnitude less than the relative input into Delaware, San Fransisco and Chesapeake Bays, which have clearly observed density driven ciruculations. Salinities generally range from 30–32 ppt with an annual variation of less than 1 ppt. Water temperature in the bay follows the surface heat flux, which becomes positive in March and negative in October. Minimum temperatures around 0°C are found in February and the maximum temperatures around 20°C are found in August. Horizontal temperature gradients are small except in summer, when 4–5°C difference between head and mouth are found due to the relatively smaller heat capacity of the shallower water.

Hydrographic surveys have shown that Vineyard Sound is always more saline and more dense than Buzzards Bay. In Buzzards Bay, salinity increases with distance from the chief source of freshwater input at the head of the bay. Differential heat capacity causes the shallow regions of the bay to become warmer in summer and colder in winter so that horizontal temperature gradients reverse with season.

Vertical stratification can develop during the spring and summer which may significantly alter the structure of forced wind and tidal response. The bay is well mixed October though February when the heat flux is negative and the water column is unstable. In March the heat flux becomes positive,

and combined with increased freshwater input, stratification may develop. In summer, the freshwater input has decreased, and vertical stratification is due primarily to surface heat flux. In September, the surface begins to cool, overturning takes place, and by late October most of the region is well mixed in the vertical. In the August 1982 and May 1983 surveys, mid-bay stations (in water depths of 10–15 m) typically showed top-to-bottom density differences of 0.5 $\sigma_t$ units while in top-to-bottom vertical differences in October 1982 and January 1983 were less than 0.05 $\sigma_t$ units. In addition, the August cruise showed that vertical stratification can vary significantly over several tidal cycles, and longer term measurements of are necessary to properly describe the variation of the spring and summer vertical density structure.

Hydrographic surveys show that horizontal density differences are generally of the order 2 $\sigma_t$ units over the length of the bay in spring and summer but only 1 $\sigma_t$ unit in fall and winter. On the basis of a simple, static, frictional model in which the along-bay pressure gradient balances vertical stress divergence, such gradients give rise to a large scale estuarine circulation of order 1 cm $s^{-1}$.

# Chapter 3

# Tidal forcing

## 3.1 Introduction

Tidal currents usually dominate instantaneous observations of current over most of Buzzards Bay, and due to the nonlinear nature of tidal flow in the bay, both generate and affect the dissipation of lower frequency flows. The purpose of this chapter is, therefore, to describe both the principal and the low-frequency currents associated with the tide in Buzzards Bay.

Tides along the U.S. East Coast are dominated by the lunar semi-diurnal component $M_2$ (12.42 hrs) due to response characteristics of the North Atlantic (Platzman, 1975) and the near resonance in the Gulf of Maine (Garrett, 1972). The local effect of the tide generating force over the shelf is small, so that tides in this region can be modeled as the response to boundary forcing at the shelf break by the open ocean tides. The $M_2$ tide arrives nearly simultaneously along the shelf, but the contrast in shelf characteristics together with the resonant nature of the Gulf of Maine causes distinctly different tidal regimes in the Western Gulf of Maine, Georges Bank, and the shelf south of Cape Cod. Brown (1984) describes the tide over Georges Bank as a progressive gravity wave influenced by rotation, while in the western Gulf of Maine, a standing rotary Kelvin wave is a better description. South of Cape Cod the shelf response is like a standing wave. Fig. 3.1 shows the difference of response in more detail. These regional tidal characteristics in turn have a direct effect on the tides in Buzzards Bay.

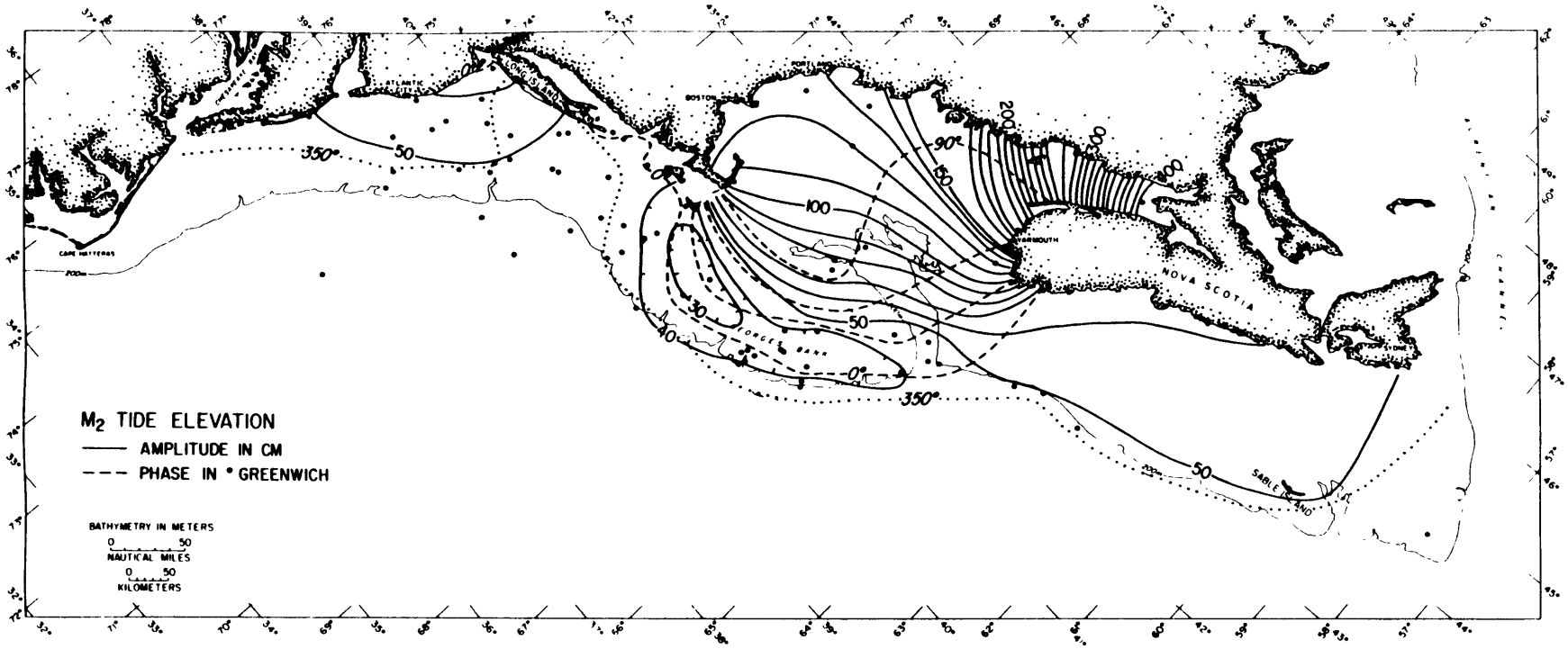


Figure 3.1: Co-amplitude and co-phase lines for $M_2$ elevation on the New England Shelf. From Moody *et al.* (1984)

## 3.2 Elevation response

Tidal phenomena in Buzzards Bay and Vineyard Sound were first investigated by A. Redfield (1953). He modeled the tidal elevation at a given point as the interference of two damped progressive waves travelling in opposite directions. Buzzards Bay is essentially a semi-enclosed basin, and the two waves correspond to an incident wave from the southern New England shelf and its reflection from the head of the bay. Both are of nearly equal magnitude, resulting in a standing wave-like response. From a physical point of view, the natural period of the bay (2 hours) is substantially less than the dominant tidal period (12.4 hours), so that the bay is in near equilibrium with the shelf tide. In contrast, Redfield argued that Vineyard Sound behaves as a straight, and the interference of the Gulf of Maine tidal wave from the east with the southern New England shelf wave from the southwest causes rapidly changing phase and tidal range. As a consequence, high water in Vineyard Sound is of decreased amplitude, and occurs 2–4 hours after Buzzards Bay (Fig. 3.2).

Results of least squares harmonic analysis (Foreman, 1978) from all tide gauge and pressure stations longer than two weeks is presented in table 3.1. Error estimates were computed according to Filloux and Snyder (1979). The principal variation in amplitude of the tidal elevation in Buzzards Bay is due to the 14.8 day spring-neap cycle evidenced by $S_2/M_2$ beating and the 27.6 day perigee-apogee cycle evidenced by $N_2/M_2$ beating. The amplitude of $S_2$ and $N_2$ are of similar magnitude and about 20% of $M_2$. Thus spring tides and perigean tides are 20% stronger while neap and apogean tides are 20% weaker. About every 7 months, perigean-spring tides result in tidal elevation and currents up to 40% above normal. This increases the likelihood of coastal flooding if accompanied by high winds, and Wood (1976) discusses this phenomenon in great detail, as well as listing all spring-perigean tidal events through 1999.

## 3.3 Tidal currents

Tidal currents in the bay and in Vineyard Sound, as anticipated from the tidal elevation response, are in marked contrast. In the bay, average speeds range from less than 10 cm $s^{-1}$ near the head of the bay, to 50 cm $s^{-1}$

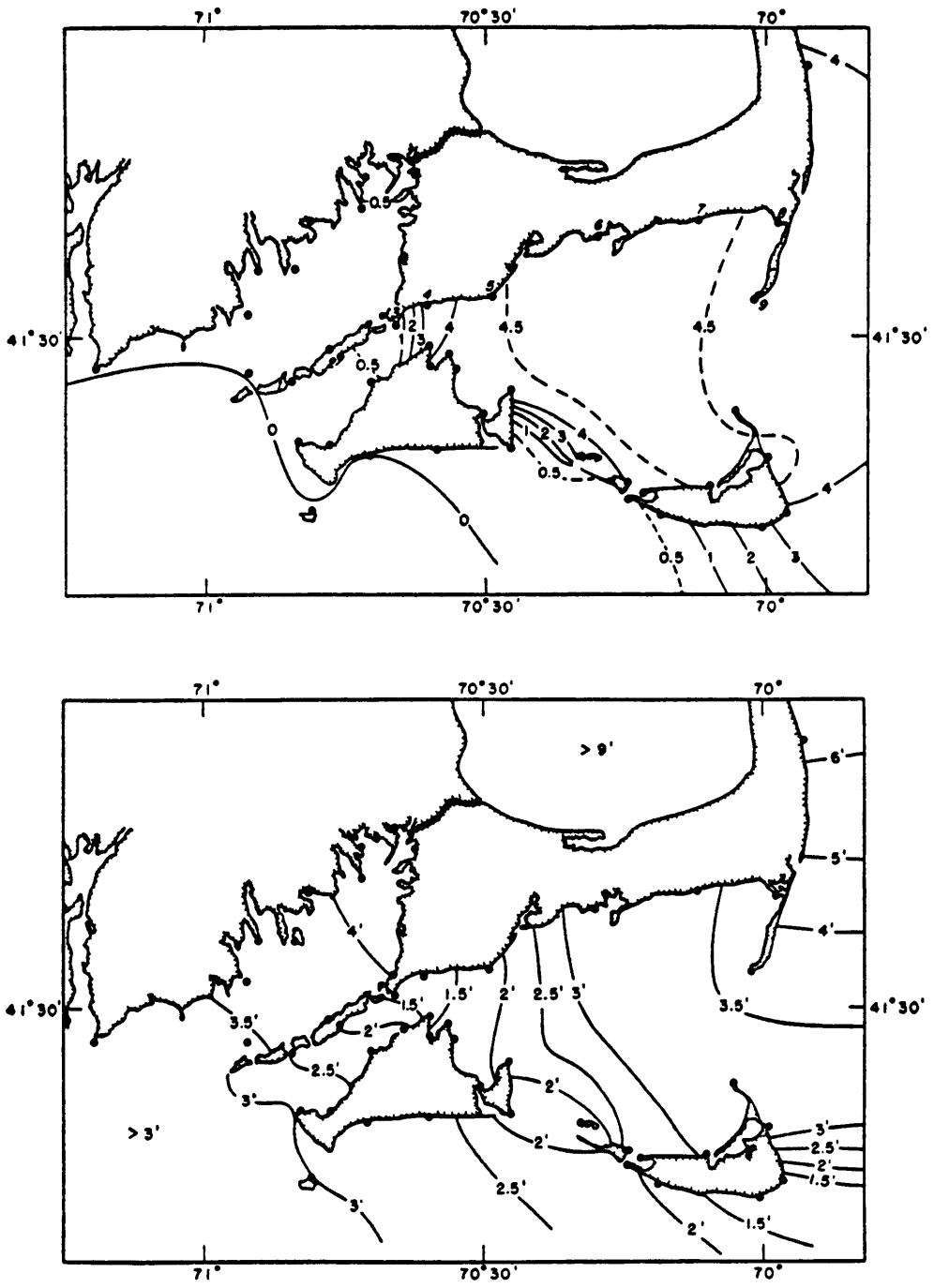


Figure 3.2: (a)Co-phase lines for tidal elevation expressed in lunar hours (12 lunar hours=12.42 hours). (b)Co-range lines for tidal range in feet. From Redfield (1953).

| STN | START | STOP | N2 AMP CM | N2 PHASE DEG G | M2 AMP CM | M2 PHASE DEG G | S2 AMP CM | S2 PHASE DEG G |
|---|---|---|---|---|---|---|---|---|
| 1 | 841108 | 841217 | 13.5 0.8 | 342.5 3.4 | 55.4 0.8 | 8.6 0.8 | 14.6 0.8 | 30.7 3.6 |
| | 850219 | 850329 | 15.2 0.8 | 353.8 3.2 | 53.7 0.8 | 5.2 1.0 | 13.6 0.8 | 27.3 2.8 |
| | 850409 | 850618 | 14.5 1.2 | 346.3 4.6 | 53.1 1.2 | 5.3 1.2 | 11.7 1.2 | 33.9 5.2 |
| | 850626 | 850807 | 12.1 0.8 | 349.2 3.8 | 56.0 0.8 | 6.7 0.8 | 11.7 0.8 | 30.8 5.0 |
| 2 | 840809 | 850119 | 13.3 1.2 | 349.4 5.6 | 51.3 1.2 | 7.6 1.4 | 11.5 1.2 | 22.8 6.4 |
| 5 | 841109 | 841212 | 12.1 0.6 | 337.2 3.2 | 50.6 0.6 | 3.6 0.8 | 13.1 0.6 | 25.2 3.2 |
| 7 | 840906 | 841022 | 15.4 0.8 | 348.2 3.2 | 50.7 0.8 | 7.0 1.0 | 10.9 0.8 | 25.1 3.4 |
| 8 | 841025 | 850114 | 12.4 1.0 | 345.6 5.0 | 51.2 1.0 | 7.1 1.2 | 13.3 1.0 | 28.7 5.4 |
| | 850128 | 850318 | 12.5 1.2 | 357.2 5.4 | 50.5 1.2 | 5.6 1.2 | 12.9 1.2 | 27.6 4.2 |
| | 850329 | 850501 | 14.4 1.0 | 352.4 3.8 | 49.9 1.0 | 4.8 1.2 | 11.9 1.0 | 30.4 3.6 |
| 11 | 840824 | 850118 | 16.2 1.4 | 349.5 4.6 | 55.1 1.4 | 11.3 1.4 | 12.5 1.4 | 28.1 6.0 |
| 12 | 841127 | 850303 | 12.4 1.2 | 357.0 5.6 | 55.4 1.2 | 11.6 1.2 | 15.4 1.2 | 32.8 5.4 |
| 13 | 840101 | 850101 | 7.7 0.2 | 21.1 1.8 | 22.8 0.2 | 36.2 0.6 | 5.7 0.2 | 35.5 2.4 |

| STN | START | STOP | O1 AMP CM | O1 PHASE DEG G | K1 AMP CM | K1 PHASE DEG G | M4 AMP CM | M4 PHASE DEG G |
|---|---|---|---|---|---|---|---|---|
| 1 | 841108 | 841217 | 5.9 1.6 | 198.5 14.6 | 6.9 1.6 | 182.4 10.2 | 8.5 0.8 | 42.5 6.0 |
| | 850219 | 850329 | 4.3 1.0 | 203.0 12.6 | 5.0 1.0 | 174.8 16.4 | 8.4 1.0 | 29.7 7.0 |
| | 850409 | 850618 | 5.0 0.8 | 204.1 9.0 | 6.7 0.8 | 167.8 6.4 | 8.7 1.2 | 34.3 7.4 |
| | 850626 | 850807 | 5.5 0.8 | 198.4 7.8 | 6.7 0.8 | 165.6 5.6 | 8.8 1.2 | 36.5 7.2 |
| 2 | 840809 | 850119 | 4.9 0.6 | 200.8 7.6 | 6.9 0.6 | 175.9 5.6 | 6.9 0.6 | 36.5 5.6 |
| 5 | 841109 | 841212 | 5.7 0.8 | 191.5 8.2 | 6.8 0.8 | 179.4 5.8 | 6.3 0.8 | 33.7 7.0 |
| 7 | 840906 | 841022 | 5.4 0.8 | 202.4 7.4 | 7.4 0.8 | 181.8 7.8 | 6.5 0.6 | 29.8 5.8 |
| 8 | 841025 | 850114 | 4.9 1.0 | 199.1 11.0 | 6.6 1.0 | 173.2 6.8 | 6.7 0.8 | 36.4 7.2 |
| | 850128 | 850318 | 4.7 1.0 | 203.0 11.6 | 5.8 1.0 | 183.0 11.6 | 6.9 0.8 | 30.6 7.0 |
| | 850329 | 850501 | 5.0 0.4 | 202.4 5.4 | 7.0 0.4 | 167.6 4.8 | 7.3 1.0 | 29.6 8.6 |
| 11 | 840824 | 850118 | 5.2 0.8 | 197.8 8.6 | 7.2 0.8 | 179.1 6.6 | 8.6 1.0 | 41.3 6.4 |
| 12 | 841127 | 850303 | 4.8 1.2 | 201.1 13.2 | 6.5 1.2 | 179.9 9.0 | 8.9 1.2 | 43.6 7.8 |
| 13 | 840101 | 850101 | 6.3 0.4 | 202.9 3.2 | 7.0 0.4 | 189.0 3.0 | 5.3 0.2 | 355.3 3.2 |

Table 3.1: Harmonic analysis of sea level and pressure in Buzzards Bay. For each component, the amplitude in cm and Greenwich phase estimates are listed with 95% confidence limits.

at the bay mouth, while in Vineyard Sound, speeds of 70–100 cm $s^{-1}$ are typical (Haight, 1938). In addition, the large phase and amplitude difference between the bay and the sound leads to extremely large currents in the holes joining the two regions: average currents of 130 cm $s^{-1}$ in Quicks Hole, 150 cm $s^{-1}$ in Woods Hole, and 120 cm $s^{-1}$ in Robinsons Hole. In both bay and sound, tidal ellipses from current meter data are essentially rectilinear with aspect ratio $|\gamma| \equiv |\frac{MIN}{MAJ}| < 0.1$, except at stations 5 and 6 near Quicks Hole, where the significant minor axis ($\gamma = -0.2$) reflects flow toward the hole after high water (Fig. 3.2 and Table 3.3). The variation of tidal current in Buzzards Bay with the spring/neap and apogee/perigee cycles is similar to the variation in elevation. As before, $N_2$ and $S_2$ major axes are of similar magnitude, about 20% of $M_2$, and their ellipse orientations coincide with the $M_2$. Thus 20% larger surface elevations accompany a 20% stronger current field. In Vineyard Sound, current meter data show a modulation of 10% due to the spring/neap cycle and a 5% modulation due to the perigee/apogee cycle.

Also seen from table 3.1 and table 3.2 is the significant size of the constituent $M_4$, a "shallow water" tide that is generated by interaction of the $M_2$ tide with itself through the non-linearity of the system. From the governing shallow water equations, one expects large $M_4$ when the tidal amplude $\eta$ is a significant fraction of the total water depth $H$, or in regions where advective terms are large, such as near rapid changes in bathymetry or coastline. The amplitude ratio $M_4/M_2$ is one measure of the non-linearity of the flow, and is about 0.2 in Buzzards Bay, 0.2 in Vineyard Sound, compared to values of 0.01 on the southern New England shelf. If the bay was in equilibrium with the shelf tide, then by continuity the $M_4/M_2$ ratio in Buzzards Bay would be greater for currents than for elevation, because the current contribution from a single constituent would be proportional to the elevation multiplied by the frequency of the constituent. Since the $M_4$ frequency is twice that of $M_2$, the $M_4/M_2$ for current would be about twice that of elevation. The $M_4/M_2$ current ratios are not larger by a factor of two, however, indicating local generation or modification of $M_4$. The $M_4$ component can give asymmetry in the tidal curve, depending on its relation to $M_2$, which has implications for sediment transport and other processes that depend non-linearly on current (Speer, 1985). Defining a phase angle

| STN | START | STOP | M2 MAJOR CM/S | M2 MINOR CM/S | M2 ORIEN DEG T | M2 PHASE DEG G | M4 MAJOR CM/S | M4 MINOR CM/S | M4 ORIEN DEG T | M4 PHASE DEG G |
|---|---|---|---|---|---|---|---|---|---|---|
| 4A | 840824 | 850116 | 25.7 0.4 | -0.4 0.5 | 39.9 1.0 | 296.4 1.0 | 6.4 0.5 | 0.3 0.4 | 35.0 4.0 | 312.5 4.2 |
| 4B | 840824 | 841208 | 22.1 0.5 | 0.9 0.5 | 36.2 1.4 | 296.1 1.2 | 5.9 0.5 | 0.1 0.5 | 35.9 4.6 | 309.3 5.4 |
| 5A | 840827 | 841219 | 24.9 0.7 | -4.9 0.6 | 75.0 1.4 | 312.2 1.6 | 5.2 0.6 | -0.5 0.4 | 66.2 4.2 | 323.5 6.2 |
| 5B | 840827 | 841219 | 21.5 0.7 | -3.9 0.6 | 70.8 1.6 | 310.2 2.0 | 5.2 0.5 | -0.4 0.4 | 59.5 4.6 | 321.6 5.4 |
| 6A | 840828 | 850116 | 22.5 0.5 | -4.5 0.4 | 75.9 1.2 | 306.2 1.4 | 3.0 0.4 | -1.3 0.5 | 18.8 12.6 | 265.6 10.6 |
| 6B | 840828 | 851208 | 21.4 0.8 | -4.3 0.7 | 72.7 2.2 | 305.9 2.4 | 2.9 0.4 | -1.3 0.5 | 24.1 13.2 | 269.6 12.2 |
| 1 | 841108 | 850114 | 9.5 0.5 | 0.8 0.5 | 14.0 3.2 | 297.2 3.2 | 1.9 0.3 | -0.1 0.2 | 19.7 7.0 | 333.8 9.2 |
| | 850128 | 850329 | 7.9 0.6 | 1.4 0.4 | 18.4 3.4 | 282.5 4.4 | 1.8 0.3 | -0.3 0.3 | 15.2 8.6 | 310.0 9.4 |
| | 850409 | 850619 | 7.8 0.6 | 2.1 0.5 | 22.1 4.0 | 275.1 5.0 | 1.9 0.3 | -0.1 0.3 | 19.0 8.6 | 307.0 10.4 |
| | 850626 | 850814 | 8.4 0.7 | 2.6 0.5 | 20.9 4.4 | 277.4 5.6 | 1.8 0.3 | -0.3 0.3 | 14.4 8.4 | 310.8 10.8 |
| 7 | 840906 | 841022 | 10.6 0.4 | 1.4 0.4 | 32.5 2.2 | 284.4 2.4 | 2.4 0.3 | 0.9 0.3 | 33.1 9.4 | 299.3 8.8 |
| | 841025 | 850114 | 14.5 0.5 | -1.2 0.5 | 47.2 1.8 | 289.5 2.0 | 3.3 0.4 | 0.7 0.4 | 34.9 7.4 | 315.9 7.8 |
| | 850114 | 850328 | 14.8 0.4 | -0.7 0.4 | 48.7 1.6 | 287.7 1.6 | 3.5 0.3 | 0.6 0.3 | 34.5 5.8 | 307.2 5.6 |
| | 850328 | 850619 | 12.4 0.5 | 0.3 0.5 | 44.3 2.4 | 287.7 2.6 | 3.4 0.4 | 0.5 0.4 | 40.1 6.8 | 303.2 7.2 |
| | 850619 | 850814 | 10.9 0.7 | 1.4 0.6 | 52.8 3.4 | 284.6 3.6 | 3.7 0.4 | 0.2 0.4 | 43.8 5.8 | 304.4 5.8 |
| 8 | 841025 | 850114 | 13.3 0.6 | 0.6 0.6 | 45.2 2.4 | 292.7 2.4 | 3.2 0.4 | -0.3 0.4 | 40.6 6.4 | 312.2 6.6 |
| | 850128 | 850328 | 12.0 0.5 | 1.1 0.4 | 58.7 2.0 | 283.2 2.4 | 3.2 0.4 | -0.3 0.4 | 51.2 6.4 | 307.0 6.8 |
| 14 | 860225 | 860428 | 75.3 1.1 | 2.3 1.0 | 55.8 0.8 | 24.0 0.8 | 2.7 0.5 | -0.4 0.5 | 27.2 10.0 | 265.8 11.0 |

| STN | START | STOP | N2 MAJOR CM/S | N2 MINOR CM/S | N2 ORIEN DEG T | N2 PHASE DEG G | S2 MAJOR CM/S | S2 MINOR CM/S | S2 ORIEN DEG T | S2 PHASE DEG G |
|---|---|---|---|---|---|---|---|---|---|---|
| 4A | 840824 | 850116 | 7.2 0.4 | 0.1 0.4 | 40.7 3.6 | 271.0 3.4 | 6.1 0.4 | -0.1 0.5 | 40.7 4.2 | 306.4 4.2 |
| 4B | 840824 | 841208 | 6.1 0.5 | 0.3 0.5 | 38.0 4.8 | 268.3 4.6 | 4.2 0.6 | -0.1 0.6 | 38.2 5.0 | 312.5 5.0 |
| 5A | 840827 | 841219 | 7.4 0.7 | -1.5 0.6 | 75.7 4.6 | 289.4 5.6 | 5.7 0.7 | -0.9 0.6 | 69.9 5.6 | 330.5 6.6 |
| 5B | 840827 | 841219 | 6.4 0.7 | -0.7 0.6 | 67.9 5.4 | 286.7 6.4 | 5.4 0.7 | -0.6 0.6 | 65.0 6.0 | 329.0 7.0 |
| 6A | 840828 | 850116 | 5.9 0.5 | -1.3 0.4 | 75.8 4.4 | 276.3 5.6 | 4.7 0.5 | -1.2 0.4 | 72.4 5.4 | 323.0 6.8 |
| 6B | 840828 | 851208 | 5.8 0.8 | -0.8 0.7 | 71.7 7.6 | 273.5 8.6 | 5.0 0.8 | -0.9 0.7 | 68.6 8.6 | 323.0 9.4 |
| 1 | 841108 | 850114 | 2.1 0.5 | 0.3 0.5 | 18.7 14.2 | 261.0 14.8 | 3.2 0.5 | 0.1 0.4 | 24.0 11.4 | 330.2 11.8 |
| | 850128 | 850329 | 2.1 0.6 | 0.2 0.4 | 21.6 12.0 | 279.5 15.6 | 1.5 0.7 | 0.1 0.6 | 28.7 10.4 | 300.0 12.4 |
| | 850409 | 850619 | 2.5 0.6 | 0.3 0.5 | 19.7 11.6 | 255.9 15.0 | 1.6 0.6 | -0.3 0.5 | 10.1 15.6 | 334.5 21.4 |
| | 850626 | 850814 | 1.9 0.7 | 0.4 0.5 | 11.1 16.2 | 257.1 23.0 | 1.7 0.5 | 0.0 0.4 | 347.6 28.2 | 318.3 41.2 |
| 7 | 840906 | 841022 | 3.4 0.4 | 0.6 0.4 | 35.1 7.6 | 254.4 8.0 | 1.6 0.6 | 0.4 0.5 | 25.2 8.8 | 305.5 9.8 |
| | 841025 | 850114 | 3.1 0.5 | 0.1 0.4 | 49.8 8.4 | 264.2 9.2 | 4.0 0.4 | -0.2 0.4 | 48.3 9.0 | 318.9 8.8 |
| | 850114 | 850328 | 3.4 0.4 | 0.5 0.4 | 46.1 7.0 | 271.6 7.0 | 2.6 0.5 | -0.2 0.4 | 43.2 6.6 | 286.2 6.8 |
| | 850328 | 850619 | 3.8 0.5 | -0.1 0.5 | 46.3 8.4 | 261.0 8.2 | 2.4 0.6 | -0.3 0.5 | 38.7 12.0 | 328.7 12.4 |
| | 850619 | 850814 | 2.2 0.6 | 0.4 0.7 | 44.0 18.0 | 253.4 17.8 | 3.2 0.4 | 0.0 0.5 | 17.2 21.2 | 294.5 18.2 |
| 8 | 841025 | 850114 | 3.1 0.6 | 0.2 0.6 | 43.1 10.4 | 269.0 10.2 | 3.8 0.5 | 0.2 0.5 | 49.4 11.4 | 324.6 11.6 |
| | 850128 | 850328 | 2.9 0.5 | 0.1 0.4 | 51.7 9.0 | 282.0 9.4 | 2.4 0.5 | 0.2 0.5 | 48.9 7.8 | 296.4 8.2 |
| 14 | 860225 | 860428 | 14.5 1.1 | 0.1 1.0 | 56.9 4.2 | 359.4 4.4 | 8.6 1.4 | 0.1 1.3 | 56.9 3.8 | 53.5 4.2 |

Table 3.2: Harmonic analysis of current in Buzzards Bay and Vineyard Sound. Major and minor axis amplitudes in cm $s^{-1}$, the orientation of the major axis in degrees true, and the Greenwich phase estimates are given with 95% confidence limits.

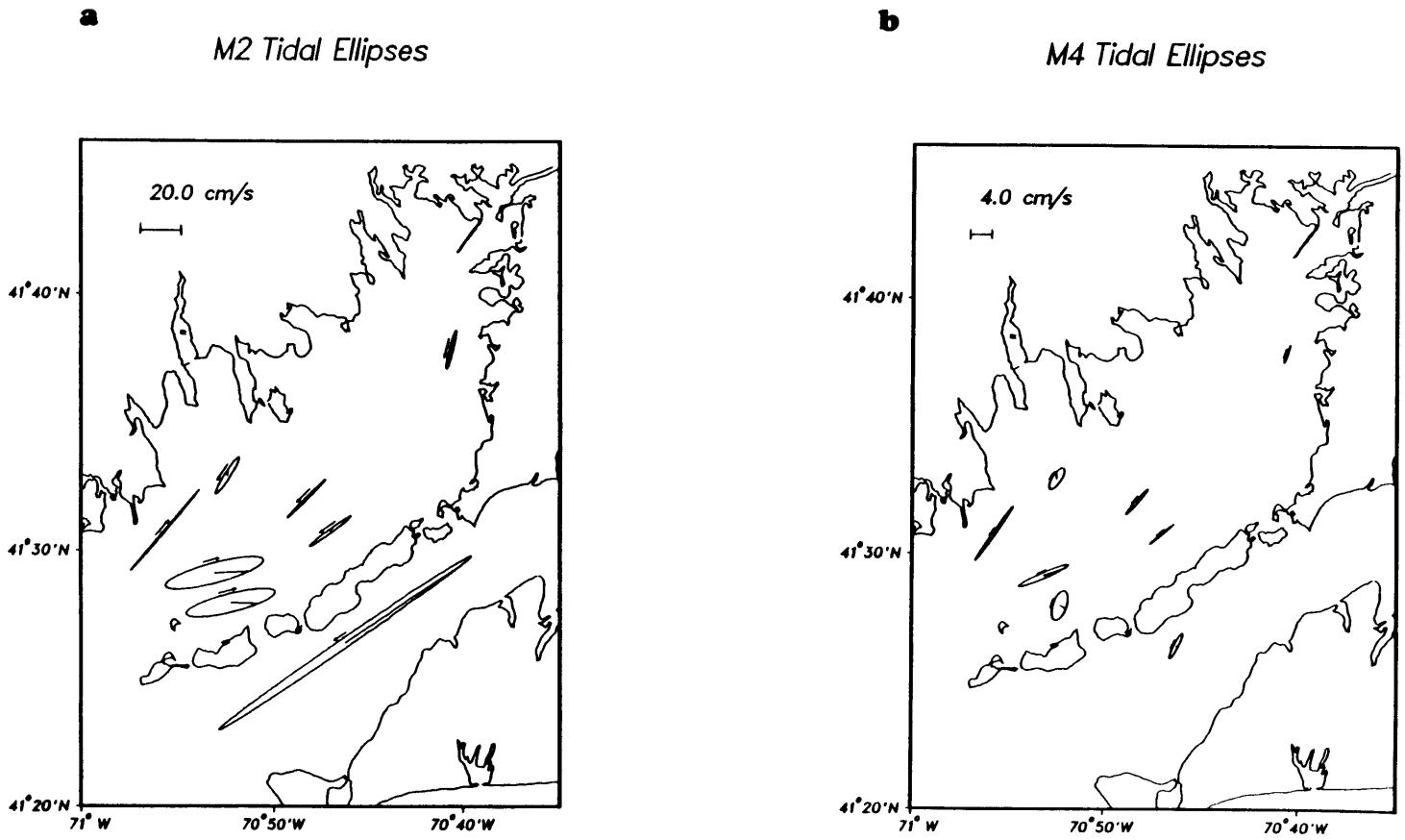


Figure 3.3: Tidal ellipses in Buzzards Bay region. The $M_2$ ellipses are drawn twice the size of the of the tidal excursion. The other constituents are drawn at eight times the size of the tidal excursion. (a) $M_2$ (12.42 hrs) ellipses. (b) $M_4$ (6.21 hrs) ellipses. (c) $S_2$ (12 hrs) ellipses. (d) $N_2$ (12.66 hrs) ellipses.

**c**

*S2 Tidal Ellipses*

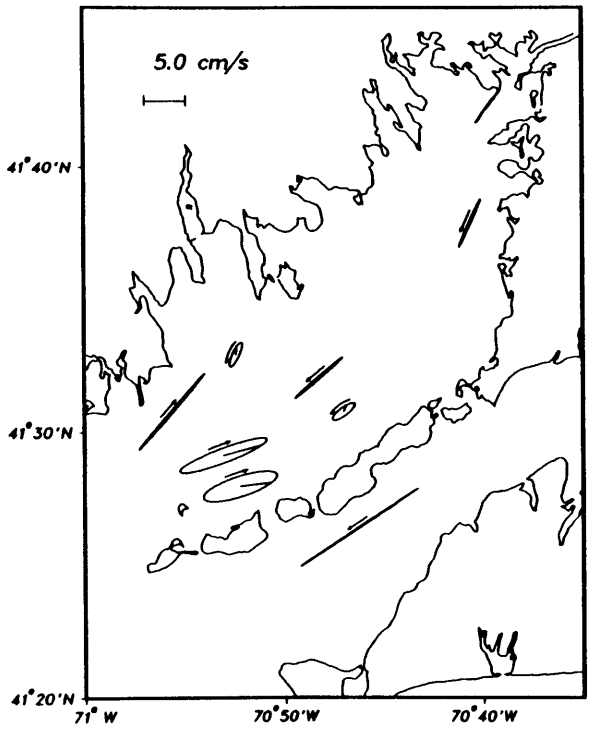


**d**

*N2 Tidal Ellipses*

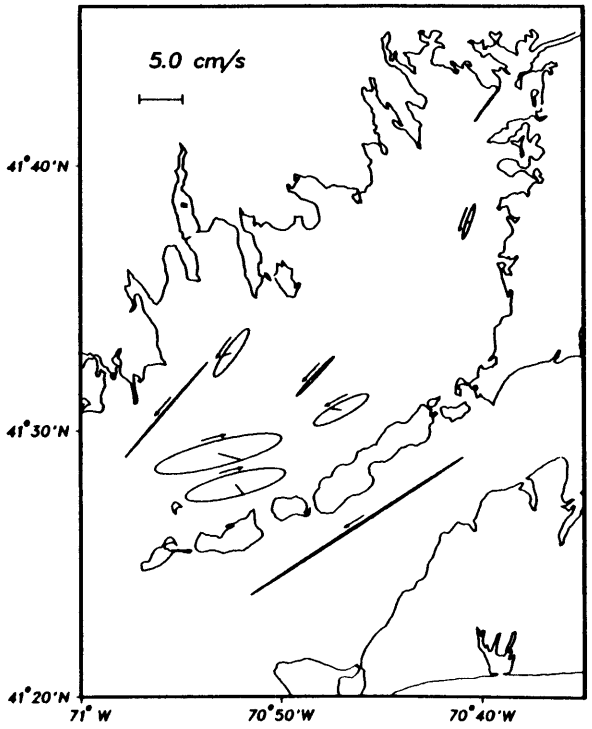

difference by

$$\theta_d = 2\theta_{M2} - \theta_{M4},$$

where $\theta$ is the phase angle, then for $90° < \theta_d < 270°$ the current is ebb dominant, which means that a longer, slower flood is followed by a shorter, quicker ebb. For $270° < \theta_d$ or $\theta_d < 90°$, then the current is flood dominant. Values of $\theta_d$ at station 1 in the upper bay are 240°–260°, indicating slight ebb dominance, whereas values of $\theta_d$ at stations 4 and 5 in the lower bay are 280°–300°, indicating slight flood dominance. At station 6, the $M_2$ and $M_4$ major axes are not aligned, and interpretation is more complicated.

## 3.4 Vertical structure of the tide

In the study of the bay, it is often desirable to estimate tidal current characteristics at a level in the water column where measurements are not available. To do this requires a model of the bottom boundary layer, a topic that has been studied by many authors and whose reviewers include Soulsby (1983) and Grant & Madsen (1986). In Buzzards Bay, the dominance of $M_2$ with a frequency greater than $f$, combined with the shallowness of the region results in a depth-limited time-dependent boundary layer structure, with shear extending throughout the water column and the current occurring significantly earlier at the bottom than at the surface. Since several stations have a significant $M_2$ minor axis and show rotation of the ellipse orientation with depth, rotational effects are kept here for generality. If the tide is represented by the dominant component $M_2$, then the governing equations can be represented as

$$i\sigma\hat{u} - f\hat{v} = -g\frac{\partial\hat{\eta}}{\partial x} + \frac{1}{\rho}\frac{\partial}{\partial z}\left(A_v\frac{\partial\hat{u}}{\partial z}\right),$$

$$i\sigma\hat{v} + f\hat{u} = -g\frac{\partial\hat{\eta}}{\partial y} + \frac{1}{\rho}\frac{\partial}{\partial z}\left(A_v\frac{\partial\hat{v}}{\partial z}\right),$$

where

$$u = \hat{u}e^{i\sigma t},$$
$$v = \hat{v}e^{i\sigma t},$$
$$\eta = \hat{\eta}e^{i\sigma t},$$

with the boundary conditions

$$\frac{\partial \hat{u}}{\partial z} = \frac{\partial \hat{v}}{\partial z} = 0 \text{ at } z = h,$$

$$\hat{u} = \hat{v} = 0 \text{ at } z = z_o.$$

Several more assumptions are necessary to determine vertical structure. First, an eddy viscosity profile must be supplied. Near the bottom, $A_v$ should approach $\kappa u_\star z$, which satisfies the law-of-the-wall:

$$u = \frac{u_\star}{\kappa} \ln\left(\frac{z}{z_o}\right)$$

where $\kappa = .4$ is Von Karman's constant, $z_o$ is the effective roughness height and $z$ is the distance from the bed. The profile of $A_v$, however, should reflect the fact that $A_v$ can not increase linearly throughout the entire water column, and Tee (1979) found that a sub-layer model (linear increase, then constant), gave nearly identical results as a parobolic model, and concluded that although the linear growth of $A_v$ at the bed was essential, the details of the $A_v$ profile away from the bed were less important. The profile chosen here is an exponential profile advocated by Long (1981), which has the advantage of simplicity:

$$A_v = \kappa u_\star z e^{-\frac{z}{\delta}}.$$

The scale length $\delta$ should be related to distance from the bottom if the boundary layer is depth-limited, and here the choice of $\delta = h/2$ was chosen. Runs with $\delta = h/4$ were not significantly different. For linearity, $u_\star$ is chosen as

$$u_\star = \sqrt{|\tau_b|_{max}/\rho},$$

where $|\tau_b|_{max}$ is the maximum bottom stress. Thus the model will represent the maximum velocity profile rather well, but will have too much viscosity at other stages of the cycle. Another parameter to be supplied is $z_o$, which is also assumed constant. This, of course, is a great simplification considering that storms in Buzzards Bay can change the effective roughness by an order of magnitude (Grant, personal communication) through surface wave effects described in Grant & Madsen (1979). At the USGS tripod stations 1, 3, 7 and 8, $M_2$ ellipse parameters were obtained at 1 m above bottom, and $u_\star$ was calculated from the law-of-the-wall and the major axis amplitude.

Runs were obtained with limiting values of $z_o = 0.01$ cm and $z_o = 1.0$ cm, corresponding to bottom drag coefficients of $C_{100} = 1.09 \times 10^{-3}$, and $C_{100} = 6.75 \times 10^{-3}$ respectively. At the WHOI transect stations 4, 5 & 6, $u_*$ was calculated from the law-of-the-wall averaging the 5 and 10 m data with the limiting values of $z_o$, then the pressure gradient iterated until the solution minimized the error in major axis amplitude at the two instruments.

Fig. 3.4 shows major and minor amplitude, phase, inclination, and eddy viscosity structure at station 5 and station 8. The model shows the proper tendencies, but is unable to represent the magnitude of the shear, rotation and phase lag of the observations. Stratification, an effect not included in this model, could significantly alter the eddy viscosity profile and hence affect the shear, yet conditions were well mixed over most of the experiment. Typical characteristics of the model in Buzzards Bay is that the bottom current leads the surface current by about 2–3° of $M_2$ phase (4–6 minutes) and is rotated several degrees to the left with respect to the surface current vector while the speed increases nearly logrithmically with distance from the bottom. Depth averaged ellipse statistics from the model are presented in table 3.3. The WHOI transect stations 4, 5 and 6 in the lower bay show that the major axis amplitude of the current is fairly constant (20–23 cm $s^{-1}$) across the moorings, but that the current arrives somewhat later as the water depth increases, presumably due to decreased frictional effects. The maximum current occurs first at station 4, then station 6, and finally at station 5 in the deeper center part of the bay, about 30 minutes after station 4.

The average cross-sectional tidal current can also be estimated from the tidal data, since the volume flux at each transect can be computed from continuity if the bay bay is approximated as a 1-D channel closed on one end. The mean cross-sectional flow in a semi-enclosed channel is

$$u = R(x)\frac{\partial \bar{\eta}}{\partial t},$$

where

$$R(x) = \left(\frac{\text{area of bay enclosed by transect}}{\text{cross section of transect}}\right),$$

and $\bar{\eta}$ is the average elevation in the area enclosed by the transect. In a nearly steady state, the average bay elevation is essentially constant, so

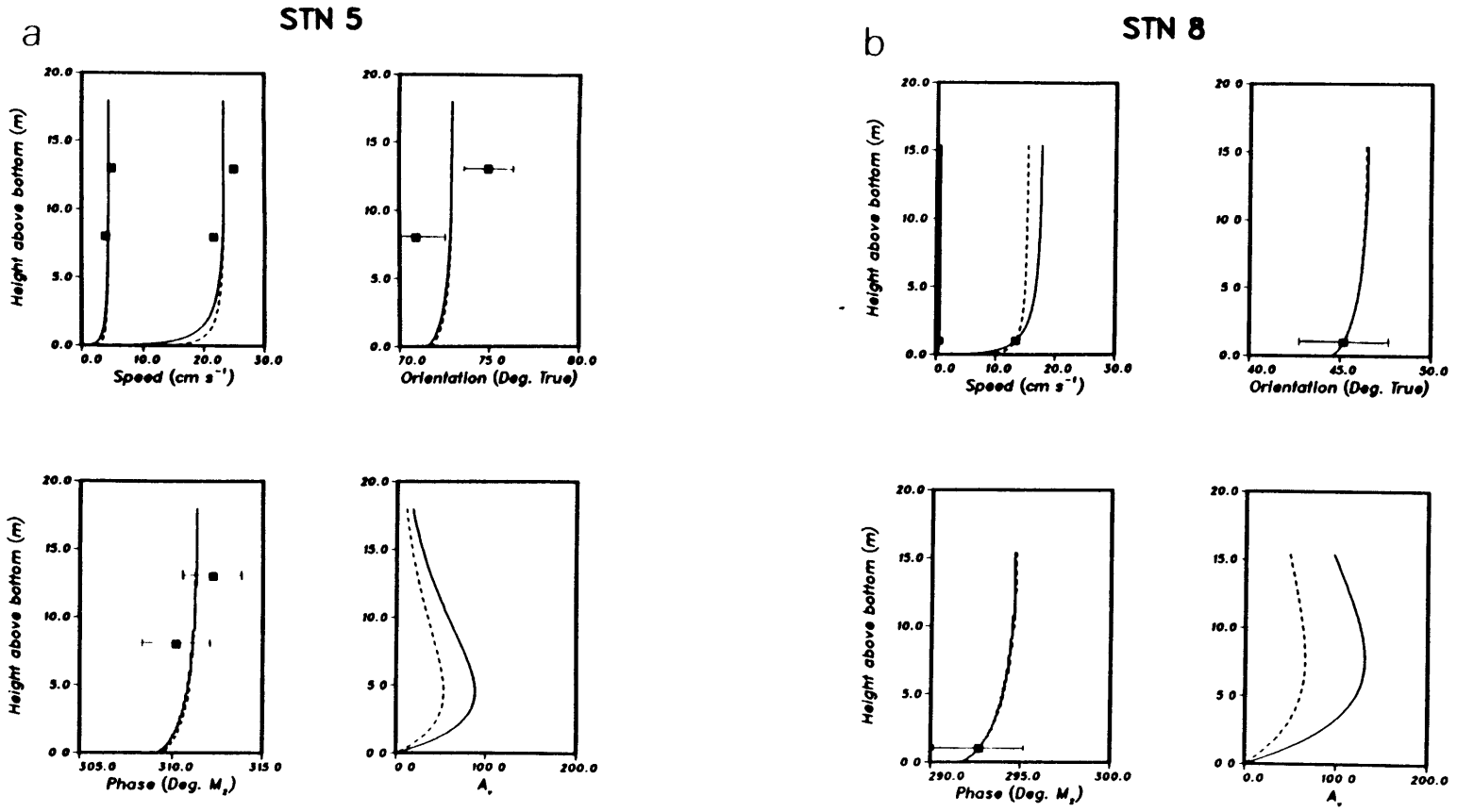


Figure 3.4: Modeled vertical $M_2$ current structure at: (a) station 5 (instruments at 5 and 10 m) ; (b) station 8 (bottom tripod 1 m above bottom). Major and minor axis speeds, inclination, phase and eddy viscosity of the model is shown along with the observations. Solid line: $z_o$ = 1.0 cm. Dashed line: $z_o$ = 0.01 cm. Horizontal error bars denote 95% confidence limits. Error bars on speed are too small to be seen.

| Stn | $z_o = 1.00$ cm | | | | $z_o = 0.01$ cm | | | |
|---|---|---|---|---|---|---|---|---|
| | Major cm $s^{-1}$ | Minor cm $s^{-1}$ | Inc $\phi$ | Phase $\theta$ | Major cm $s^{-1}$ | Minor cm $s^{-1}$ | Inc $\phi$ | Phase $\theta$ |
| 1 | 11.5 | .9 | 15.1° | 298.8° | 10.4 | .7 | 14.9° | 298.7° |
| 2 | 12.7 | 1.6 | 33.4° | 285.8° | 11.6 | 1.4 | 33.4° | 285.8° |
| 4 | 22.7 | .2 | 37.9° | 296.1° | 23.2 | .3 | 37.9° | 296.1° |
| 5 | 22.0 | −4.1 | 72.7° | 310.9° | 22.6 | −4.2 | 72.7° | 310.9° |
| 6 | 20.9 | −4.2 | 74.1° | 305.8° | 21.4 | −4.2 | 74.1° | 305.8° |
| 8 | 16.7 | .6 | 46.2° | 294.3° | 14.9 | .5 | 46.2° | 294.3° |

Table 3.3: Depth-averaged $M_2$ ellipse parameters from vertical structure model. Major and minor axis amplitude, inclination $\phi$ in degrees true, and phase angle $\theta$ (360°= 12.42 hrs) are shown.

that any sea level gauge may be used to compute $\partial\bar{\eta}/\partial t$. Values of $R(x)$ were obtained from digitization of bathymetric charts.

For the $M_2$ tide,

$$u_{M_2} = R(x)\eta_{M_2}\omega\cos(\omega_{M_2}t),$$

where

$$\omega_{M_2} = \frac{2\pi}{12.42 \text{ hours}},$$

and $\eta_{M_2}$ is the average tidal elevation in the enclosed area. Using the elevation amplitude from New Bedford of 52 cm, the cross-sectional mean $M_2$ tidal currents $\bar{u}_{cont}$ are shown in table 3.4, along with the cross-sectional mean obtained by averaging the $M_2$ major axis currents computed from the vertical structure model at each mooring in the section $\bar{u}_{model}$. The close correspondence between the two estimates suggests that the 1-D continuity calculation gives a reasonable estimate of the current over much of the section (except close to the walls, of course, where the current must approach zero).

| Transect | Area enclosed $m^2$ | Cross-section $m^2$ | $R(x)$ | $\bar{u}_{cont}$ cm $s^{-1}$ | $\bar{u}_{model}$ cm $s^{-1}$ |
|---|---|---|---|---|---|
| USGS1 | $1.02 \times 10^8$ | $0.86 \times 10^8$ | 1186 | 9.1 | 11.5 |
| USGS2 | $3.16 \times 10^8$ | $1.50 \times 10^8$ | 2107 | 15.3 | 16.7 |
| WHOI | $4.68 \times 10^8$ | $1.65 \times 10^8$ | 2836 | 20.7 | 21.9 |

Table 3.4: Mean cross-sectional tidal current estimated from continuity ($\bar{u}_{cont}$) and from the vertical structure model ($\bar{u}_{model}$).

## 3.5 Tidal rectification

Nonlinear processes, in addition to generating harmonics such as $M_4$, also may generate mean sea level departures or mean currents. This mechanism of residual current generation has been actively studied in recent years and the progress to date is summarized by Zimmerman (1981) and Robinson (1983). These studies have shown that significant tidal rectification is to be expected in regions where tidal currents interact with complicated bathymetry and topography.

One of the most striking features of the moored current measurements is the steadiness and regularity of the flow on time scales greater than a few days as evident in the low-passed vector plots from the WHOI transect moorings (Fig. 3.5). It is apparent that there is both a mean component and a modulation of the flow at two weeks and a month in the same direction, suggestive of tidally rectified flow. Following Butman, *et al.* (1983), a time series of tidal energy was created by squaring the component of hourly averaged tidal velocity in the direction of the major axis at each site. This tidal energy time series was then compared to the component of low passed current in the direction of the mean. Fig. 3.6 shows the remarkable correlation at station 6B between the envelope of the tide and the amplitude of the low-frequency current in the direction of the mean.

The variance in the along-mean direction for the 15–30 day band and coherence with the tidal magnitude is shown in table 3.5. Coherence between tidal energy and along-mean flow at 15 days and 30 days is the highest at the 5 m instruments 5A and 6A, where tidal rectification accounts for

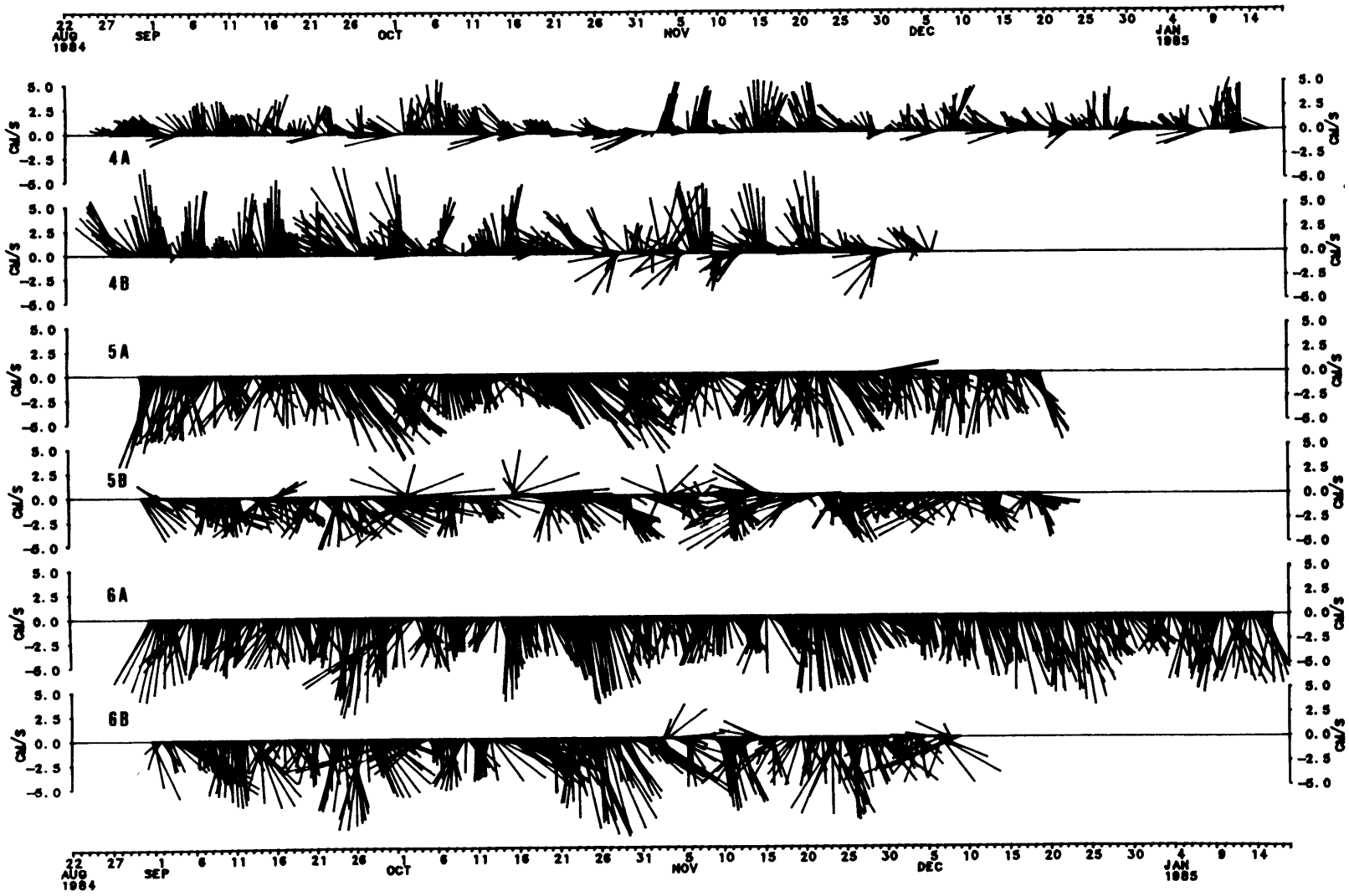


Figure 3.5: Low-passed (33 hr) currents from WHOI transect moorings 4, 5 and 6. True North is directed upwards.

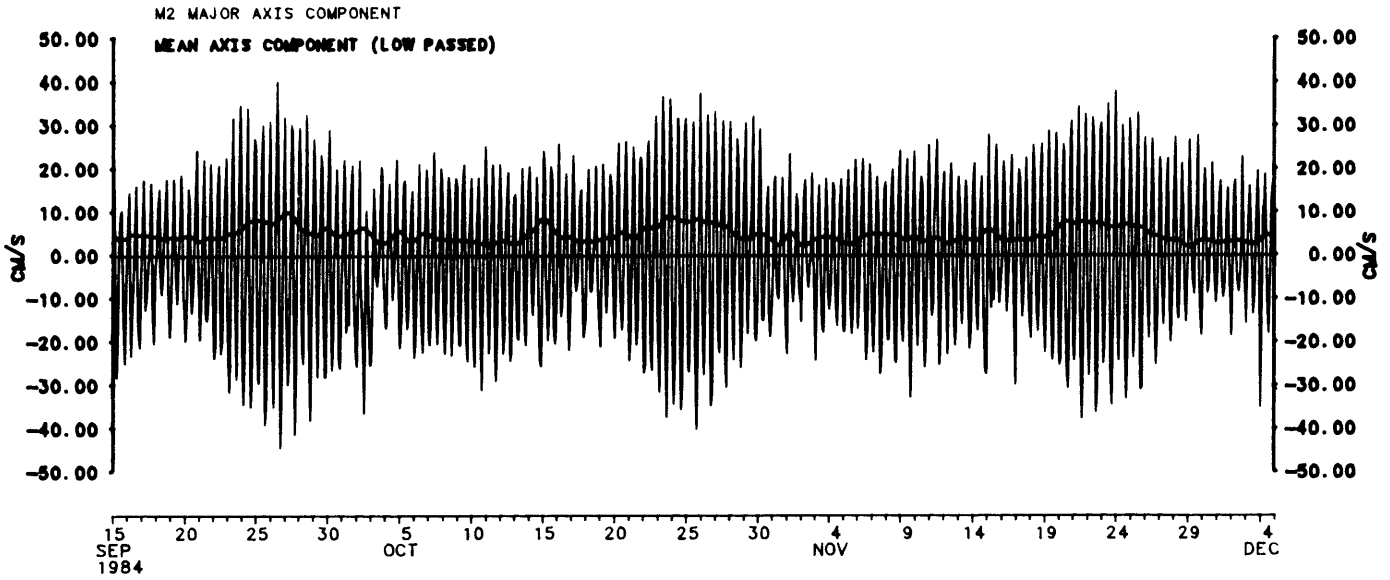


Figure 3.6: The component of the tidal current in the direction of the major axis (thin line) and the component of the low-frequency flow in the direction of the mean (heavy line) at station 6A. Note the strong visual correlation at a period of one month.

| | 29.3 days | | 14.7 days | |
|---|---|---|---|---|
| Stn | Variance $cm^2\ s^{-2}$ | Coherence | Variance $cm^2\ s^{-2}$ | Coherence |
| 4A | .17 | (.13) | .05 | .62 |
| 4B | .39 | .71 | .44 | (.54) |
| 5A | 1.21 | .95 | .89 | .93 |
| 5B | .67 | .74 | .67 | .73 |
| 6A | .70 | .96 | .61 | .94 |
| 6B | 1.56 | .56 | 1.24 | .74 |

Table 3.5: Variance of low-passed along-mean flow and coherence with tidal strength. Coherence in parenthesis are below the 90% confidence limit of 0.59. The 95% confidence limit is 0.67.

about 90% of the energy, and in general seems related to the magnitude of the mean flow observed at the sites (table 3.6).

Butman, *et al.* were able to calculate upper bounds for the rectified mean flow on Georges Bank using a simple dynamical model, but no model has yet been attempted for Buzzards Bay due to its complex topography. For lack of a such a model, it is assumed that the tidally rectified flow due to the interaction of $M_2$ with another component is proportional to

$$(A_{M2}\cos\omega_{M2}t + A_m\cos\omega_m t)^2,$$

where the subscript $m$ represents modulation with either $S_2$ or $N_2$. This seems reasonable since the $M_2$, $S_2$, and $N_2$ ellipses are nearly rectilinear and have similar orientations (Fig. 3.3). If this term is averaged over a tidal cycle, the high frequency terms drop out, and only two components remain,

$$\frac{1}{2}A_{M2}^2 + \frac{1}{2}A_m^2 + A_{M2}A_m\cos[(\omega_{M2} - \omega_m)t].$$

The ratio $R_m$ of the modulated component to the mean component is then

$$R_m = \frac{2A_{M2}A_m}{A_{M2}^2 + A_m^2}.$$

| STN | 4 | | 5 | | 6 | |
|---|---|---|---|---|---|---|
| | $\|u\|$ cm s$^{-1}$ | $\theta$ | $\|u\|$ cm s$^{-1}$ | $\theta$ | $\|u\|$ cm s$^{-1}$ | $\theta$ |
| A | 2.0 | 318° | 4.7 | 194° | 4.9 | 184° |
| B | 3.0 | 326° | 2.1 | 202° | 3.3 | 201° |

Table 3.6: Observed mean currents at the WHOI transect.

The estimate of the mean $U_{0m}$ is,

$$U_{om} = \frac{\sqrt{2\sigma_m^2 \gamma_m^2}}{R_m},$$

where $\sigma_m^2$ is the total variance at the modulation frequency and $\gamma_m^2$ is the squared coherence of the modulated component with the tidal envelope (table 3.5). The values of $R_m$ are obtained from the least squares harmonic analysis given in table 3.2. Since there are two distinct periods of modulation, there are two estimates of the mean due to tidal rectification listed in table 3.7. The similarity of the independent estimates of the mean (when significant) indicates that the calculations are consistent.

Since the observations clearly under-resolved the residual flow field, a nonlinear barotropic tidal model of Buzzards Bay and Vineyard Sound was developed (Capotondi, 1987). The numerical scheme was similiar to that of Flather and Heaps (1975) except that an upwind differencing scheme was used to compute the advective terms. Since this scheme is known to be highly diffusive, the effects of artificial viscosity were reduced by using grid spacing of 250 m (Fig. 3.7). The model was forced by $M_2$ elevation only on the open boundaries, and bottom friction was adjusted to best match $M_2$ observations in the interior ($C_D = 2.5 \times 10^{-3}$). The model was run for 5 tidal cycles until equilibrium conditions had been reached, and the mean current obtained by averaging over the subsequent tidal period. The $\log_{10}$ of the mean current for the entire domain is shown in Fig. 3.8. Evident is the complex small scale nature of the resulting mean flow field. A comparison with the observations, plotted on a linear scale in Fig. 3.9, shows that the predicted structure is indeed consistent with the observations. In addition,

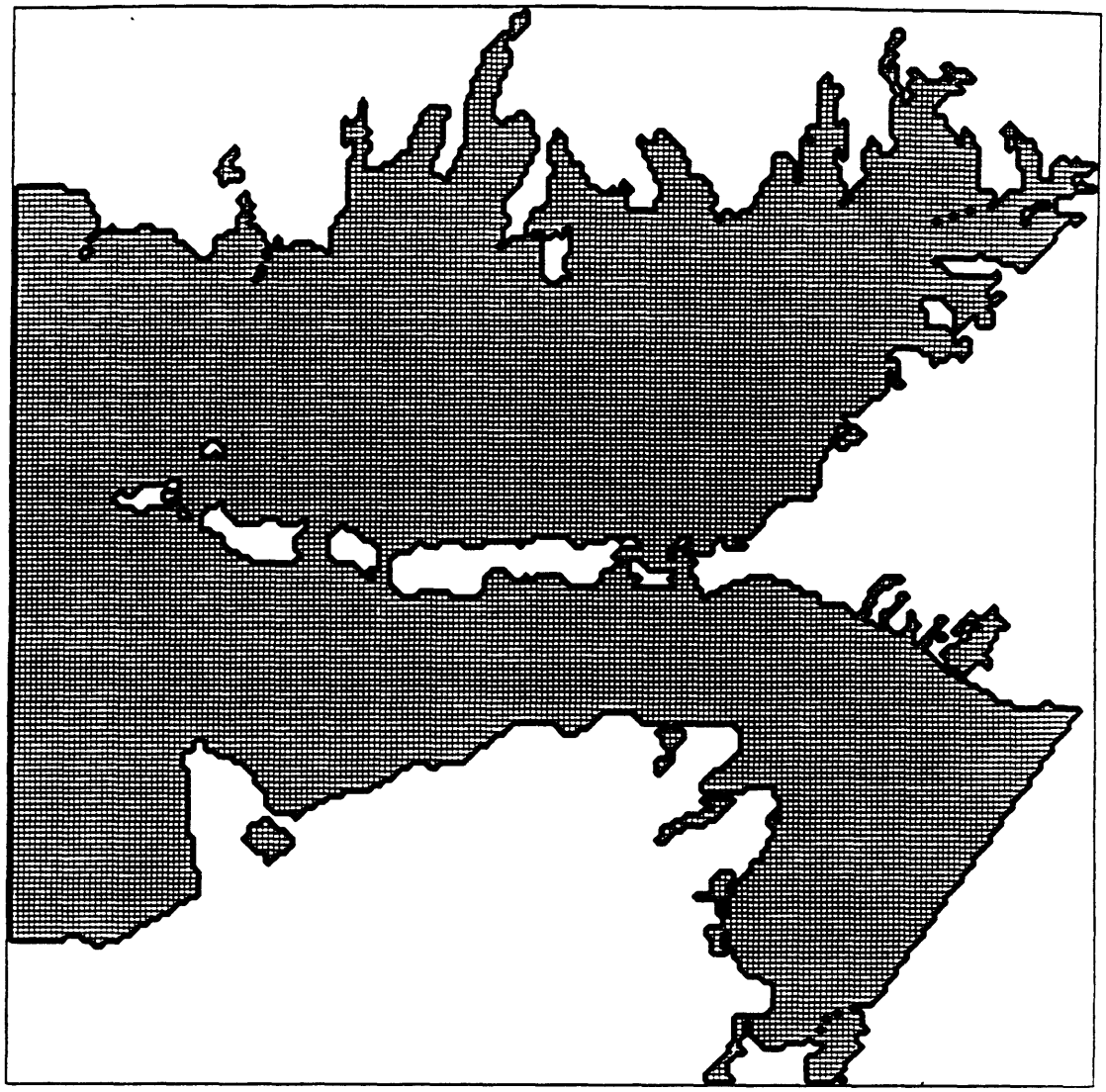

Figure 3.7: Finite-difference grid for 2-D nonlinear tidal model of Buzzards bay and Vineyard Sound. Grid spacing is 250 m.

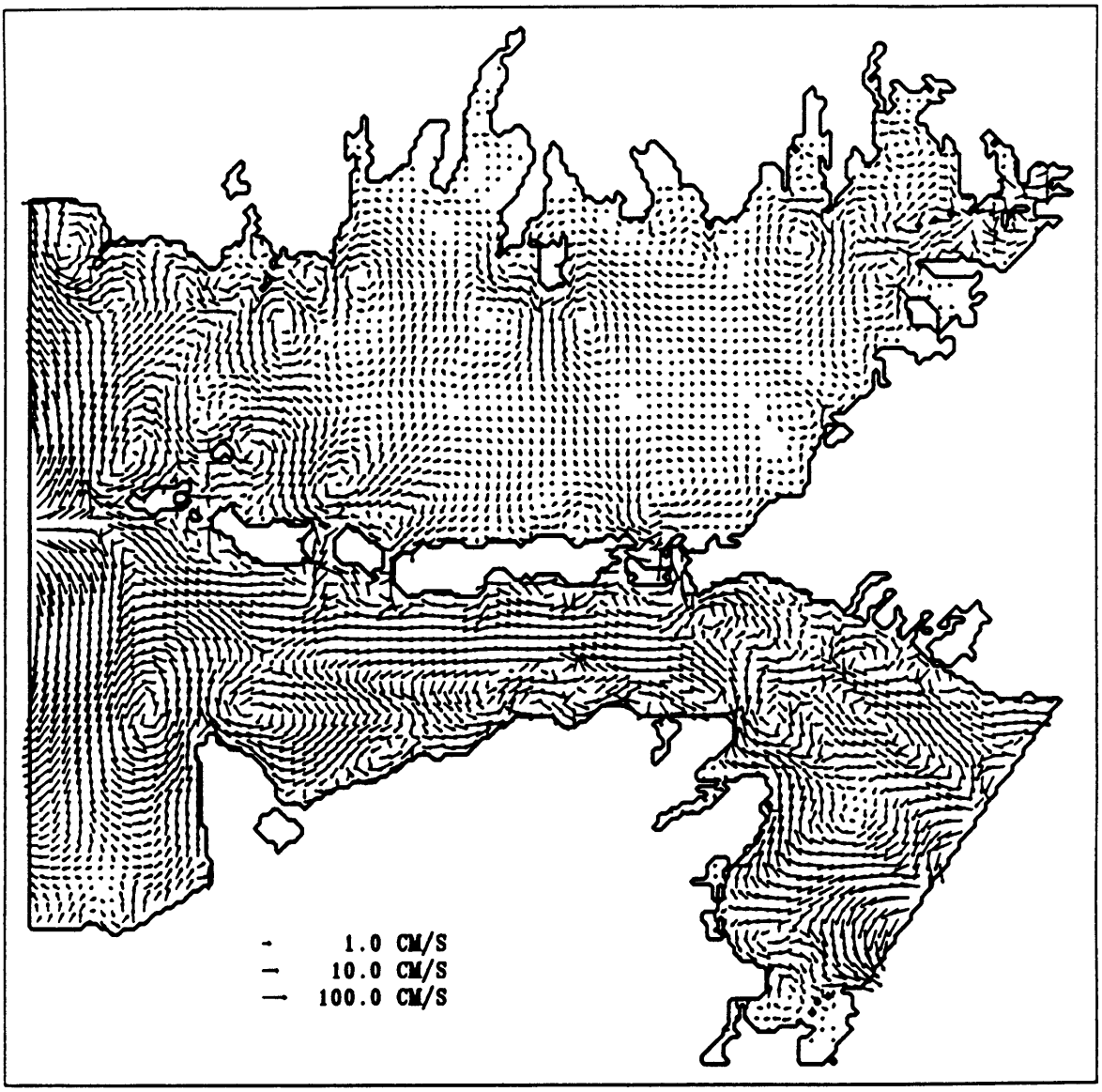


Figure 3.8: $\text{Log}_{10}$ of mean Eulerian current predicted by model. Model was forced by $M_2$ elevation on open boundaries. Results here show average current over a tidal cycle.

| | $N_2$ | | $S_2$ | |
|---|---|---|---|---|
| Stn. | $R_{N2}$ | $U_{oN2}$ cm $s^{-1}$ | $R_{S2}$ | $U_{oS2}$ cm $s^{-1}$ |
| 4A | .52 | – | .45 | 0.4 |
| 4B | .51 | 1.2 | .42 | – |
| 5A | .55 | 2.7 | .44 | 2.8 |
| 5B | .55 | 1.6 | .48 | 1.7 |
| 6A | .49 | 2.3 | .41 | 2.5 |
| 6B | .50 | 2.0 | .45 | 2.6 |

Table 3.7: Separate estimates of the mean flow due to tidal rectification from analysis of the modulation due to the $N_2$ and $S_2$ components. The similar estimates of the mean flow suggest that the calculations are consistent.

the mean flow at stations 7 and 3 also seem to be consistent with the predicted residual flow.

When the scale of these residual eddies is large compared to the tidal excursion, it is appropriate to relate these Eulerian mean flow features to a Lagrangian mean flow field. When the scale of these features is comparable to the tidal excursion, however, the significance of the residual eddies, as Zimmerman (1976) and Uncles (1982) have shown, is to disperse material carried on the dominant along-bay tide via the mechanism of "tidal random walk". Basically, one can conceive of an eddy deflecting the path of a particle carried on an otherwise rectilinear tide, so that a Lagrangian residual displacement results over a tidal cycle. This displacement may be such that on the subsequent tide cycle, the particle encounters a different eddy or a different part of the same eddy, so that a different displacement occurs. These displacements act to diffuse tracers on scales larger than the tidal excursion, and the mechanism can be the dominant diffusive process in regions of strong tidal rectification. Zimmerman derived an expression for effective diffusivity of such eddies when Gaussian eddies are homogeneous, isotropic and only consecutive residual displacements are correlated. Despite these simplifications, he obtained values that matched estimates from salt flux calculations in the Dutch Wadden Sea. Using Zimmerman's method in

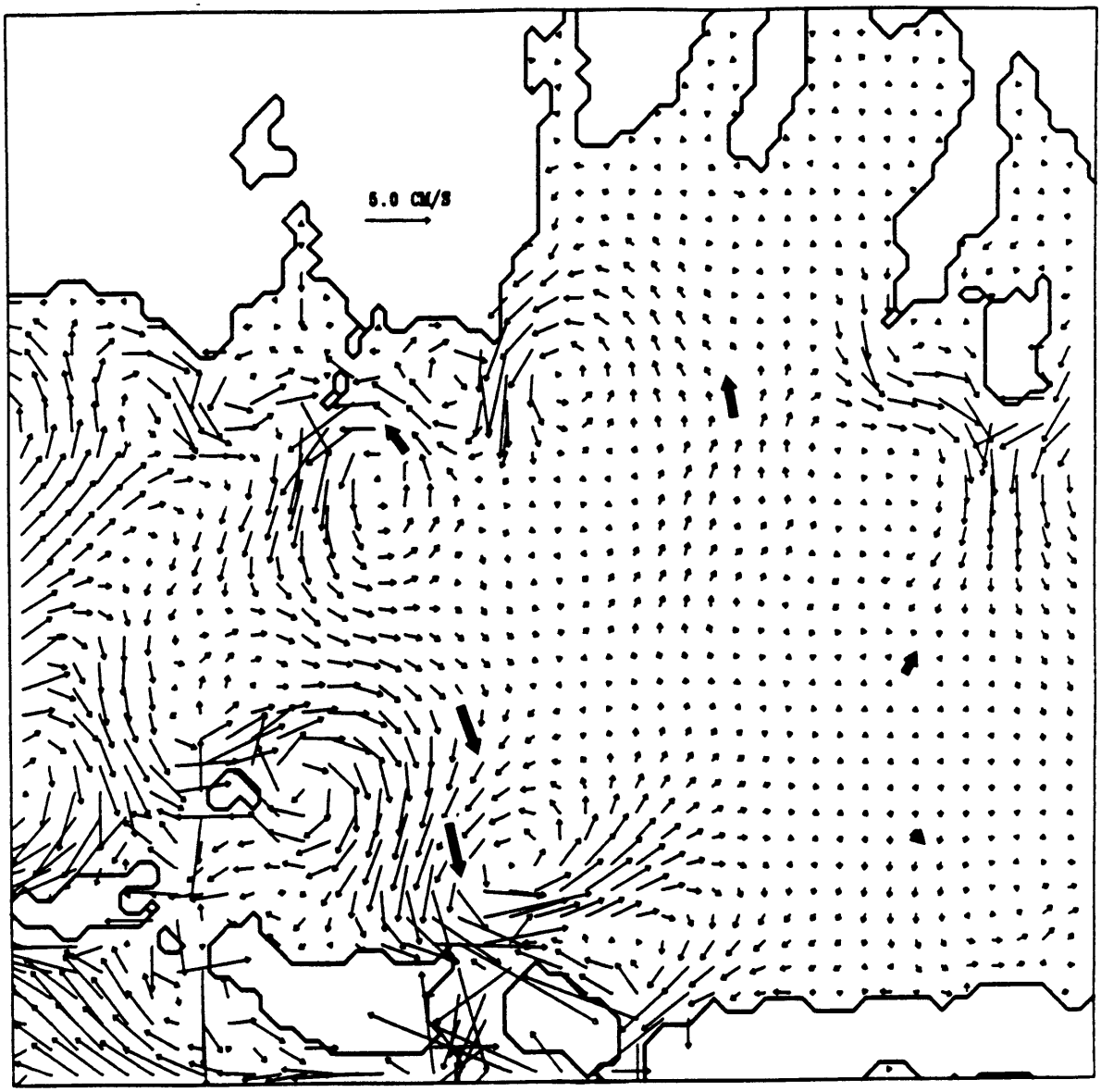


Figure 3.9: Comparison of model predictions with observed means at current meter sites. The structure of the predicted mean flow is consistent with the mean observations, although the magnitude agreement is only approximate.

Buzzards Bay, with a tidal excursion of 4 km, a residual gyre scale of 1/3 bay width or about 5 km, residual velocity scale of 4 cm $s^{-1}$ and a tidal velocity scale of 20 cm $s^{-1}$, then $\lambda = 1$, $\nu = .04$ and from Zimmerman's Fig. 4 on page 427, we find that the effective longitudinal diffusivity, $\kappa_{11}$ is approximately $2 \times 10^6$ $cm^2$ $s^{-1}$. This is clearly an order of magnitude estimate, but gives an idea of the effectiveness of this mixing process. The time scale of decay for a wavelength L is

$$T = \left( \frac{\left(\frac{L}{2\pi}\right)^2}{\kappa} \right),$$

so that high wavenumber structure decays more rapidly, with the time scale of decay proportional to the square of the wavelength. As an example, for $\kappa = 2 \times 10^6 cm^2$ $s^{-1}$, the decay scale for a 20 km wavelength structure is 28 hours while for a 10 km wavelength the decay scale is just 7 hours. In addition, since tides and tidal residual currents are stronger near the mouth, and weaker near the head, the effective dispersion caused by tidal effects must similarly be stronger at the mouth and weaker at the head. This is important, since increased dispersion near the mouth provides a preferred pathway for material to be transported down the bay. Additional work is needed to address the significance of this effect.

## 3.6 Summary

The tides are the dominant signal in Buzzards Bay, with typical elevation ranges of order one meter and current amplitudes of 15–50 cm $s^{-1}$. The response is like a standing wave in Buzzards Bay, the time of high water occuring nearly simultaneously over the bay, the head lagging the mouth by only 20 minutes. In addition, there is little amplification from the mouth to the head, since the natural period of the bay (2-3 hours) is substantially less than the semi-diurnal period (12.42 hrs). A homogeneous model of the vertical tidal structure indicates that the bottom flow leads the surface flow by 5–10 minutes and is veered 5–10 degress anti-clockwise. In the lower bay, the data suggest that the homegeneous model underestimates the vertical structure, indicating perhaps that the stress parameterization is not adequately specified.

The effect of tidal forcing is also evident in the low-frequency flow field, where nonlinear interaction of the semi-diurnal tide with the complex geometry and bathymetry generates mean flow modulated at 15 and 28 days. This tide-induced residual circulation dominates the mean flow measures in the lower bay and accounts for 60–95% of the variance at two weeks and one month. A non-linear barotropic tidal model of Buzzards Bay and Vineyard Sound reveals that the lower bay mean circulation consists of small scale eddies of 2–5 km and amplitudes of 1-5 cm $s^{-1}$. These residual gyres act to disperse tracer carried on the dominant flow and, since the mechanism is more active near the mouth of the bay than at the head, should provide a preferred path for the transport of material down the bay.

# Chapter 4

# Meteorological Forcing

## 4.1 Introduction

While the previous chapter suggested that tidally driven residuals dominate the mean and very low-frequency (15–30 day) flow in the lower bay, wind driven flows dominate the entire low-frequency spectrum in the upper bay and are clearly important in the lower bay as well. Current measurements show that a moderate wind stress of 1 dyn $cm^{-2}$ along the axis of the bay can drive a 5–10 cm $s^{-1}$ flow against the wind in the deeper regions of the bay, and a simple model consistent with this data suggests stronger 10–15 cm $s^{-1}$ flow downwind in the shallow regions (i.e. along the northwest shore). A current of 5–10 cm $s^{-1}$ over three days advects a parcel 10–20 km, a significant fraction of the bay, and several times the length of the tidal excursion, illustrating the importance of wind driven flow on particle transport. In this chapter, the response of the bay to wind and pressure forcing is investigated.

In a series of papers studying subtidal forcing in Chesapeake Bay, Wang (1978, 1979a, 1979b) described the role of forcing by coastal sea level. In the Chesapeake, he found that coastal sea level events at 5–20 days often forced barotropic flows larger than local wind driven flow. In contrast, sea level fluctuations at 2–3 days were found to be locally generated by wind forcing, and were attributed to the lowest seiche mode of the bay. Garvine (1985), with simple scaling arguments, showed that since the natural period of most estuaries is much less than the period of energetic wind forcing, the estuary is essentially in equilibrium with the coastal sea level. Thus the barotropic

flow is dominated by the non-local wind effect on the shelf, while the local sea level gradient is dominated by local wind stress acting along the axis of the bay.

In Buzzards Bay, it is this local wind response that dominates currents generated by meteorological forcing, with non-local wind driving on the shelf and atmospheric pressure variations playing a secondary role. Because the depth varies across the bay, wind along the axis causes downwind transport in the shallows along the northwestern shore and return flow in the deeper regions to the southeast, which leads to large particle excursions, mixing and exchange with Rhode Island Sound water. Non-local wind and atmosperic pressure variations determine the average bay level, however, and are important for consideration of coastal flooding. First the meteorological response will be examined via the statistics of the low-passed wind, current and pressure measurements, then a simple model of local wind response will be presented.

## 4.2 Wind in Buzzards Bay region

Winds along the Mid-Atlantic Bight are generally northwestly in winter and southwesterly in summer (Saunders, 1977). Wind roses from 20 years of data at Otis Air Force Base on Cape Cod (Fig. 4.1) show this seasonal pattern quite clearly, the southwesterly tendency in summer augmented substantially by the local sea breeze. Storms often blow from the north or northeast, which is aligned roughly along the axis of the bay. Wind data for the study period was obtained from the US Army Corps of Engineers at the New Bedford Hurricane Barrier (anemometer height: 15 m above sea level), and was converted to wind stress computed from the quadratic drag law $\tau = \rho C_D |u| u$ with $C_D$ increasing linearly with wind speed over 11 m $s^{-1}$ according to Large and Pond (1981). The low-passed time series of New Bedford wind stress for the study period is shown in Fig. 4.2.

With additional wind data collected by C. Butman and the USGS (B. Butman), a comparison of low passed stress between New Bedford and nearby stations (Fig. 1.3) was carried out using complex or vector correlation. Vector pairs are written as

$$w_1 = u_1 + iv_1,$$

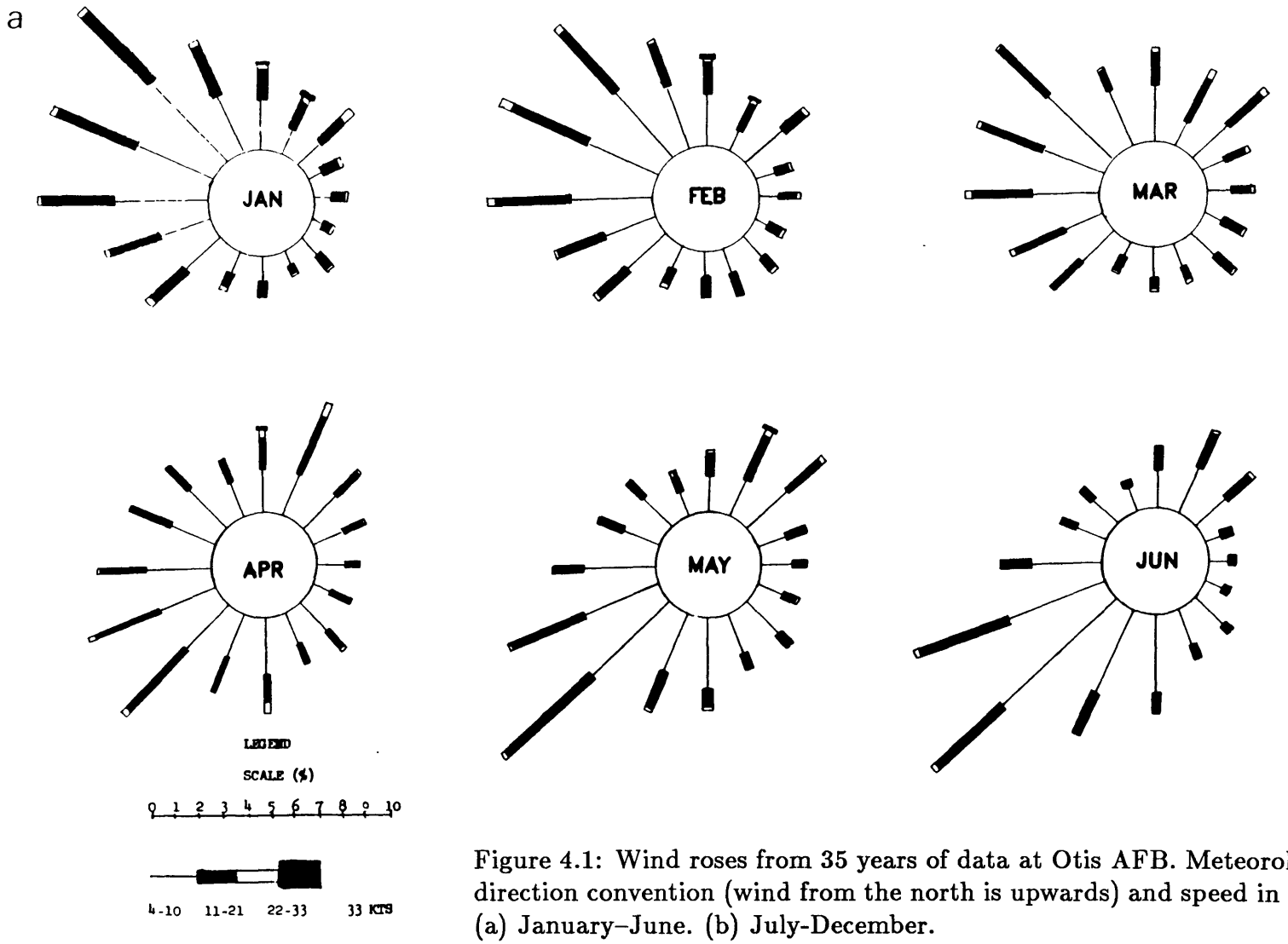


Figure 4.1: Wind roses from 35 years of data at Otis AFB. Meteorological direction convention (wind from the north is upwards) and speed in knots. (a) January–June. (b) July-December.

b

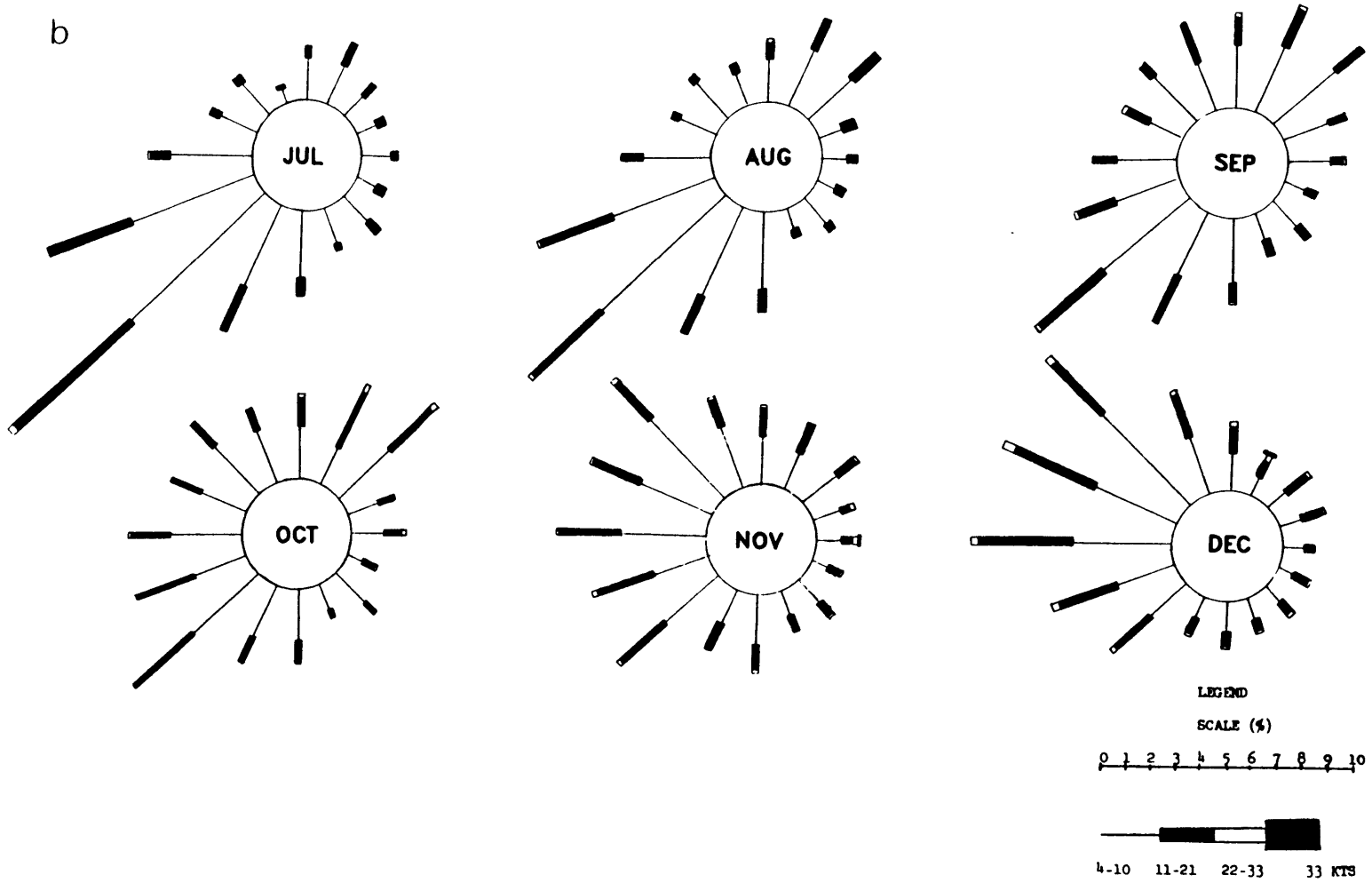
JUL
AUG
SEP
OCT
NOV
DEC
LEGEND
SCALE (%)
0 1 2 3 4 5 6 7 8 9 10
4-10
11-21
22-33
33 KTS

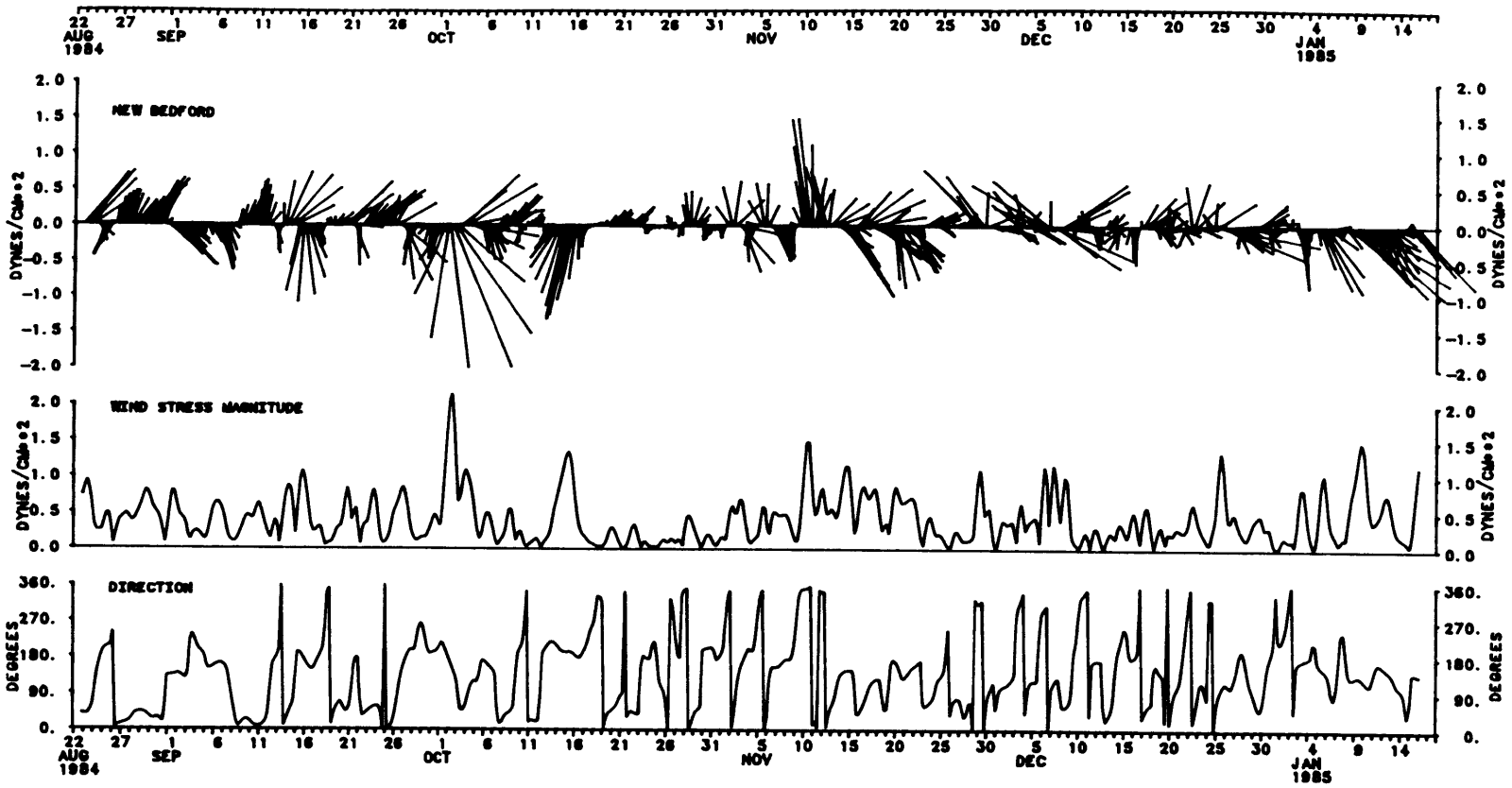


Figure 4.2: Low-passed (33 hr) wind stress vectors, magnitude and direction from New Bedford. Oceanographic direction convention (wind towards the north is upwards) is used.

| Station | Start-Stop | $r$ | $\theta$ | $\sigma_{NB}$ dyn cm$^{-2}$ | $b$ |
|---|---|---|---|---|---|
| Otis AFB | 841001 850116 | .84 | -18.9 | .51 | 1.00 |
| Wings Neck | 820120 820326 | .95 | -3.0 | .86 | .98 |
| Wings Neck | 820702 820926 | .90 | 5.1 | .70 | .75 |
| Buzz Bay LT | 850821 850912 | .92 | 9.6 | .75 | 1.27 |
| Nantucket LS | 820815 820926 | .64 | 5.8 | .73 | .46 |

Table 4.1: Comparison of low-frequency wind stress from station pairs in the Buzzards Bay region. Vector correlation $r$, rotation angle $\theta$, variance of New Bedford record $\sigma_{NB}$, and regression coefficient $b$.

$$w_2 = u_2 + iv_2,$$

and the complex inner correlation $C$ as

$$C = \frac{\langle w_1 w_2^* \rangle}{\sqrt{\sigma_{w1}^2 \sigma_{w2}^2}},$$

where $\sigma_w^2 = \langle ww^* \rangle$. A correlation coefficient r, which varies from 0 to 1 giving the degree of relatedness of the two series, or the amount of $\sigma_{w2}$ explained by $w_1$ is defined by

$$r = \sqrt{(\Re C)^2 + (\Im C)^2},$$

and the average difference angle between the two vectors is given by the phase $\theta$

$$\theta = \arctan \frac{\Im C}{\Re C}.$$

A regression coefficient $b$ can be defined which describes how much magnitude of $w_2$ is obtained per unit input of $w_1$,

$$b = r \frac{\sigma_{w2}}{\sigma_{w1}}$$

Table 4.1 shows the results of the analysis. New Bedford is well correlated with Wings Neck and the Buzzards Bay Light Tower, which suggests that

| STN | 4<br>$cm^2\ s^{-2}$ | 5<br>$cm^2\ s^{-2}$ | 6<br>$cm^2\ s^{-2}$ |
|---|---|---|---|
| A | 3.3 | 10.3 | 5.4 |
| B | 8.6 | 17.1 | 13.8 |

Table 4.2: Total current variance in 2–30 day band.

New Bedford is an adequate representation of wind over the entire bay, although it appears from the values of $b$ that in the summer the magnitude of the low-frequency wind stress is larger at the mouth and weaker at the head. Otis AFB give a somewhat poorer representation of Buzzards Bay low-passed wind stress, and Nantucket Lightship, on the shelf, shows substantial differences.

## 4.3 Wind, elevation and current spectra

Rotary spectra of wind stress and current was computed over the period 84/08/31–84/11/29 using 30 day pieces (Hanned and overlapped by 50%) yeilding a basic frequency interval of 0.033 cpd and 10 degrees of freedom for no frequency averaging. The wind stress total spectrum has a maximum at 15 days with a root mean square (rms) amplitude of 0.21 dyn $cm^{-2}$ and decreases roughly linearly with increasing frequency (Fig. 4.3a). The study period was not particularly energetic, with a total variance of 0.29 $dyn^2\ cm^{-4}$ over the low-frequency band (2–30 days).

The surface mooring current energy levels drop steeply from 30 to 10 days, and drop at a lesser slope to 2 days (Fig. 4.3b). As discussed in chapter 3, a significant fraction of the energy at 15–30 days is explained by tidal rectification, from 8% at 4A to 75% at 6A. Total variance over 2-30 days is shown in table 4.2. Similar structure is observed in the lower instrument spectra (stns 4B, 5B, and 6B), except at 4B, where 15-30 day energy is particularly low. Total variance is these instruments is 1.6 to 2.9 times larger than in the surface instruments.

Sea level data was collected for the study period from Woods Hole, Wings Neck and New Bedford in the bay, and Newport and Nantucket

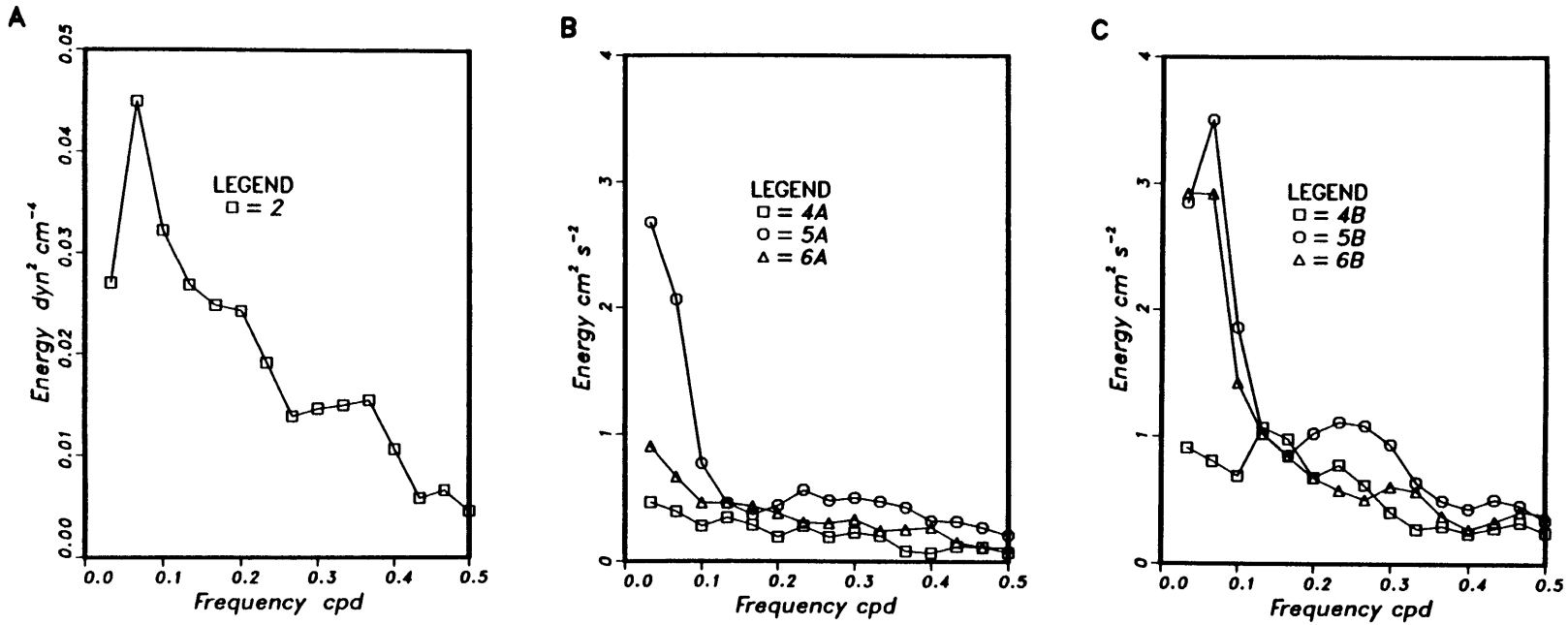


Figure 4.3: Total spectrum (sum of anti-clockwise and clockwise energy) of low-passed (a) New Bedford wind stress, (b) upper current meter, and (c) lower current meter data.

Island on the adjoining shelf. The sea level response is important because mass conservation allows the calculation of barotropic shelf exchanges and associated currents in the bay from the average sea level variation in time. Sea level gradient, in addition, is dynamically important in the local wind response. Sea level spectra are red, and show weak peaks at 3.3 and 2.3 days (Fig. 4.4). Coherence between all stations was greater than 0.90, with stations in the bay coherent at greater than 0.95 over the 2–30 day band. A empirical orthogonal function decomposition for the three bay stations revealed that over 90% of the sea level energy was contained in a single "pumping" mode, the average sea level of the bay simply rising and falling, while 7% was contained in an along-bay "set-up" mode, rising motion at the head of the bay coinciding with sinking motion at the mouth of the bay, and vice versa. The transfer functions between stations in the bay and in Rhode Island Sound (Newport) are not significantly different from unity, which suggests that the pumping mode represents the bay and Rhode Island Sound fluctuating in unison. This pumping mode drives a simple barotropic current through continuity which is greatest at the mouth and decreases to zero at the head, while the set-up mode, in conjunction with local wind stress, drives a more complicated response. The pumping response will be examined first briefly.

## 4.4 Non-locally forced response

The pumping mode, or rise and fall of average bay level is due almost exclusively to variations in non-local wind and atmospheric pressure. From these fluctuations in bay level, the associated flow of current in and out of the bay can be quantified. Miller (1958) was the first to look at subtidal sea level response to wind in the region, studying wind and elevation in Nantucket Sound. Miller claimed that fluctuations in air pressure were immediately and fully compensated by fluctuations in sea level at 1 mb to 1 cm, the "inverse barometer effect". With the resulting time series (presumably incoherent with air pressure), he found a symmetric average sea level response to the wind at 80° true, roughly the along-shelf direction. He obtained a transfer function of .015 m $(\mathrm{m\ s^{-1}})^{-1}$, a linear relation between coastal sea level and wind speed but with no dynamical basis. More recently, Noble and Butman (1979) examined subtidal sea level re-

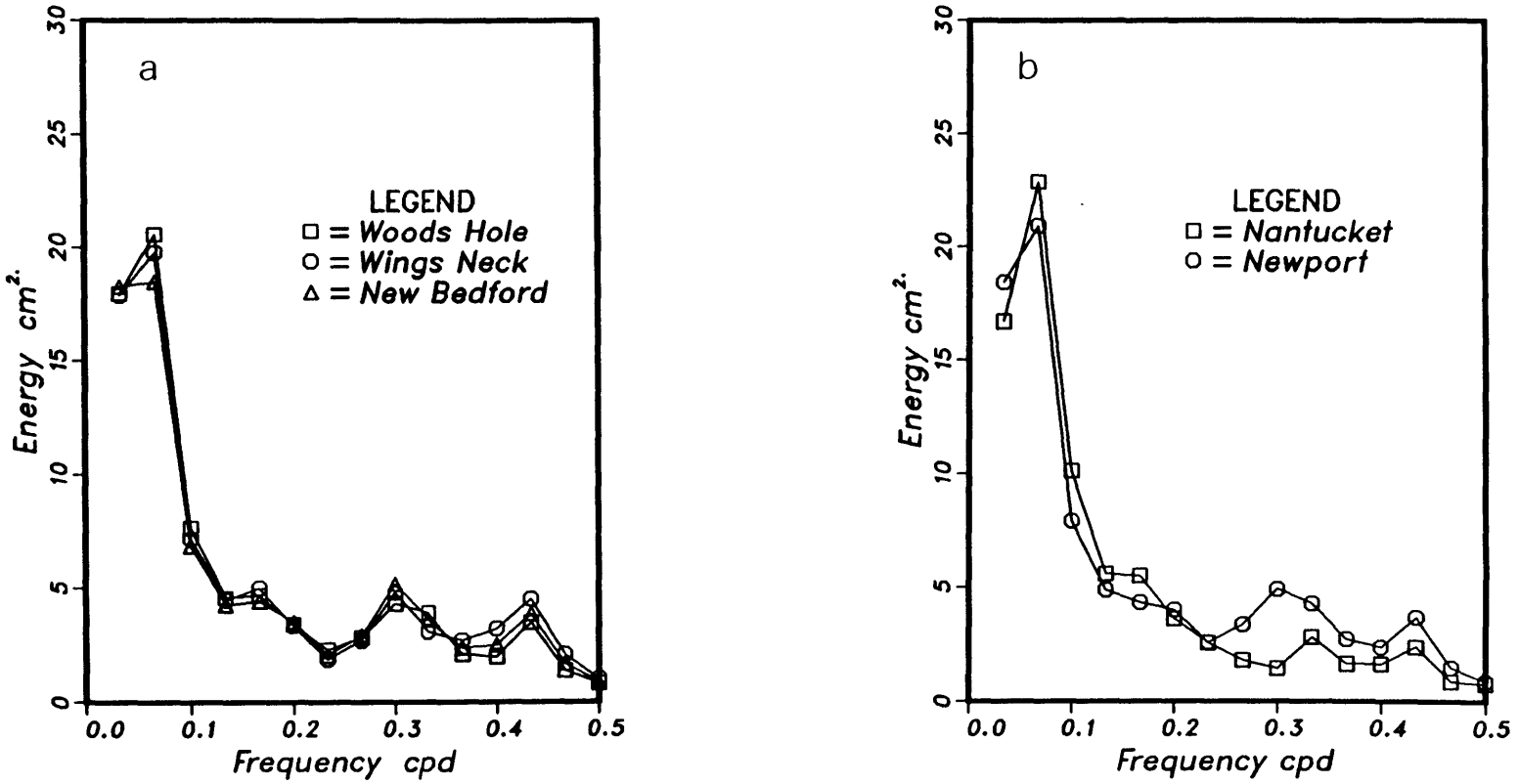


Figure 4.4: Spectra of low-passed sea level. (a) Stations inside the bay. (b) Stations outside the bay.

sponse along the U.S. East Coast, using a dynamical model in which coastal sea level was proportional to alongshelf wind stress, via cross-shelf Ekman transport. The transfer function obtained at Nantucket was 23 cm (dyn $cm^{-2})^{-1}$ for the alongshore wind component.

Ideally, a functional relationship could be found which would predict sea level variation with wind and pressure as inputs. In the bay, unfortunately, wind, atmospheric pressure and average sea level are all highly correlated, and the two inputs are not separable. In addition, since the bay responds to atmospheric pressure gradients, rather than local atmospheric pressure, additional data would be required to adequately describe the relevant forcing mechanism. Luckily, as will be seen next, the current driven by these fluctuations appear small compared to currents driven by local wind.

Regardless of whether the average sea level fluctuations in Buzzards Bay can be sucessfully modeled as a function of wind and air pressure, these fluctuations imply the existence of currents which may be inferred from mass conservation. A time series of $\partial\bar{\eta}/\partial t$ was computed using the low-passed sea level record from New Bedford chosen as represnetative of the bay. Time series of cross-sectional mean velocities can then be computed using the $R(x)$ values given in table 3.4. Time series of inferred current at the WHOI transect shows that even near the mouth, the currents associated with sea level fluctuations are quite weak, with a maximum speed of 3 cm $s^{-1}$ (Fig. 4.5). There was no significant coherence between the inferred current and the along axis components of velocity at any of the WHOI transect moorings. For the 2–30 day band, the total variance in $\partial\bar{\eta}/\partial t$ was $1.93\times10^{-8}$ $cm^2$ $s^{-2}$, corresponding to a current at the WHOI transect with a variance of 0.16 $cm^2$ $s^{-2}$, an order of magnitude less than the total current variance at these moorings. Since the currents associated with the low-frequency sea level fluctuations are greatest near the mouth, it can be concluded that the pumping mode is of secondary importance in driving circulation in the rest of the bay as well.

## 4.5 Local wind forced response

In shallow estuaries and embayments, often local wind stress is the dominant mechanism for current generation. Wind over a bounded basin initially drives water downwind, establishing an adverse pressure gradient. If

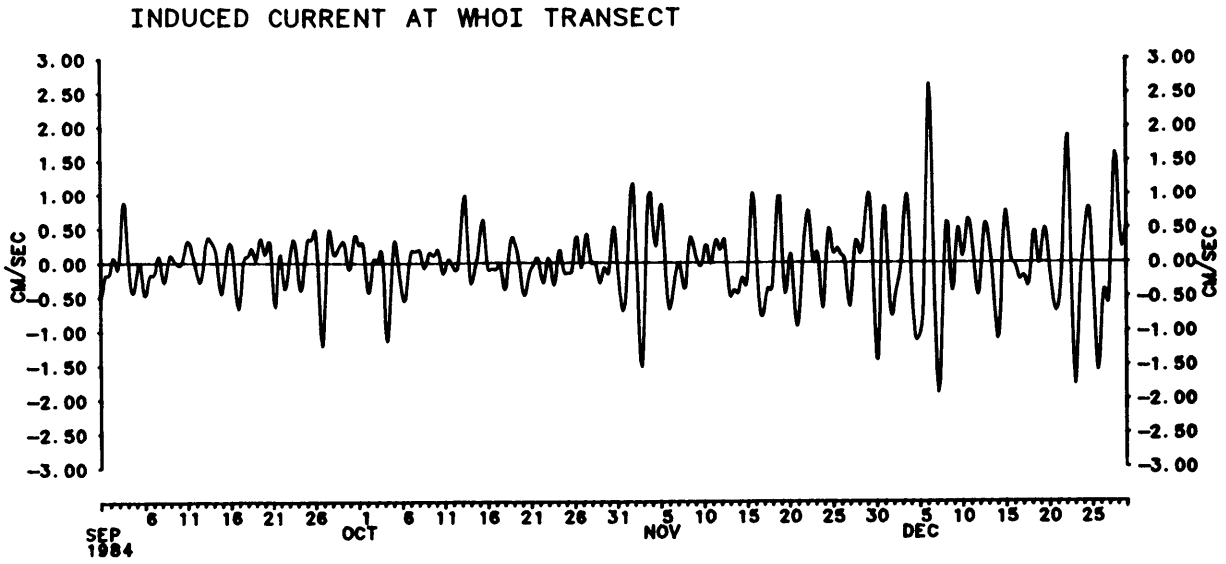


Figure 4.5: Inferred along-bay current near the mouth of the bay induced by low-frequency (less than .5 cpd) sea level variation. The RMS amplitude is 0.4 cm $s^{-1}$.

| STN | 4<br>$cm^2\ s^{-2}$ | 5<br>$cm^2\ s^{-2}$ | 6<br>$cm^2\ s^{-2}$ |
|---|---|---|---|
| A | 1.8 | 3.8 | 2.6 |
| B | 4.5 | 6.7 | 4.6 |

Table 4.3: Along-bay current variance in 2–7.5 day band.

the natural period of the bay is much less than the period of the forcing, a quasi-equilibrium balance is established between surface stress, pressure gradient and dissipative frictional forces acting on the induced currents. As previously mentioned, a significant amount of the total current variance at the WHOI transect can be explained by tidal rectification effects. To isolate the local response, the analysis will concentrate on the 2–7.5 day band. Rotary sprectrum computations for this band reveal narrow ellipses aligned with the local along-bay coordinate, within 20° of the $M_2$ tidal ellipse orientations while the wind stress ellipse is alligned nearly north/south. Principal axes from 2–7.5 day band-passed data are shown in Fig. 4.6. Along-axis currents over the entire bay were most coherent with along-axis winds (20°–200°in the upper bay, 60°–240°in the lower bay), so that the wind response is most efficient for wind along the axis of the bay.

Concentrating on the energetic along-bay response, coherence and phase calculations between along-bay current and wind stress components showed that while the lower instruments (4B, 5B and 6B) at the WHOI transect were coherent as expected, the upper instruments (4A, 5A and 6A) show little or no coherence with along-bay winds. The upper instruments, as previously mentioned, also have decreased energy levels in along-bay current relative to the lower instruments (table 4.3). Structure is seen in the horizontal as well, with the greatest energy at the central mooring at station 5.

Some of the observed response may be explained by a steady model in which an along-axis equilibrium is reached between wind stress, pressure gradient and frictional resistance. If the bay is approximated as a longitudinal channel of varying cross section, and narrow enough so that wind stress and pressure gradient are constant across the channel, then the appropriate

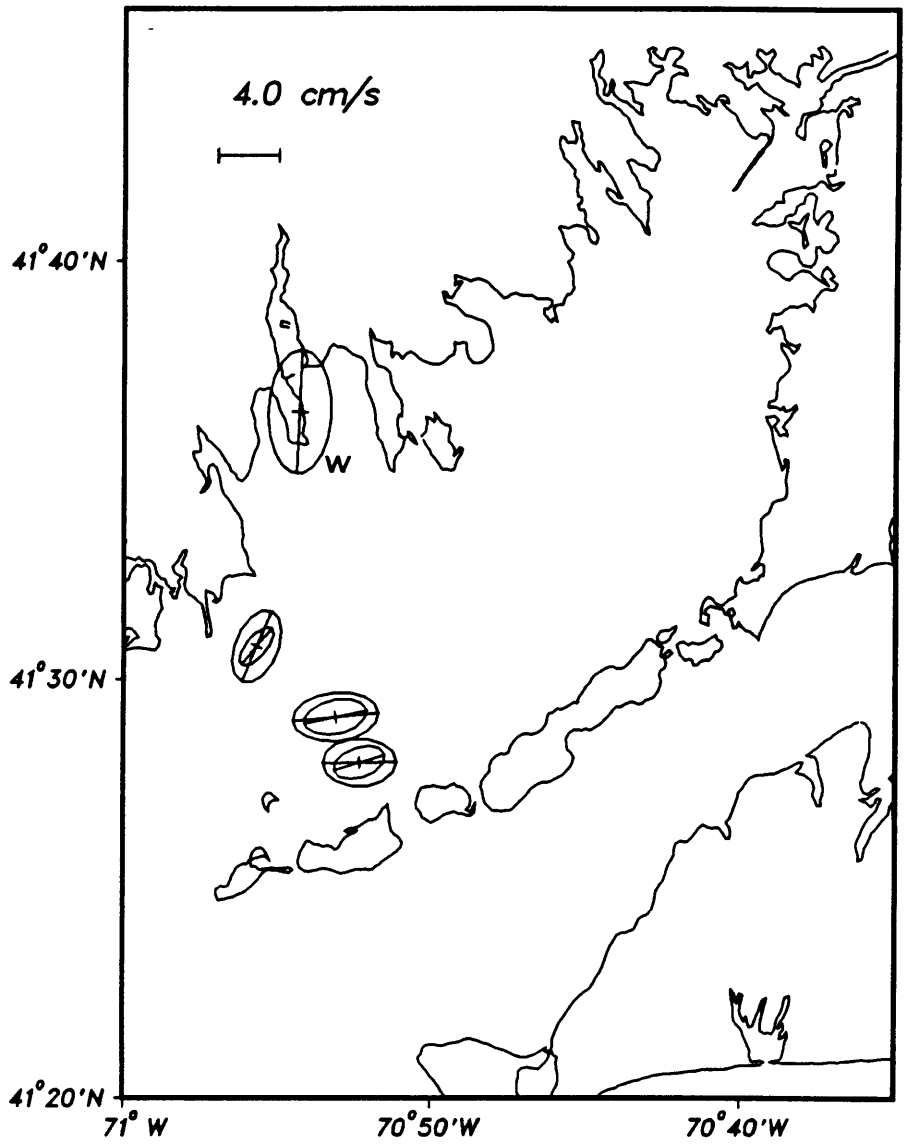


Figure 4.6: Principal axis wind stress ("W") and current ellipses from 2–7.5 day band. The major axis of wind stress is 0.4 dyn $cm^2$.

momentum equation is

$$\frac{\partial u}{\partial t} = -g\frac{\partial \eta}{\partial x} + \frac{\partial \tau^x}{\partial z}.$$

In addition, it is assumed that the current is in quasi-equilibrium with the wind forcing, since the frictional time scale $h/u_*$ is typically 2–3 hours, much shorter than the period of forcing. The balance then is given by

$$g\frac{\partial \eta}{\partial x} = \frac{\partial \tau^x}{\partial z} = const.$$

Since the average bay level is not rising or falling for this mode, mass conservation for an enclosed bay requires that

$$\iint u\, dy\, dz = 0.$$

The simplest model of response is that of a narrow 1-D basin with constant depth. If the bottom boundary layer is approximated by a no-slip condition and the interior stresses are modeled with a constant eddy viscosity formulization, then the problem simplifies to solving

$$g\frac{\partial \eta}{\partial x} = \frac{A_v}{\rho}\frac{\partial^2 u}{\partial z^2},$$

with

$$\tau^x = \rho A_v \frac{\partial u}{\partial z} = \tau_0^x \text{ at } z = 0,$$
$$u = 0 \text{ at } z = -h,$$

where z is the vertical coordinate measured upwards from the sea surface, h is the bottom depth, $\tau_0^x$ is the surface wind stress and $A_v$ is the constant vertical eddy viscosity. Integrating twice and applying the boundary conditions leads to a parabolic profile for velocity,

$$u = \frac{g}{2A_v}\frac{\partial \eta}{\partial x}(z^2 - h^2) + \frac{\tau_0^x}{\rho A_v}(z + h).$$

Requiring the depth averaged transport to be zero gives the relation between surface slope and wind stress,

$$\frac{\partial \eta}{\partial x} = \frac{3}{2}\frac{\tau_0^x}{\rho g h},$$

which upon substitution gives an expression for $u$ as a function of wind stress, eddy viscosity and depth,

$$u = \frac{\tau_0^x}{4\rho A_v}(h+z)\left(1+\frac{z}{1/3h}\right).$$

At one third the water depth, $u$ is zero, while the magnitude of response is proportional to wind stress and inversely proportional to eddy viscosity. Current is strong downwind near the surface, and is slower upwind at depth.

This simple model provides an explanation for reduced energy levels and lack of coherence with the along-bay wind at the upper instruments. These measurements were made at 5 m depth in water that was 15.5, 18.1, 16.0 m deep, roughly coincident with the zero velocity crossover predicted at 1/3 the total depth. The model also predicts an upwind current response for the lower instruments at 10 m.

A more realistic parameterization of the bottom boundary layer is a quadratic drag law, and in view of the relatively large tidal currents, linearization is appropriate (Hunter, 1975), so that

$$\tau_b^x = \frac{4}{\pi}\rho C_{100}|u_{tidal}|u_{100},$$

where $C_{100}$ is the bottom drag coefficient at 1 m, $|u_{tidal}|$ is the tidal amplitude at 1 m, and $u_{100}$ is the wind-driven bottom velocity at 1 m.

A more realistic parameterization of the interior stresses is given by a parabolic eddy viscosity $A_v$ profile which approximates log layers at the surface and bottom,

$$A_v = ku_\star z\left(1-\frac{z}{h}\right)$$

where Von Karman's constant $k = .4$, and $u_\star$ is defined by

$$u_\star = \frac{1}{2}\sqrt{\frac{\tau_s}{\rho}} + \frac{1}{2}\sqrt{\frac{\tau_b}{\rho}}.$$

This choice of $u_\star$ somewhat crudely combines surface and bottom effects but is chosen for simplicity, consistent with the nature of this modeling effort. To find a solution for a given cross section, the wind stress is specified, and the sea level gradient is interated until the zero transport

condition is reached. For the WHOI transect (stations 4, 5 and 6) a constant depth cross-section predicts a structure not much different from the analytic solution, except that the maximum in upwind flow is deeper due to the decreased eddy viscosity near the boundaries (Fig. 4.7a). Adding cross-channel depth variability causes the response to change dramatically (Fig. 4.7b), as first pointed out by Csanady (1973). The most obvious feature is the rapid downwind flow in the shallow regions and the slower upwind return flow in the deeper regions. This is because of the wind stress dominating the integrated pressure gradient in the shallows driving transport downwind, and integrated pressure gradient dominating wind stress in the deeper regions driving transport against the wind. The vertical structure is determined by the extent of the vertical mixing, which in turn is a function of the surface and bottom stress. Fig. 4.7b shows that with realistic bathymetry, the deepest part of the section should show up-wind current over the whole water column. This provides an explanation for a curious result of a drifter study (Signell, unpublished) in which it was observed that surface drifters in the center of the bay showed quite sluggish response (2–5 cm $s^{-1}$) for winds of 20 m $s^{-1}$. In addition, the model with cross-channel structure provides an explanation for why elevated energy levels were present at the central mooring: the response is greater because the water depth is further away from the zero line. The model, however, indicates that the upper instrument at the central mooring (5A) should be coherent with the alongshore wind, a response that is not observed. Probably the most suspect simplification in the model is that of constant cross-section along the bay, because variations in the actual width and depth are large. In addition, the interior stress distribution may be improperly represented by the parabolic eddy viscosity profile, resulting in improper vertical current structure.

Assuming the model gives at least a crude representation of the response to local wind driving, the predicted currents are an effective mechanism for transport and mixing. For example, consider an alongbay event of 1 dyn $cm^{-2}$ over 3 days, say from the northeast. Water along the northwestern side, within about 3 km of the coast, has an average velocity of 10 cm $s^{-1}$, which results in a displacement of 25 km, sufficient to transport water from New Bedford out of the bay into Rhode Island Sound, assuming the response is similar to the WHOI transect along this section. From a

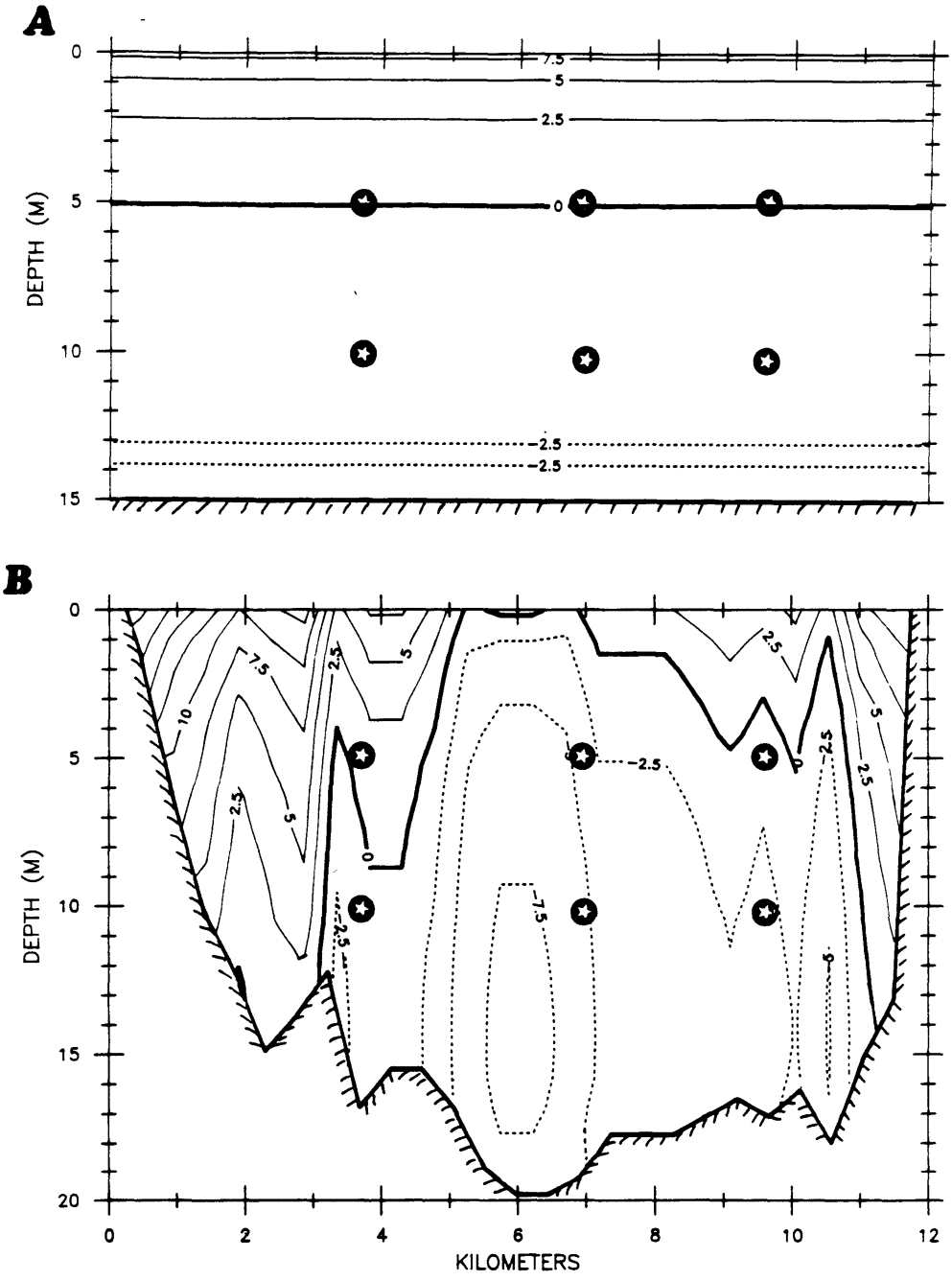


Figure 4.7: Steady wind forced model runs at WHOI transect. Wind stress is 1 dyn $cm^{-2}$ into the page and $u_{rms}$ is 15 cm $s^{-1}$. Dashed lines indicate flow in opposite direction of wind stress and stars indicate instrument locations. (a) Constant cross-section depth. (b) Variable cross-section depth.

mixing point of view, the same wind results in a transport of 2400 $m^3\ s^{-1}$ in and out of the bay, enough to exchange roughly 15% of the bay volume over the three days.

## 4.6 Summary

Local forcing by the wind dominates the current response from the 2–30 days at all stations except in regions of strong tidal rectification, where the 15–30 day currents are dominated by the modulation of the rectified flow. Wind on the shelf and atmospheric forcing drive average sea level variation in the bay, but the currents associated with these variations are weak, representing approximately 10% or less of the variance at their maximum strength at the mouth. The low-passed current variablility is polarized along the axis of the bay, and is most sensitive to winds in this direction. A steady state model which appears to represent the basic characteristics of the observations suggests that the along bay current response is one of strong downwind flow in the shallow northwestern side of the transect, and weaker return flow over the deeper regions of the transect to the southeast. The model also indicates that the local wind response is an effective mechanism for mixing, transport and bay renewal.

# Chapter 5

# Conclusions

Tidal and local wind forcing are the two most important mechanisms determining subtidal circulation in Buzzards Bay. Density driven flow is not apparent in current measurements, and calculations from hydrographic surveys together with drainage basin information suggests that density gradients drive large scale currents less than 1 cm $s^{-1}$ in magnitude. Although vertical stratification can exist in the spring and summer, in fall and winter, when the current measurements described here were obtained, the entire region is well mixed. Wind forcing dominated the 2–10 day band over the entire bay, while the 10 day to mean band in lower Buzzards Bay (south of New Bedford) appears dominated by small scale (3–5 km) tide-induced residual eddies.

The current response to wind is polarized along the axis of the bay and is principally driven by the component of local wind along this axis. Wind driven effects on the shelf do not drive significant currents in the bay, but account for greater than 90% of the low-frequency energy in sea surface displacement in the bay. At the WHOI transect, all three moorings were in water deeper than the cross-sectional average. At the lower instruments the transfer function between along-bay wind stress and along-bay currents indicates 5–10 cm $s^{-1}$/dyn $cm^{-2}$ currents directed against the wind and is larger at the central deepest mooring (station 5). These currents are nearly in phase with the forcing since the frictional time scale is of order 2–12 hours. A simple steady dynamical model that is consistent with basic features of the observed response predicts that 15–20 cm $s^{-1}$/dyn $cm^{-2}$ downwind transport will occur in the shallower regions where wind stress overcomes the integrated adverse pressure gradient. The understanding of

the wind reponse is far from complete, however. The model presented here is very sensitive to the bottom depth, and has a very crude eddy viscosity profile. In addition, the model ignores along-bay variations in cross-section, a poor assumption in Buzzards Bay.

While the local wind response dominates low-frequency circulation in the upper bay, in the lower bay, where tidal currents are stronger and the bathymetry complex, tide-induced residual currents are an important component of the subtidal circulation. Between 50–90% of the energy at 15 and 30 days in the observed along-mean flow component can be attributed to tidal rectification, and the mean flow predictions of a depth-averaged nonlinear tidal model are consistent with observed means in the lower bay. The model predicts residual eddy scales of 3–5 km with magnitudes of 2–5 cm $s^{-1}$ in Buzzards Bay.

There are several implications of these results with respect to transport and dispersion of passive tracers. First, the lack of an energetic density driven circulation indicates that mean transport should be thought of as a diffusive phenomenon resulting from the combined effect of local wind events and the nonlinearity of the tidal flow. Sporatic 2–5 day up-bay and down-bay wind events will advect material downwind in the shallows and upwind in the deeper regions, and subsequent dispersion due to tide-induced residual eddies will act to erode strong cross-channel gradients so that the process is irreversible. According to the model presented here, a northeaster blowing at 1 dyn at the bay mouth would transport 21,000 $m^3$ $s^{-1}$ to the southwest along the shore and 21,000 $m^3$ $s^{-1}$ to the northwest in the deeper regions, resulting in an exchange of 15% of the bay volume in 3 days. Dispersion by tide-induced residual eddies, on the other hand, should be a more continuous diffusive process modulated at 14 and 27 days and which in addition to homogenizing cross-channel structure, provides a preferred pathway for down-bay transport due to increased effective diffusion of stonger residual eddies.

Future work is planned to study the dispersion problem in more detail. This study has described the dominant mechanisms of dispersion, but more accurate modeling of the wind response together with calculation of tide-induced dispersion directly from the numerical tidal model is necessary before dispersion can be adequately quantified.

## REFERENCES


**Anraku M.**, 1964. Influence of the Cape Cod Canal on the hydrography and on the copepods in Buzzards Bay and Cape Cod Bay, Massachusetts. 1. Hydrology and distribution of copepods. *Limnol. Oceanog.*, **9**, 46–60.

**Beardsley R.C., Boicourt W.C.**, 1981. On estuarine and continental-shelf circulation in the Middle Atlantic Bight. *Evolution of Physical Oceanography, Scientific Surveys in Honor of Henry Stommel,* B.A. Warren and C. Wunsch, Eds., The MIT Press, 198–233.

**Brown W.S.**, 1984. A comparison of Georges Bank, Gulf of Maine, and New England Shelf tidal dynamics. *J. Phys. Oceanogr.*, **14**, 145–167.

**Bue C.D.**, 1970. Stream flow from the United States into the Atlantic Ocean during 1931–60. Contributions to the hydrology of the United States. *Geol. Surv. Water Supply Pap.*, **1899-I**, 36 p.

**Bumpus D.F.**, 1973. Arms of the Sea. *Coastal and Offshore Environmental Inventory: Cape Hatteras to Nantucket Shoals,* University of Rhode Island Marine Publication Series No. 2, Marine Experiment Station, 1-34–1-36.

**Butman B., Folger D.**, 1979. An instrument system for long-term sediment transport studies on the continental shelf. *J. Geophys. Res.*, **84**, 1215–1220.

**Butman B., Noble M., Chapman D.C., Beardsley R.C.**, 1983. An upper bound for the tidally rectified current at one location on the southern flank of Georges Bank. *J. Phys. Oceanogr.*, **13(8)**, 1452–1460.

**Capotondi A., Signell R.P., Sonnad V., Beardsley R.C.**, 1987. Tide-induced residual circulation simulation on a parallel computer. In preparation.

**Csanady G.T.**, 1973., Wind-induced barotropic motions in long lakes. *J. Phys. Oceanogr.*, **3**, 429–438.

**Chase J.**, 1972., Oceanographic Observations along the East Coast of the United States, 1970. *United States Coast Guard Report No. 53*, 154 p.

**Conomos T.J., Smith R.E., Gartner J.W.**, 1985. Environmental setting of San Francisco Bay. *Hydrobiologia*, **129**, 1–12.

**Farrington J.W., Tripp B.W., Davis A.C., Sulanowski J.**, 1982. *One view of the role of scientific information in the solution of enviro-economic problems.* In: Proceedings of the International Symposium on Utilization of Coastal Ecosystems, Planning, Pollution, Productivity, 22–27, November 1982. Rio Grande, R.S. Brazil, in press.

**Filloux J.H., Snyder R.L.,** 1979. A study of tides, setup and bottom friction in a shallow semi-enclosed basin. Part I: Field experiment and harmonic analysis. *J. Phys. Oceanogr.*, **9**, 158–169.

**Flather R.A., Heaps N.S.,** 1975. Tidal computations for Morecambe Bay. *Geophys. J.R. Astr. Soc.*, **42**, 489–517.

**Foreman M.G.G.,** 1977. Manual for tidal heights analysis and prediction. *Pacific Marine Science Report 77-10,* Institute of Ocean Sciences, Patricia Bay, Sidney, B.C. 97 pp.

**Garrett C.,** 1972. Tidal resonance in the Bay of Fundy and Gulf of Maine. *Nature,* **238**, 441–443.

**Garvine R.W.,** 1985. A simple model of estuarine subtidal circulation forced by local and remote wind stress. *J. Geophys. Res.*, **90**, 11945–11948.

**Gilbert T., Clay A., Barker A.,** 1974. Site selection and study of ecological efforts of disposal of dredged materials in Buzzards Bay, Mass. *New England Aquarium, Tech. Rep. to the U.S. Army Corps of Engineers.*

**Goldsmith T.L.,** 1986. Balancing the budget: a study of pond level change. *Unpublished document.*

**Grant W.D., Madsen O.S.,** 1979. Combined wave and curent interaction with a rough bottom. *J. Geophys. Res.*, **84(C4)**, 1797–1808.

**Grant W.D., Madsen O.S.,** 1986. The continental-shelf bottom boundary layer. *Ann. Rev. Fluid Mech.*, **18**, 265–305.

**Guswa J.H., LeBlanc D.R.,** 1981. Digital models of ground-water flow in the Cape Cod aquifer system, Massachusetts. *U.S. Geol. Surv. Water Res. Invest.*, Open-file Rep. No. 80-67.

**Haight P.J.,** 1938. *Currents in Narragansett Bay, Buzzards Bay, and Nantucket and Vineyard Sounds,* Special Publication No. 208, U.S. Government Printing Office.

**Hunter J.R.,** 1975. A note on quadratic friction in the presence of tides. *Estuarine and Coastal Marine Science,* **3**, 473–475.

**Large W.G, Pond S.,** 1981. Open ocean momentum flux measurements in moderate to strong winds. *J. Phys. Oceanogr.*, **11**, 324–336.

**Long C.E.,** 1981. A simple model for time dependent stabily stratified turbulent boundary layers. *Univ. of Wash. Dept. of Oceanog. Spec. Rep. No. 95.*

**Miller A.R.,** 1958. The effects of winds on water levels on the New England Coast. *Limnology and Oceanography,* **3(1)**, 1–14.

**Moody J.A., Butman B., Beardsley R.C., Brown W.S., Daifuku R., Irish J.D., Mayer D.A., Mofjeld H.O., Petrie B., Ramp S., Smith P., Wright W.R.**, 1984. Atlas of tidal elevation and current observations on the Northeast American Continental Shelf and Slope. *U.S. Geological Survey Bulletin 1611*, U.S. Government Printing Office, 122p.

**Noble M., Butman B.**, 1979. Low-frequency wind-induced sea level oscillations along the east coast of North America. *J. Geophys. Res.*, **84**, 3227–3236.

**Platzman G.W.**, 1975. Normal modes of the Atlantic and Indian Oceans. *J. Phys. Oceanogr.*, **5**, 201–221.

**Redfield A.C.**, 1953. Interference phenomena in the tides of the Woods Hole region. *J. Mar. Res.*, **12**, 121–140.

**Robinson I.S.**, 1983. Tidally induced residual flows. Chapter 7 in: Physical Oceanography of Coastal and Shelf Seas., ed. B. Johns, *Elsevier Oceanography Ser.*, No. 35, 321–356.

**Rosenfeld L.R., Signell R.P., Gawarkiewicz G.G.**, 1984. Hydrographic study of Buzzards Bay, 1982–1983. Woods Hole Ocean. Inst. Tech. Rpt. WHOI-84-5 (CRC-84-01), Woods Hole, MA, 140 pp.

**Saunders P.M.**, 1977. Wind stress over the Eastern Continental Shelf of North America. *J. Phys. Oceanogr.*, **7**, 555–566.

**Soulsby R.L.**, 1983. The bottom boundary layer of shelf seas. Chapter 5 in: Physical Oceanography of Coastal and Shelf Seas., ed. B. Johns, *Elsevier Oceanography Ser.* No. 35, 189–266.

**Speer P.E.**, 1984. Tidal distortion in shallow estuaries. *PhD thesis, Joint Program in Oceanography and Ocean Engineering, Woods Hole Oceanographic Institution.* 210p.

**Sumner F.B., Osburn R.C., Cole L.J., Davis B.M.**, 1913. A biological survey of the waters of Woods Hole and vicinity. *Bull. U.S. Bureau of Fisheries,* Part 1, **31**, 544 pp.

**Tee K.T.**, 1979. The structure of three dimensional tide-generating currents. Part 1: ocsillating currents. *J. Phys. Oceanogr.*, **9**, 930–944.

**Uncles R.J.**, 1982. Residual currents in the Severn Estuary and their effects on dispersion. *Oceanol. Acta.*, **5(4)**, 403–410.

**Wandle S.W., Morgan M.A.**, 1984. Gazetteer of hydrologic characteristics of streams in Massachusetts–coastal river basins of the South Shore and Buzzards Bay. *U.S. Geologic Survey Water Resources Investigations Report 84-4288*, 32p.

**Wang D-P., Elliott A.J.**, 1978. Nontidal variability in the Chesapeake Bay and Potomac River: Evidence for nonlocal forcing. *J. Phys. Oceanogr.*, **8**, 225–232.

**Wang D-P.**, 1979a. Subtidal sea level variations in the Cheaspeake Bay and relations to atmospheric forcing. *J. Phys. Oceanogr.*, **9**, 413–421.

**Wang D-P.**, 1979b. Wind-driven circulation in the Chesapeake Bay, Winter 1975. **9**, 564–572.

**Weaver G.**, 1982. PCB contanimation in and around New Bedford, MA. *Environ. Sci. and Technol.*, **18(1)**, 22A–27A.

**Wood F.J.**, 1976. The strategic role of perigean spring tides. U.S. Government Printing Office, Washington, D.C. 538p.

**Zimmerman J.T.F.**, 1976. Mixing and flushing of tidal embayments in the Western Dutch Wadden Sea, Part II: Anaysis of mixing processes. *Netherlands Journal of Sea Research*, **10(4)**, 397–439.

**Zimmerman J.T.F.**, 1981. Dynamics, diffusion and geomorphological significance of tidal residual eddies. *Nature*, **290**, 549–555.